# COLLISION-INDUCED QUADRUPOLAR SPECTRA OF MOLECULAR HYDROGEN IN THE FORST OVERTONE REGION AT 77,201 AND 295K



EDWARD GERARD VAN NOSTRAND


CENTRE FOR NFLD. STU
NOV 30 1985
MEMORIAL UNIVERSITY
OF NEWFOUNDLAND

CANADIAN THESES ON MICROFICHE

I.S.B.N.

THESES CANADIENNES SUR MICROFICHE

National Library of Canada
Collections Development Branch

Canadian Theses on
Microfiche Service

Ottawa, Canada
K1A 0N4

Bibliothèque nationale du Canada
Direction du développement des collections

Service des thèses canadiennes
sur microfiche

## NOTICE

The quality of this microfiche is heavily dependent upon the quality of the original thesis submitted for microfilming. Every effort has been made to ensure the highest quality of reproduction possible.

If pages are missing, contact the university which granted the degree.

Some pages may have indistinct print especially if the original pages were typed with a poor typewriter ribbon or if the university sent us a poor photocopy.

Previously copyrighted materials (journal articles, published tests, etc.) are not filmed.

Reproduction in full or in part of this film is governed by the Canadian Copyright Act, R.S.C. 1970, c. C-30. Please read the authorization forms which accompany this thesis.

THIS DISSERTATION
HAS BEEN MICROFILMED
EXACTLY AS RECEIVED

## AVIS

La qualité de cette microfiche dépend grandement de la qualité de la thèse soumise au microfilmage. Nous avons tout fait pour assurer une qualité supérieure de reproduction.

S'il manque des pages, veuillez communiquer avec l'université qui a conféré le grade.

La qualité d'impression de certaines pages peut laisser à désirer, surtout si les pages originales ont été dactylographiées à l'aide d'un ruban usé ou si l'université nous a fait parvenir une photocopie de mauvaise qualité.

Les documents qui font déjà l'objet d'un droit d'auteur (articles de revue, examens publiés, etc.) ne sont pas microfilmés.

La reproduction, même partielle, de ce microfilm est soumise à la Loi canadienne sur le droit d'auteur, SRC 1970, c. C-30. Veuillez prendre connaissance des formules d'autorisation qui accompagnent cette thèse.

LA THÈSE A ÉTÉ
MICROFILMÉE TELLE QUE
NOUS L'AVONS REÇUE

NL-339 (r. 82/08)

Canada

# COLLISION-INDUCED SPECTRA OF MOLECULAR HYDROGEN IN THE FIRST OVERTONE REGION AT 77, 201 AND 295 K

BY

Edward van Nostrand

A thesis submitted to the School of Graduate Studies in partial fulfillment of the requirements for the degree of Master of Science

Department of Physics

Memorial University of Newfoundland

July 1983

St. John's Newfoundland

## ABSTRACT

The collision-induced absorption spectra of molecular hydrogen in its first overtone region has been recorded with a 2 m high-pressure low-temperature absorption cell for gas densities up to 940 amagat at 77, 201 and 295 K. The observed spectra in the main region consists of pure overtone (i.e., $\Delta v = 2$) single transitions $O_2(J)$, $Q_2(J)$ and $S_2(J)$, pure overtone double transitions $Q_2(J)+Q_0(J)$ and $Q_2(J)+S_0(J)$ and double fundamental (i.e., $\Delta v = 1$) transitions $O_1(J)+Q_1(J)$, $Q_1(J)+Q_1(J)$ and $Q_1(J)+S_1(J)$; in addition, double transitions $S_2(J)+S_0(J)$ (corresponding to a first overtone vibrational-rotational transition in one molecule and a simultaneous pure rotational transition in its collision partner) and $S_1(J)+S_1(J)$ (corresponding to a simultaneous fundamental vibrational-rotational transition in each molecule of the colliding pair) have been observed for the first time for normal hydrogen at 77 K. These S + S transitions arise entirely from the contribution to the intermolecular interaction by the anisotropy of the polarizability of a molecule in the quadrupole field of its collision partner.

An analysis of the observed profiles on the basis of the theory of the quadrupole induction mechanism has been attempted using a symmetrized modified dispersion lineshape (with an extra fourth power term in the denominator) and the available matrix elements of the quadrupole moment.

polarizability and anisotropy of the polarizability of the $H_2$ molecule: it is found that the calculated intensities of the transitions involving $\Delta v = 2$ are somewhat too high. However, a reduction of the $\Delta v = 2$ quadrupole moment matrix elements by a factor of 0.68 is found to give a good agreement between the calculated absorption profiles and the experimental profiles at all the three experimental temperatures. Pressure narrowing of the $S_{\Delta v}(J) + S_{\Delta v}(J)$ transitions in the first overtone region for pure gas densities in the range 640 - 940 amagat at 77 K has been clearly observed for the first time.

A reanalysis of the absorption profiles of the $S_1(J) + S_0(J)$ transitions of the fundamental band of $H_2$ at 77 K obtained earlier in our laboratory is also reported.

## ACKNOWLEDGEMENTS

I would like to express my deep appreciation to my supervisor, Professor S.P. Reddy for his valuable guidance and encouragement throughout the course of the present work.

I would especially like to thank Dr. P. Gillard for help in the experimental work and also for many rewarding discussions.

I am also grateful for the technical assistance of Messrs. T.G. White and M. Ryan of the Physics workshop and Mr. R. Bradley for help with some of the photographic work.

I also wish to acknowledge the financial assistance from the Natural Sciences and Engineering Research Council of Canada and the Memorial University of Newfoundland.

## CONTENTS

# CHAPTER 1

# INTRODUCTION

## 1.1. Collision-Induced Absorption of Molecular Hydrogen in the Fundamental and First Overtone Regions

In their ground electronic states, isolated homonuclear diatomic molecules such as $H_2$ do not have permanent electric dipole moments and are normally infrared inactive. However, during collisions between two or more molecules a transient dipole moment can be induced which is modulated by the vibrational, rotational and relative translational motions of the molecules to give rise to infrared absorption spectra. This collision-induced absorption, first observed by Crawford *et al.* (1949) in the fundamental bands of compressed oxygen and nitrogen, was soon identified in the fundamental band of hydrogen (Welsh *et al.*, 1949). Since 1949 the collision-induced absorption spectra of the fundamental and overtone bands of gaseous $H_2$ have been studied in the pure gas and in binary mixtures with other simple gases over wide ranges of temperatures and pressures. A review of the experimental work done prior to 1971 on the induced spectrum of $H_2$ has been given by Welsh (1972) and a comprehensive bibliography on the subject has been compiled by Rich and McKellar (1976). For more recent work on the fundamental band, Reddy *et al.* (1977, 1980), Sen *et al.* (1980) and the references therein are to be consulted. Van Kranendonk (1974) and Birnbaum *et al.* (1982) have reviewed the theoretical aspects of collision-induced absorption.

The general theory of collision-induced absorption was first introduced by Van Kranendonk and Bird (1951a and 1951b) and later refined by Van

Kranendonk (1957 and 1958) by proposing the so called "exponential-4" model. In this model the induced dipole moment $\mu$, in a colliding pair of molecules consists of two additive parts, $\mu_{overlap}(R)$ and $\mu_{quad}(R)$, R being the intermolecular separation. The short-range, angle-independent, electron-overlap part is proportional to exp(-R) and the long-range, angle-dependent quadrupolar part is proportional to $R^{-4}$. The first part gives rise mainly to the broad $Q_{overlap}$ (i.e., $\Delta J=0$) components and the second part to relatively less broad O ($\Delta J=-2$), $Q_{quad}$ ($\Delta J=0$) and S ($\Delta J=+2$) components, where J is the rotational quantum number.

In the overlap induction mechanism a dipole moment is induced in the colliding molecules as a result of distortion of the electron distributions. As far as the fundamental band ($\Delta v=1$) is concerned this gives rise to a component of the single transitions $Q_1(J)$, (In the usual notation the subscripts 0,1,2, etc. attached to O,Q,S, etc. refer to $\Delta v$, the change in the vibrational quantum number, v). A distinct feature of the overlap induction is a characteristic dip in the Q branch of the fundamental band which was first observed by Crawford *et al.* (1950) in hydrogen-foreign gas mixtures and later confirmed by Chisholm *et al.* (1952) at higher gas densities. Van Kranendonk (1978) has explained this feature in terms of a destructive interference between the induced dipoles in successive collisions with the resulting lineform $D(\Delta\nu) = 1-\gamma[\ ]+(\Delta\nu/\delta_c)^2]^{-1}$ where $\delta_c$ is the intercollisional halfwidth, $\gamma$ is a parameter describing the height of the minimum and $\Delta\nu=\nu-\nu_m$, $\nu_m$ being the molecular transition wavenumber. The lineform of the total overlap induced transition is a product of $D(\Delta\nu)$ and the intracollisional lineform $W_0^0(\Delta\nu)=[2\Delta\nu/\delta_d]^2K_2(2\Delta\nu/\delta_d)$ of Levine and Birnbaum (1967) where $\delta_d$ is the intracollisional halfwidth and $K_2$ is a

modified Bessel function of the second kind. The "symmetrized" lineform $W_0(\Delta\nu) = D(\Delta\nu)\, W_0^0(\Delta\nu)$ is converted to the observed Boltzmann modified lineshape by dividing by the factor $1+\exp(-hc\Delta\nu/kT)$. The overlap contribution to the intensity of the fundamental band of $H_2$ has been successfully represented by this lineshape for the $H_2$-foreign gas spectra by Mactaggart and Welsh (1973) and for the pure gas spectra by Reddy *et al.* (1977). A detailed kinetic theory of the intercollisional interference dips in the overlap induced Q branch has been given by Lewis and Van Kranendonk (1971, 1972a, 1972b) and Lewis (1972, 1973, 1976 and 1982).

In the quadrupole induction mechanism, the quadrupole field of one molecule induces an electric dipole in its collision partner and vice versa. The strength of this induced dipole depends on the quadrupole moment and the polarizability of the colliding molecules. For the fundamental bands, the isotropic part of the polarizability of a colliding molecule contributes to the intensity of the single transitions $O_1(J)$, $Q_1(J)$ and $S_1(J)$ and the double transitions $Q_1(J)+O_0(J)$ and $Q_1(J)+S_0(J)$. (In a single transition, only one molecule of the colliding pair undergoes a change in its rotational and/or vibrational state. In a double transition both molecules of the collision pair simultaneously absorb a single photon.) The anisotropic component of the polarizability of a colliding molecule, however, contributes to the intensity of the transitions mentioned above as well as to the transitions of the form $S_1(J)+S_0(J)$. These transitions have been investigated in detail by Sen *et al.* (1980) and are also considered in the present work (see Chapter 5). Most lineshapes which have been used to describe the quadrupolar absorption have been modified Lorentzians. The lineshape used for the quadrupolar components in the present

work is given in detail in Chapter 3.

A third part of the induced dipole moment is the intermediate range $\mu_{hexa}(R)$ which results from the polarization of a molecule by the hexadecapole field of its collision partner and is proportional to $R^{-6}$. It gives rise to the $U_1(J)$ $(\Delta J=+4)$ single transitions and $Q_1(J)+U_0(J)$ double transitions in the collision induced fundamental band of $H_2$. These transitions, first observed by Gibbs *et al.* (1974), have been studied in detail by Reddy *et al.* (1980) and later by Gillard (1983) at higher densities.

Although the three types of induction discussed here contribute to the hydrogen fundamental band (see for example Reddy *et al.*, 1977, 1980 and Sen *et al.*, 1980), the overlap induction does not appear to contribute to the intensity of the first overtone region (see for example McKellar and Welsh, 1971).

A basic feature of the collision-induced absorption is the broad transition halfwidths. According to Van Kranendonk (1957), the width of the lines is due to the short duration of the induced dipole and the uncertainty principle, $\Delta E = h/(2\pi\Delta t)$. If the collision duration is given by $\Delta t = \bar{R}/\bar{V}$ where $\bar{R}$ is the range of the induction mechanism and $\bar{V}$ is the relative velocity of one molecule with respect to its collision partner, then the resulting width of the line in $cm^{-1}$ is of the order of

$$\Delta\nu = \frac{1}{2\pi c\,\Delta t} = \frac{\bar{V}}{2\pi c\bar{R}}$$

Because of the presense of $\bar{R}$, the short-range overlap induction will give rise to broader transitions than the long-range quadrupolar induction. Also, the relative kinetic energy of the molecules can be approximated by $\frac{1}{2}m\bar{V}^2 \approx \frac{3}{2}kT$ which shows a $T^{1/2}$ dependence for the halfwidth. This is

evident in the observed spectra where the halfwidths of the quadrupolar components vary from 50 $cm^{-1}$ at 77 K to greater than 100 $cm^{-1}$ at room temperature (see for example Reddy *et al.*, 1977).

The halfwidth of the collision-induced quadrupolar-induced transitions also has a notable density dependence at high densities. De Remigis *et al.* (1971) observed a definite decrease in the halfwidth in the fundamental band of $H_2$ in $H_2$ - Ar mixtures for gas densities above 300 amagat. Zaidi and Van Kranendonk (1971) explained the line narrowing in terms of a diffusional effect in which the linewidth is proportional to the diffusion constant and thus is approximately proportional to the density. This simple explanation has been criticized by Lewis and Tjon (1978) who showed that it is sometimes inapplicable. Later Mactaggart *et al.* (1973) studied in detail the same effect in the fundamental band in the binary mixtures $H_2$-Ar, $H_2$-Kr and $H_2$-Xe. The present work discusses the first observation of diffusional pressure narrowing in the first overtone region of $H_2$ in the pure gas.

The collision-induced absorption of hydrogen in the first overtone region was first observed by Welsh *et al.* (1951) at 80 and 300 K with 85 cm and 30 cm transmission cells for gas densities up to 426 and 676 amagat, respectively. It was suggested that the absorption corresponds to a superposition of two bands, namely, the true overtone band ($\Delta v = +2$) and a band arising from simultaneous fundamental vibrational ($\Delta v = +1$) transitions of both colliding molecules. This was later confirmed by Hare and Welsh (1958) who studied the absorption of $H_2$ in the first overtone region with a path length of 4 cm at 298 K for gas densities up to 1100 amagat. The observed spectra showed that both the pure overtone and

double fundamental transitions have very nearly the same shape at low as well as high densities and that there was no indication of any splitting of the absorption peaks. It was therefore proposed that the transitions arise from the same mechanism as the $Q_{quad}$ and S lines of the fundamental band, namely the quadrupolar induction. For reasons not fully understood, the observed collision-induced absorption of hydrogen in the first overtone region does not seem to have any contribution from the short range electron overlap induction, as mentioned earlier.

The absorption spectrum of $H_2$ in the first overtone region, obtained at a density of 31 amagat with a path length of 13.6 m at 24 K, was analyzed by Watanabe *et al.* (1971) on the basis of the theory of the quadrupolar induction using a Boltzmann modified dispersion lineshape (Kiss and Welsh, 1959) for the individual components. However, it was found that a systematic discrepancy existed between the experimental and calculated profiles. The relative intensities of the single transitions were too large compared to the double transitions. Watanabe (1971) suggested that this discrepancy could probably be due to the different density dependence of single and double transitions on the absorption arising from ternary collisions and reanalyzed the spectrum, applying a density correction. Although there was some improvement, there were still unexplained differences between the observed and calculated spectrum.

McKellar and Welsh (1971) studied the first overtone region of $H_2$ in the pure gas and in binary mixtures with Ar and $N_2$ with a path length of 137 m in the temperature range 85 to 116 K and analyzed the absorption profiles. This analysis revealed that systematic discrepancies still exist between the experimental and calculated profiles.

More recently Silvaggio *et al.* (1981) made an analysis of the absorption in the first overtone region at 122 and 273 K using the theoretical lineshape of Birnbaum and Cohen (1976). The fit between the observed and predicted profiles was reasonable, however the observed absorption was quite weak so that a detailed comparison between observed and theoretical profiles was difficult. Earlier Goorvitch *et al.* (1981) analyzed the fundamental band of hydrogen using the same lineshape, and on comparison with the results using a modified dispersion lineshape (Mactaggart and Hunt, 1969), concluded that either lineshape was satisfactory.

Typical collision-induced quadrupolar transitions in the first overtone region are shown in Fig. 1. The wavenumbers for the rotational and vibrational levels were calculated from the molecular constants of free $H_2$ (Foltz *et al.*, 1966). The single transitions $O_2(1)$, $Q_2(1)$ and $S_2(1)$ and the double transitions $Q_2(1)+S_0(1)$ and $S_2(1)+S_0(1)$ are all representative of the pure overtone ($\Delta v=2$) band, whereas the $Q_1(1)+O_1(2)$, $Q_1(1)+Q_1(1)$, $Q_1(1)+S_1(1)$ and $S_1(1)+S_1(1)$ transitions correspond to both molecules making a fundamental ($\Delta v=1$) transition. The $S_2(1)+S_0(1)$ and $S_1(1)+S_1(1)$ transitions arise solely from the anisotropy of the polarizability and their intensities can be used as a measure of its contribution to the first overtone region. These transitions are relatively weak compared to those arising from the isotropic part of the polarizability.

The intensity of the collision-induced transitions while dependent on the matrix elements of the quadrupole moment and polarizability are also very much dependent upon the population of the initial states. The

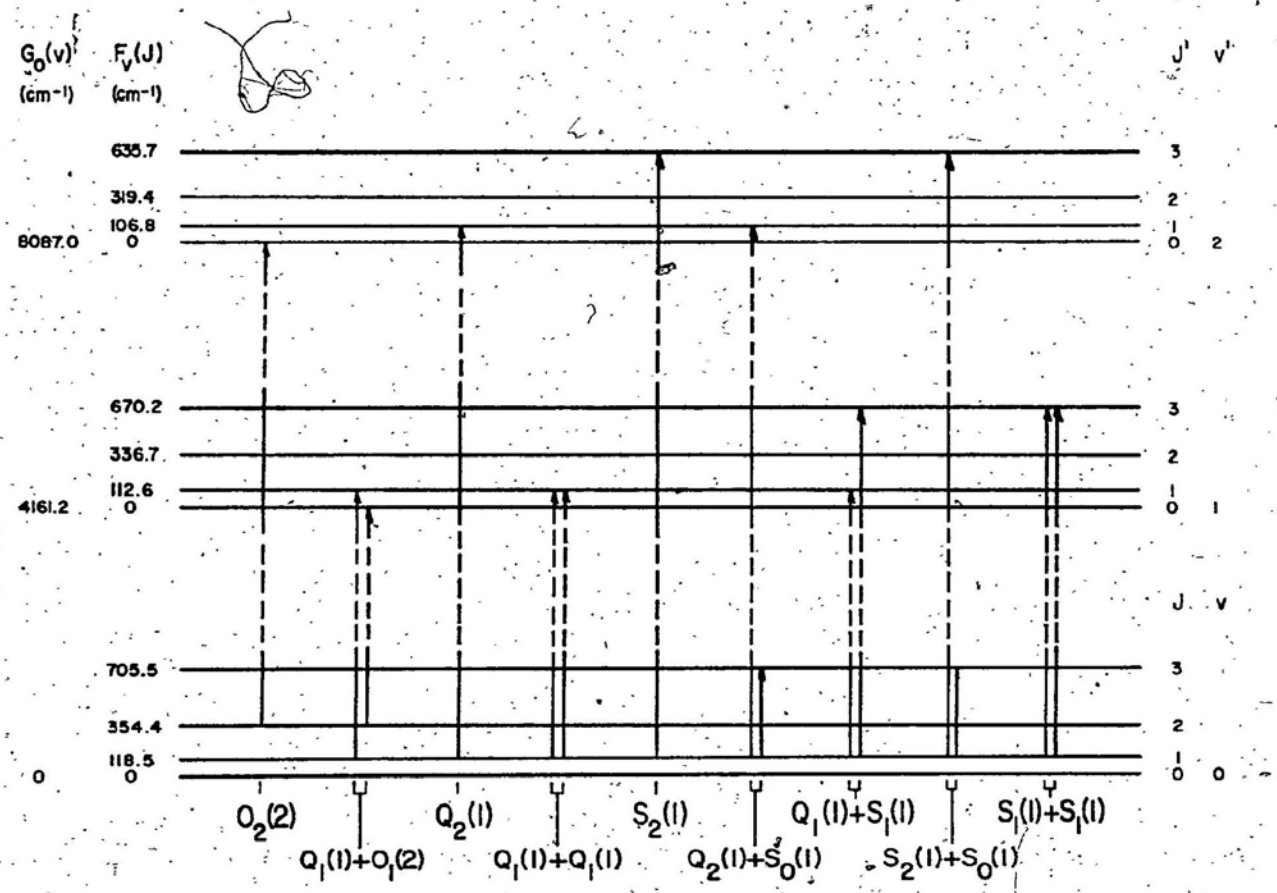


Fig. 1. Energy level diagram of $H_2$ showing some representative induced quadrupolar transitions in the first overtone region.

number of molecules N(J) in a rotation level J of the ground vibrational state of a symmetric diatomic gas in thermal equilibrium at temperature T depends on I) (2J+1) fold degeneracy ($g_J$), II) (2T+1) fold degeneracy ($g_T$) (due to nuclear spin) and III) the Boltzmann factor $\exp(-E_J/kT)$, i.e., $\exp(-F_0(J)hc/kT)$. (Note that temperature T should not be confused with total nuclear spin T). The nuclear spin I of the H atom is 1/2 and the total nuclear spin of the $H_2$ molecule has two (i.e., 2I+1) values, T=1 (parallel spins) and 0 (antiparallel spins). Symmetric and antisymmetric rotational levels have even and odd T values, respectively. Since the ground electronic state of $H_2$ is $^1\Sigma_g^+$, the even rotational levels (J=0,2,...) are symmetric and hence have T=0 (i.e., $g_T = 1$) and the odd rotational levels (J=1,3,...) are antisymmetric and hence have T=1 (i.e., $g_T = 3$). Therefore

$$N(J_{even}) \qquad 1(2J+1)\exp(-F_0(J)hc/kT) \ ,$$

and

$$N(J_{odd}) \qquad 3(2J+1)\exp(-F_0(J)hc/kT) \ .$$

### 1.2. The Present Study

The main aim of the present work was to obtain accurate experimental collision-induced absorption profiles of $H_2$ in the first overtone region over wide ranges of densities and temperatures, to analyze them with appropriate lineshape functions and to find whether it would be possible to obtain a better agreement between the calculated and experimental profiles than was previously acheived. Another aim was to observe and analyze the weaker transitions of the type $S_2(J)+S_0(J)$ and $S_1(J)+S_1(J)$, which occur on the high wavenumber tail of the first overtone region. Actually

the spectra have been recorded with a 2 m low-temperature high-pressure cell for gas densities up to 940 amagat at 77, 201 and 295 K. The apparatus and experimental procedure are described in Chapter 2.

When an attempt was made to analyze the experimental profiles at the three temperatures for densities up to 430 amagat on the basis of the theory of the quadrupolar induction mechanism using a symmetrized modified dispersion lineshape (with an extra fourth power term in the denominator) and available matrix elements of the quadrupole moment, polarizability, and anisotropy of the polarizability of the $H_2$ molecule; it was found that the calculated intensities of the transitions involving $\Delta v = 2$ are somewhat too high. However, when the $\Delta v = 2$ quadrupole moment matrix elements are reduced by a factor 0.68, the calculated absorption profiles agree very well with the experimental profiles at all the three temperatures. The absorption profiles, the analysis and results are presented in Chapter 3.

The purely anisotropic $S_{\Delta v}(J) + S_{\Delta v}(J)$ transitions of $H_2$ in the first overtone region have been studied for gas densities in the range 640 - 940 amagat at 77 K and a profile analysis has been carried out. Diffusional narrowing of these transitions has been clearly observed. There is an indication of the occurence of the $Q_1(J) + U_1(J)$ transition, corresponding to a $\Delta J = 4$ (i.e., U) transition in one molecule of the colliding pair. Details of this phase of the work are described in Chapter 4.

A reanalysis of the $S_1(J) + S_0(J)$ transitions in the fundamental region of $H_2$, which were initially studied by Sen *et al.* (1980), has been carried out assuming that the contribution of the overlap induction mechanism is negligible in the region of these transitions. This study is described in Chapter 5.

## CHAPTER 2

## APPARATUS AND EXPERIMENTAL TECHNIQUE

The infrared spectra of the collision-induced absorption of molecular hydrogen in its first overtone region was studied for gas pressures up to 800 atmospheres at 77, 201 and 295 K. The experimental data were obtained with two high-pressure absorption cells, a high-pressure gas handling system and an infrared recording spectrometer. In this chapter, a brief description of the apparatus and its operation will be presented.

### 2.1. The Absorption Cells and the Gas Handling System

#### (a) The 2.1 m Monel Absorption Cell

The 2.1 m transmission-type monel absorption cell which was originally designed for experiments at temperatures in the range 77 – 300 K was used in the present work only at room temperature (295 K). A schematic diagram of a cross-section of the cell is shown in Fig. 2. The cell consists of a monel tube T, 2.1 m long, 7.62 cm in outer diameter, and 2.54 cm in central bore. A polished monel light guide L with an aperture 1.0 cm x 0.5 cm runs through the full length of the cell. Synthetic sapphire windows $W_1$, 1.00 cm thick and 2.54 cm in diameter, were attached to polished monel seats S with an aperture 1.01 cm x 0.51 cm by Canadian General Electric RTV clear silicone sealant. An invar O-ring I between the seat and the body of the cell was compressed by tightening eight 3/8-24 allen-head bolts against the retaining end piece P to ensure a pressure tight seal.

Three concentric metal jackets surrounding the monel tube provided a

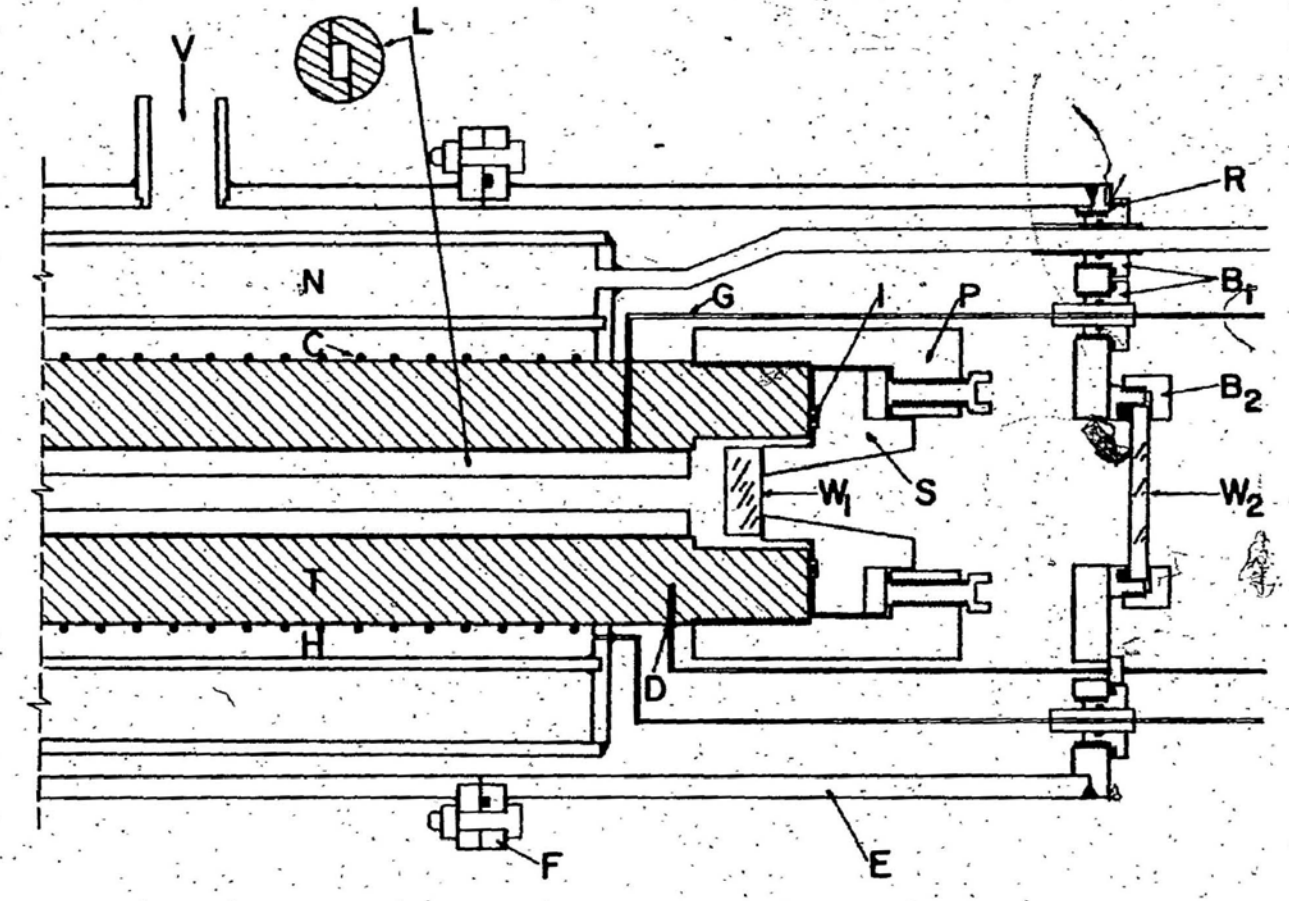


Fig. 2. A cross-section of the 2.1 m low-temperature, high-pressure monel cell.

means to regulate the temperature of the cell between 77 and 295 K. An inner cylindrical steel jacket contains a heat exchange gas H, such as helium, at pressures up to one atmosphere. By maintaining the required amount of pressure of helium gas and by adjusting the current through the coils, the cell can be maintained at the desired temperature above 77K. A copper-constantan thermocouple D was placed in the wall of the cell body to monitor the temperature. A third jacket surrounding the cell and inner jackets could be evacuated through the vacuum port V, to insulate the liquid nitrogen chamber and to prevent water vapor from condensing on the cooled windows. The end cap E which is sealed to the exterior jacket by flange F, can be removed to allow access to the inner components. Rubber O-rings R in the threaded brass fittings $B_1$ ensures a vacuum tight seal around the high pressure gas tubing G and the liquid nitrogen port. A sapphire window $W_2$, 5.08 cm in diameter and 0.3 cm thick, was sealed to the end piece with a rubber O-ring by a threaded brass ring $B_2$. Further details of the cell are given by Penney (1980).

**(b) The 2 m Stainless Steel Absorption Cell**

The low temperature experiments at 201 and 77 K were carried out with a 2 m transmission-type stainless steel absorption cell, originally designed for experiments at room temperature by Reddy and Kuo (1971) and later modified for low temperature work by Chang (1974). The cell, whose schematic cross-section is shown in Fig. 3, consists of a 2 m stainless steel tube T, 7.62 cm in diameter, and 2.54 cm in central bore. A polished stainless steel light guide L, with an aperture 1.0 cm x 0.5 cm, was inserted into the bore to ensure good transmission of radia-

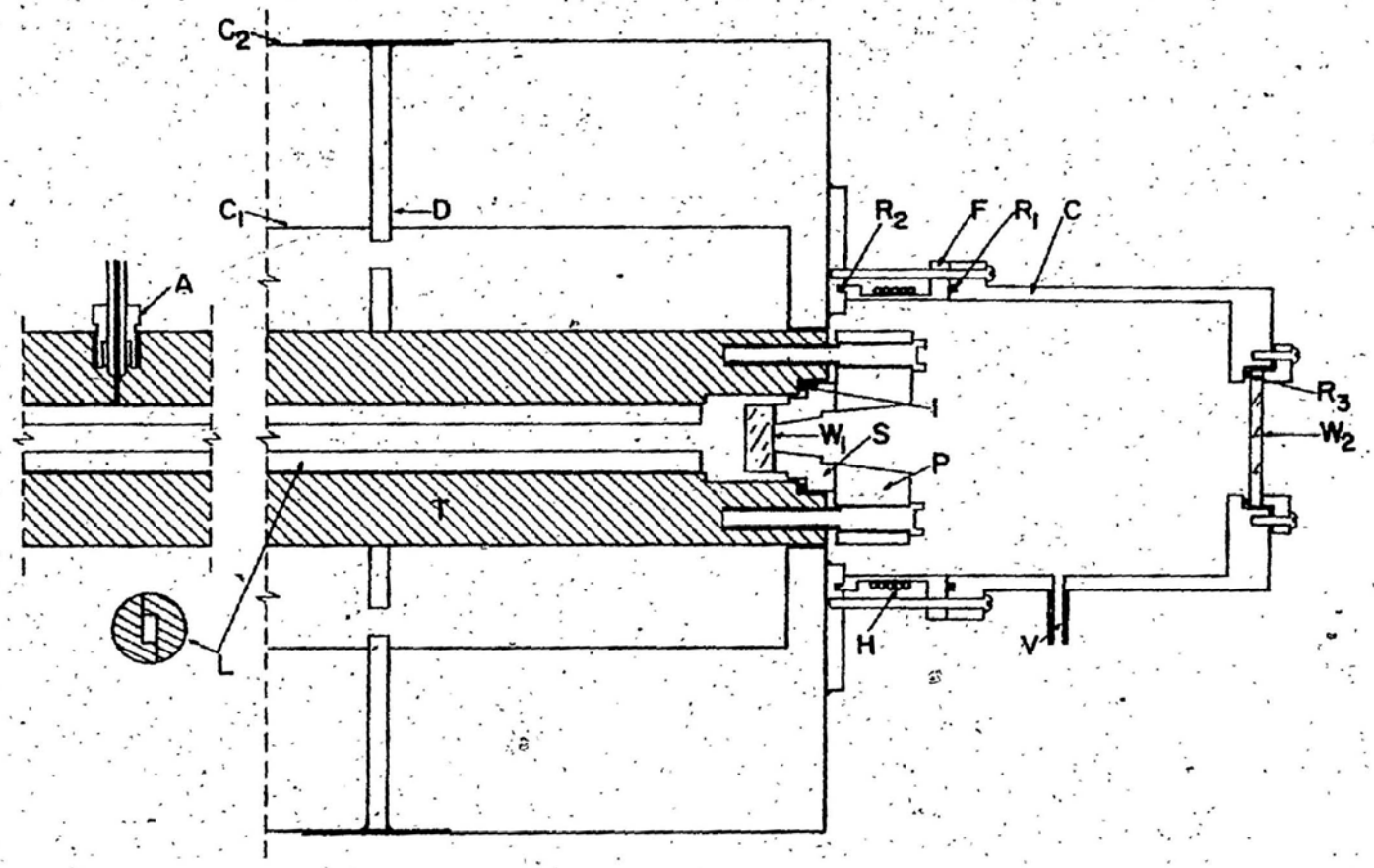


Fig. 3. A cross-section of the 2 m low-temperature, high-pressure stainless-steel cell.

tion through the cell. Synthetic sapphire windows $W_1$, 1.00 cm thick and 2.54 cm in diameter, were positioned on stainless steel seats S with a rectangular aperture equivalent to that of the light guide. An end piece P with eight Allen head bolts was used to achieve a pressure tight seal between the seat and the body of the cell by compressing an Invar O-ring I. The experimental gas is admitted into the cell through the Aminco fitting A. A stainless steel flange F at the end of the cell provides a seat for a Plexiglas end cap C. The seal was provided by tightening eight screws against a rubber O-ring $R_1$ between the cap and flange and an indium seal $R_2$ between the flange and the cell. This assembly was evacuated through the port V to prevent condensation of water vapor on the cool windows for the low temperature experiments. Heating tapes H were wound around the flange so that the rubber O-ring would not freeze. A sapphire window $W_2$, 5.08 cm in diameter and 0.3 cm thick was placed in the end cap and sealed against a rubber O-ring $R_3$ with a Plexiglas ring and three screws.

Two concentric stainless steel chambers surround the cell and provide both an insulating jacket and a chamber for the coolant. The inner chamber $C_1$, which contains the coolant, was welded to a stainless steel disc D for support. Holes were drilled in the disc to allow free flow of the coolant to the ends of the cell. The central section of the exterior chamber $C_2$ was also welded to the disc; however the two ends were free to slide over the central section to allow for the difference in the thermal expansion and contraction of the two chambers. The space between $C_1$ and $C_2$ was filled with vermiculite which acted as an insulator for the coolant.

Liquid nitrogen, which was admitted through an opening at the top of the jacket, was used as a coolant for experiments at 77 K. Its flow from a 200 litre dewar was regulated by a Rochefort Liquid Nitrogen Controller which closed or opened a solenoid valve, depending on whether or not a carbon resistor was immersed in the liquid nitrogen contained in the cell jacket. For work at 201 K the cell was cooled with a mixture of ethanol ($C_2H_5OH$) and crushed dry ice.

**(c) The Gas Handling System**

Hydrogen gas used in the present experiments was of Matheson ultra-high-purity grade and was handled in a high pressure system shown schematically in Fig. 4. The gas was admitted into the cell through a series of Aminco stainless steel high-pressure fittings and capillary tubing. From the cylinder, the gas was first passed through the coil $C_1$ of 1/4 inch copper tubing to remove any possible contaminants such as water vapor, carbon dioxide etc.. Since thermal compression was the only method used to develop high pressures, up to 12,000 psi, several stages of cooling and warming were required. A medium pressure stainless steel compressor $C_2$, immersed in liquid nitrogen, received the cooled gas from the copper coil. As $C_2$ was allowed to warm up to room temperature, the gas from it was admitted into two high-pressure stainless steel compressors $C_3$ and $C_4$ at liquid nitrogen temperature. The gas in $C_3$ was then warmed to room temperature and admitted into $C_4$, still kept at 77 K. Finally $C_4$ acted as a high-pressure gas reservoir when it was warmed up to room temperature.

The experimental gas pressures were recorded by three Bourdon tube

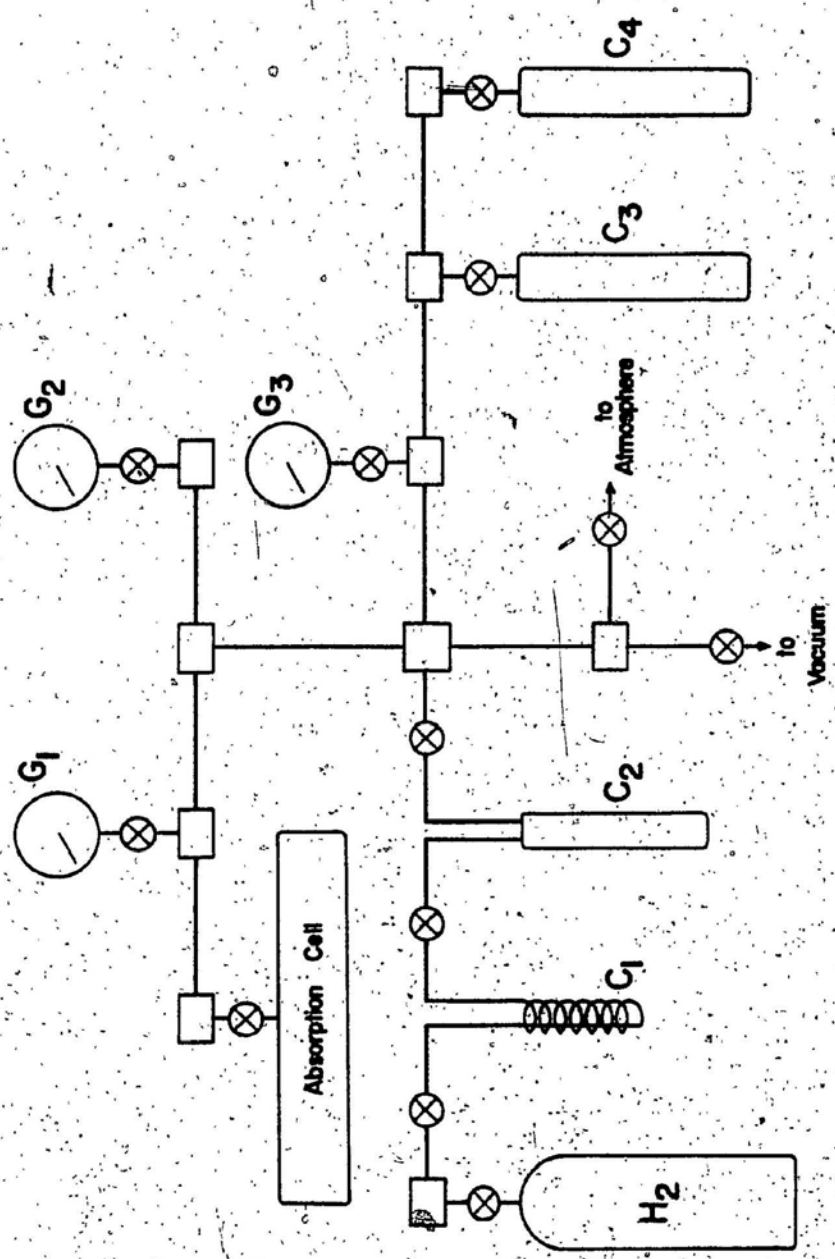


Fig. 4. The high-pressure gas handling system.

pressure gauges $G_1$, $G_2$ and $G_3$ with respective ranges 0-5000, 0-10000 and 0-20000 psi. Oil filled Bourdon tube test gauges which were calibrated against an Ashcroft dead weight pressure balance were used as calibration standards for the gauges used in the system.

## 2.2 The Optical System

### (a) The Spectrometer and Optics

The optical arrangement is shown in Fig. 5. The source of continuous infrared radiation is a Canadian General Electric FFJ 600 W Quartzline projection lamp S enclosed in a water cooled brass jacket of special design. The lamp voltage, stablized by a Sorensen ACR 2000 voltage regulator, was adjusted between 60 and 80 volts to bring the signal to noise ratio to an acceptable level. An f/4 front-coated concave mirror $M_1$ with focal length 40 cm, focused the source radiation at the entrance window of the absorption cell. The radiation leaving the exit window of the cell was then focused, by a similar mirror $M_2$, onto the entrance slit of a Perkin-Elmer model 99 double-pass prism spectrometer. The radiation was then dispersed by an LiF prism, reflected back by a Littrow mirror to complete the first pass through the prism and brought to a focus. The diverging radiation from this focus was then chopped by a tuning fork chopper at 260 Hz and sent back through the prism for a second pass. Rotation of the Littrow mirror allows different frequencies of the second pass radiation to fall on the exit slit. The radiation emerging from the exit slit was then focused onto an uncooled lead sulfide detector. The slit width maintained at 35 microns gave a spectral resolution of 16 $cm^{-1}$ at the origin of the first overtone band of hydrogen (8087 $cm^{-1}$).

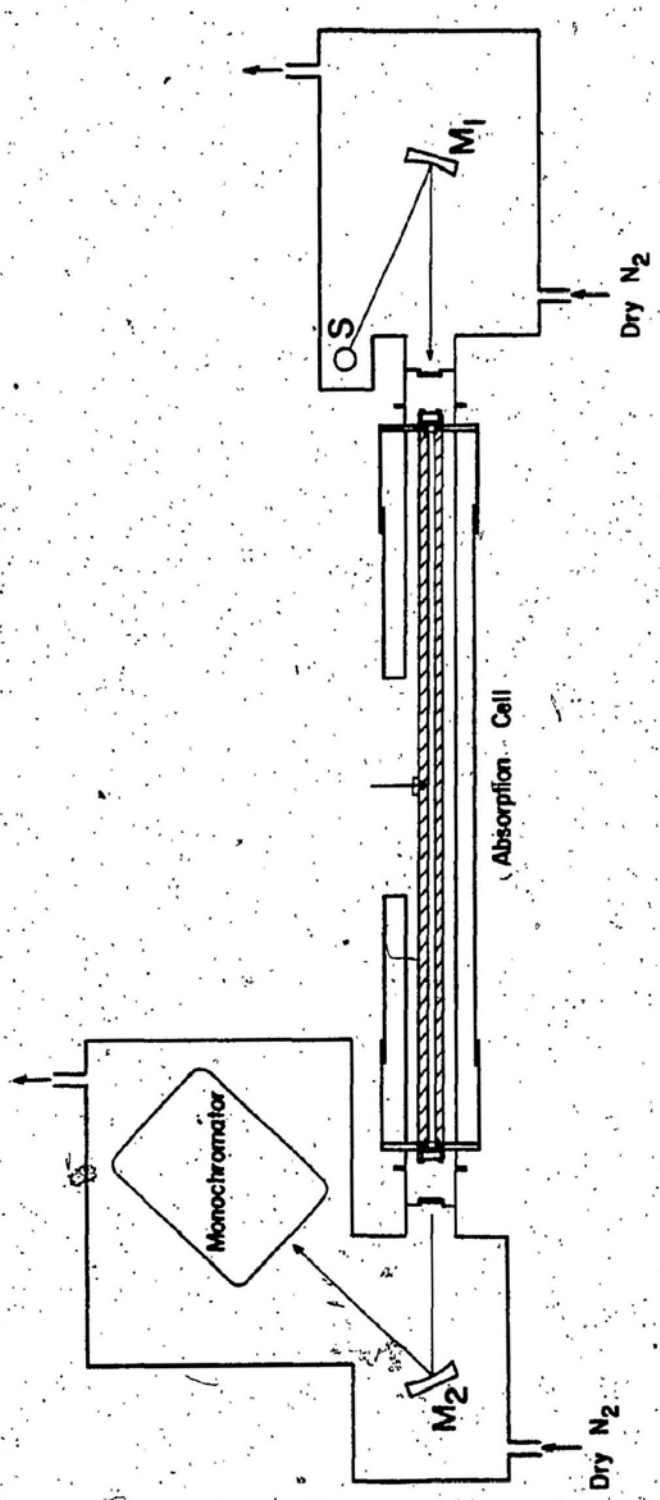


Fig. 5. The optical arrangement.

**(b) Flushing of the Optical Path with Dry Nitrogen Gas**

Atmospheric water vapor absorption, in the spectral regions 7000–7400 $cm^{-1}$ and 8700–8900 $cm^{-1}$, interferes with the recording of the hydrogen spectra in its first overtone region. To remove the water vapor from the path of the radiation, the source of radiation and the monochromator were housed in airtight enclosures as shown in Fig. 5. The source and mirror $M_1$, at one end of the cell, were enclosed in a Plexiglas box that was sealed to the endcap of the cell with a rubber gasket. The monochromator and mirror $M_2$ were located in a similar box at the other end of the cell. Dry nitrogen gas which was generated by electrically boiling liquid nitrogen contained in a 200 litre dewar was continuously flushed through the two boxes. Four days of flushing with the nitrogen was usually required to bring the water absorption to a negligible and stable level.

**2.3. Signal Detection**

The lead sulfide detector used was a photoconductive device whose resistance varies with the intensity of the radiation incident upon its surface. The detector was supplied with a constant current so that the voltage corresponds directly to the radiation intensity. This voltage was amplified by Brower Laboratories model 261 preamplifier and model LI-100 lock-in voltmeter. However, since only the chopped second pass radiation is important, the signal arising from unchopped first pass radiation and zero drift, must be removed. A 260 Hz signal from the tuning fork chopper was sent to the trigger input of the lock-in voltmeter where it was matched with the chopped radiation signal so that the unchopped radiation could be subtracted. The a.c. signal was full wave rectified and its

random noise was reduced with an RC filter. The d.c. signal leaving the lock-in voltmeter was recorded on a Hewlett-Packard model 7132A strip chart recorder.

## 2.4. Data Reduction

### (a) Calibration

The hydrogen spectra were recorded as an intensity versus the time base of the chart recorder. However the time base was converted to wavenumber ($cm^{-1}$) by taking the spectra of known emission lines of mercury (Zaidel *et al*. 1970) and absorption peaks of atmospheric water vapor (Downie *et al*. (1953) and Plyler *et al*. (1952)) in the region of the hydrogen first overtone band. The positions of these standard emission and absorption peaks were measured with respect to the prominent mercury line at 9859.5 $cm^{-1}$ and least squares fitted to a sixth order polynomial. This in turn was used to obtain a calibration chart giving the positions at intervals of 10 $cm^{-1}$ on a transparent overlay for the experimental hydrogen spectra.

### (b) Chart Reduction

If $I_0(\nu)$ is the transmitted intensity of the radiation at wavenumber $\nu$ (in $cm^{-1}$) by the evacuated cell of sample path length $l$, and $I(\nu)$ is the corresponding quantity with the cell filled with hydrogen at a given pressure, the absorption coefficient $\alpha(\nu)$ is given by

$$\alpha(\nu) = (2.303/l) \log_{10}(I_0(\nu)/I(\nu))$$

It should be noted that $I_0(\nu)$ and $I(\nu)$ are measured from the infinite

absorption line. Chart recordings of the spectrum with the cell evacuated were taken both at the beginning and end of an experiment. A proper matching of the initial and final background traces indicated the stability of the source of radiation and the signal recording system during the experiment. Several traces were also taken at each gas pressure and averaged to obtain the spectrum. A mercury emission line included in all of the traces was used as a reference for matching the traces. The quantity $\log_{10}(I_0(\nu)/I(\nu))$ was measured at intervals of 10 $cm^{-1}$. Absorption profiles were obtained by plotting $\log_{10}(I_0(\nu)/I(\nu))$ against $\nu$. The areas under the absorption profiles represent the integrated absorption coefficients $\int \alpha(\nu)\, d\nu$.

## 2.5. Isothermal Data

Recorded pressures of hydrogen at the three experimental temperatures were converted to the density in units of amagat using the pressure-density data available in the literature. (Amagat is the ratio of the density of a gas at any temperature and pressure to its density at STP). Densities of $H_2$ gas at 201 and 295 K were first obtained by a linear interpolation of the pressure-density data at −75 and −50 °C and 0 and 25 °C, respectively, given by Michels *et al*. (1959). These data were least squares fitted to a polynomial to allow interpolation of the densities for the experimental pressures. A similar procedure was followed to obtain densities for hydrogen at 77 K from the data of McCarty *et al*. (1981).

## CHAPTER 3

## COLLISION-INDUCED ABSORPTION SPECTRA OF HYDROGEN IN THE FIRST OVERTONE REGION AND THEIR ANALYSIS

A brief summary of the earlier work on the collision-induced infrared absorption of $H_2$ in its fundamental and first overtone regions and an outline of the objectives of the present research project have been given in Chapter 1. The high-pressure absorption cells and the experimental procedure have been described in Chapter 2. In the work reported in this chapter, the induced spectra of $H_2$ were recorded in the pure gas at 77, 201 and 295 K with 2 m and 2.1 m absorption cells for a number of gas densities up to 435 amagat. Table 3-1 summarizes the conditions under which the experiments were carried out.

TABLE 3-1. Summary of experimental conditions

| Temperature (K) | Absorption path length (cm) | Number of gas densities studied | Maximum density of gas (amagat) |
|---|---|---|---|
| 77 | 194.6 | 14 | 365 |
| 201 | 194.8 | 18 | 403 |
| 295 | 209.7 | 16 | 433 |

Results of the transitions of the type $S_{\Delta v}(J_1)+S_{\Delta v}(J_2)$ which occur on the high wavenumber tail of the main first overtone band and which have been studied for $H_2$ in the pure gas at 77 K in the density range 640 - 940 amagat will be described in Chapter 4.

### 3.1. Absorption Profiles

Three typical absorption profiles of $H_2$ in the pure gas in the first overtone region at each of 77, 201 and 295 K are shown in Figs. 6, 7 and 8, respectively, by plotting $\log_{10} [I_0(\nu)/I(\nu)]$ against wavenumber, $\nu$. The positions of the single transitions $O_2(2)$, $Q_2(1)$, $S_2(0)$ and $S_2(1)$, calculated from the constants of the free $H_2$ molecule (Foltz *et al.*, 1966) are marked along the wavenumber axis. For the collision-induced absorption in the first overtone region resulting from the quadrupolar induction mechanism (as discussed in Chapter 1), the isotropic part of the polarizability contributes to the intensity of the pure overtone single transitions $O_2(J)$ ($J \neq 0$ and 1), $Q_2(J)$ ($J \neq 0$) and $S_2(J)$, pure overtone double transitions $Q_2(J)+S_0(J)$ and double fundamental transitions $Q_1(J)+O_1(J)$ ($J \neq 0$ and 1 for $O_1(J)$), $Q_1(J)+Q_1(J)$ and $Q_1(J)+S_1(J)$; whereas the anisotropic part of the polarizability contributes not only to the double S transitions $S_2(J)+S_0(J)$ and $S_1(J)+S_1(J)$ exclusively but also a small amount to the other transitions mentioned here. In Figs. 6, 7 and 8, the extent of different molecular wavenumbers of the transitions are identified over the absorption peaks; the absorption peak positions and the assignments of transitions contributing to these peaks are given in Tables 3-2 and 3-3. The individual components of the absorption profiles are generally broad and have a characteristic dependence on the temperature as seen from the profiles of Figs. 6 - 8. At high temperature these are broader as the relative speed of the pairs of colliding molecules is large, resulting in a short collision duration.

The short-range electron overlap induction mechanism contributes considerably to the intensity of the induced fundamental band of $H_2$ (see

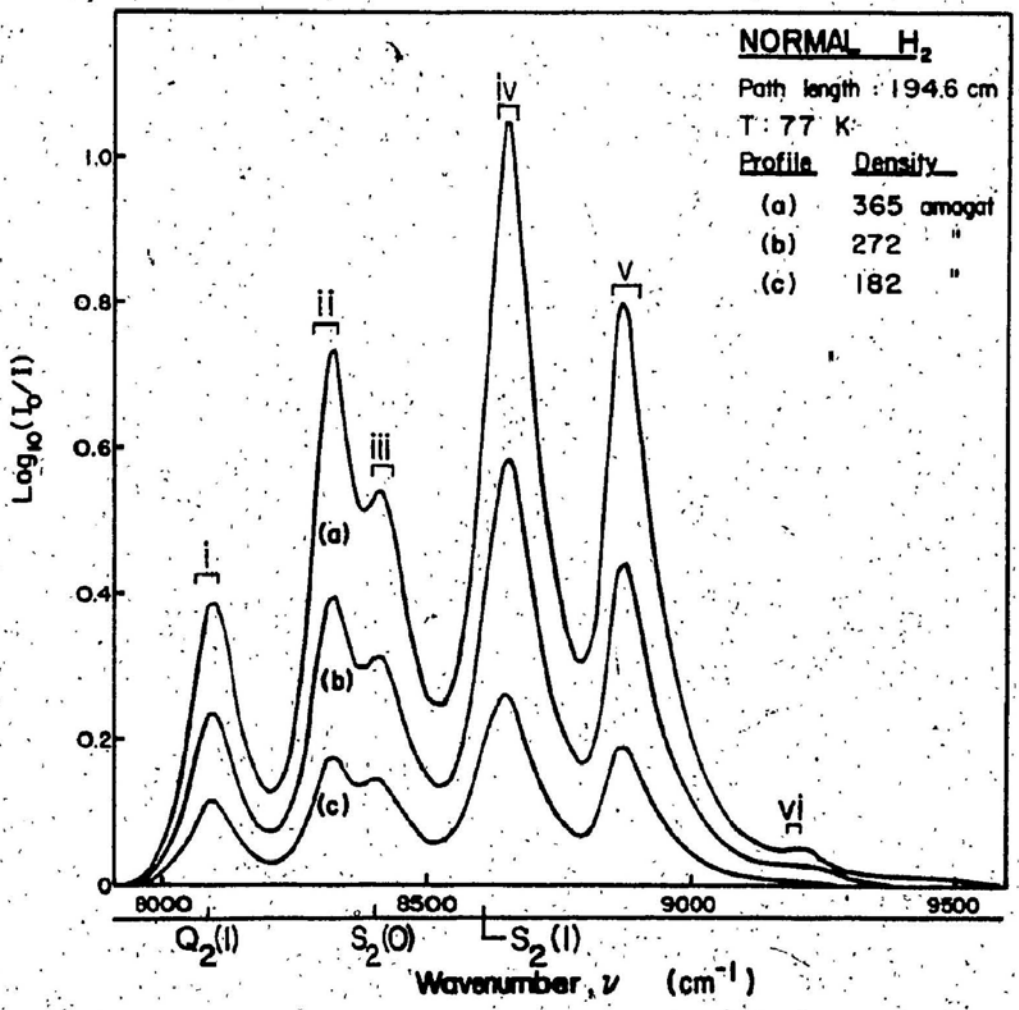


Fig. 6. Collision-induced absorption profiles of $H_2$ in the first overtone region at three different densities of the gas at 77 K. The calculated positions of $Q_2(1)$, $S_2(0)$ and $S_2(1)$ are marked along the wavenumber axis. The extents of various transitions are marked in groups i to vi. Peak positions of these groups and the assignments of the corresponding transitions are given in Table 3-2.

TABLE 3-2 Assignment of the Observed Absorption Peaks of the $H_2$ at 77 K

| Peak number | Wavenumber of observed peak | Assignment |
|---|---|---|
| I | 8085 | $Q_2(J)$, $Q_2(J)+Q_0(J)$ |
| II | 8310 | $Q_1(J)+Q_1(J)$ |
| III | 8410 | $Q_2(J)+S_0(0)$ |
| IV | 8655 | $Q_2(J)+S_0(1)$, $Q_1(J)+S_1(0)$ |
| V | 8875 | $Q_2(J)+S_0(2)$, $Q_1(J)+S_1(1)$ |
| VI | 9200 | $S_2(1)+S_0(1)$, $S_1(1)+S_1(0)$ |

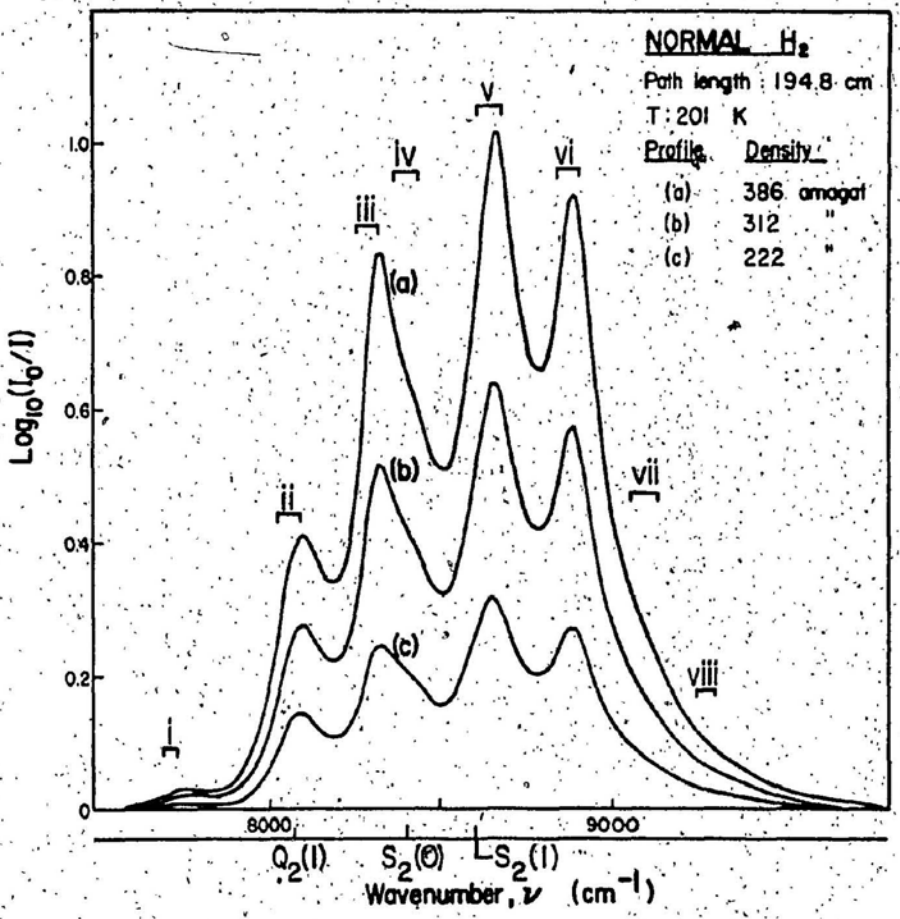


Fig. 7. Collision-induced absorption profiles of $H_2$ in the first overtone region at three different densities of the gas at 201 K. The calculated positions of $Q_2(1)$, $S_2(0)$ and $S_2(1)$ are marked along the wavenumber axis. The extents of various transitions are marked in groups i to viii. Peak positions of these groups and the assignments of the corresponding transitions are given in Table 3-3.

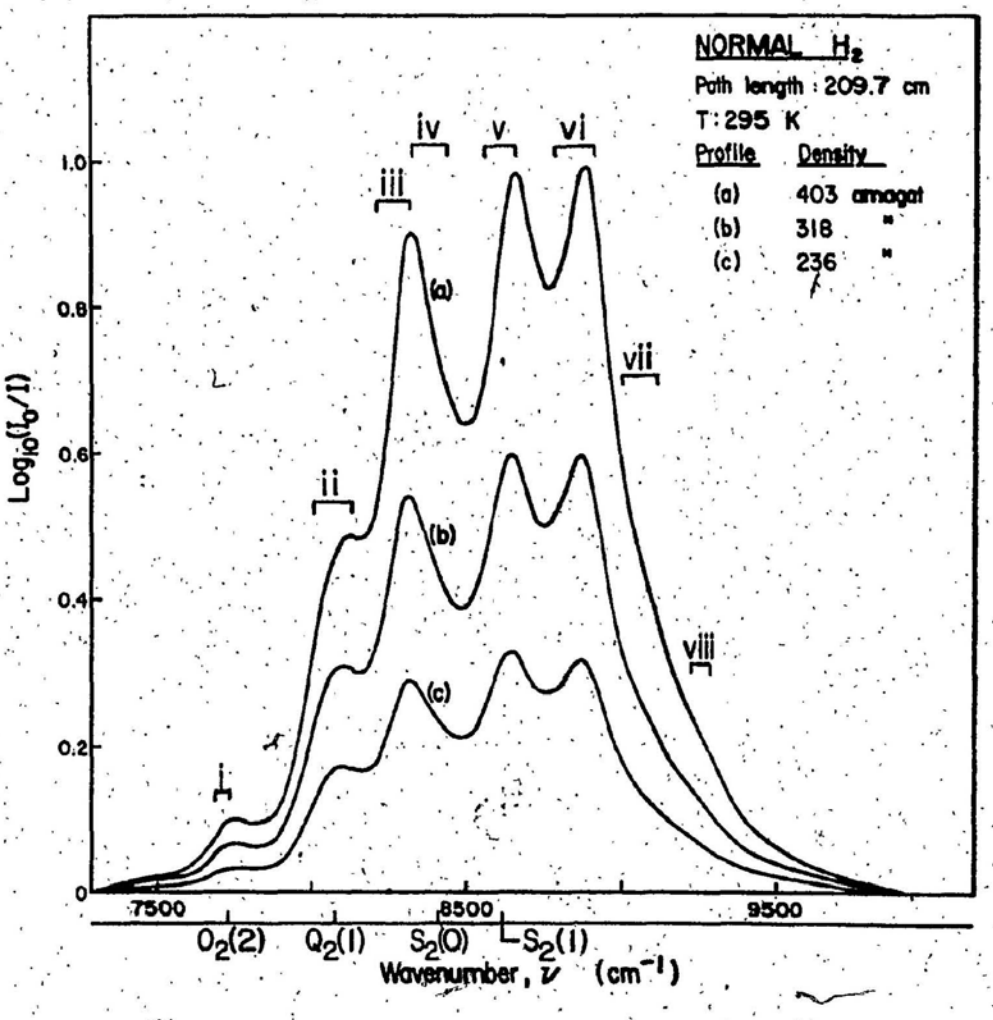


Fig. 8. Collision-induced absorption profiles of $H_2$ in the first overtone region at three different densities of the gas at 295 K. The calculated positions of $O_2(2)$, $Q_2(1)$, $S_2(0)$ and $S_2(1)$ are marked along the wavenumber axis. The extents of various transitions are marked in groups i to viii. Peak positions of these groups and the assignments of the corresponding transitions are given in Table 3-3.

TABLE 3–3 Assignment of the Observed Absorption Peaks of the $H_2$ at 201 and 295 K

| Peak number | Wavenumber of observed peak | | Assignment |
|---|---|---|---|
| | 201 K | 295 K | |
| I | 7750 | 7750 | $Q_2(J)+O_0(2),\ O_2(2)$ |
| II | 8100 | 8110 | $Q_2(J),\ Q_2(J)+Q_0(J)$ |
| III | 8325 | 8320 | $Q_1(J)+Q_1(J)$ |
| IV | - | - | $Q_2(J)+S_0(0)$ |
| V | 8660 | 8660 | $Q_2(J)+S_0(1),\ Q_1(J)+S_1(0)$ |
| VI | 8875 | 8870 | $Q_2(J)+S_0(2),\ Q_1(J)+S_1(1)$ |
| VII | - | - | $Q_2(J)+S_0(3),\ Q_1(J)+S_1(2)$ |
| VIII | - | - | $Q_1(J)+S_1(3)$ |

for example Reddy *et al.*, 1977) and gives rise to a characteristic dip in the Q branch resulting in $Q_P$ and $Q_R$ components whose separation increases with increasing density of the gas. The occurence of this dip has been interpreted in terms of the negative correlations existing between the short range dipole moments induced in successive collisions (Van Kranendonk, 1968). A distinct feature of the the induced spectra of $H_2$ in the first overtone region is the absence of the corresponding dip in the $Q_2(J)$ in Figs. 6 – 8. This absence implies that the overlap induction mechanism does not contribute to the intensity of the first overtone band. This conclusion is in agreement with the earlier observations (see for example Hare and Welsh, 1958 and McKellar and Welsh, 1971). The detailed profile analysis carried out later in this chapter also supports this conclusion. However, McKellar and Welsh (1971) have found that the overlap induction mechanism contributes to the intensity of the induced second overtone band of $H_2$ and very recently Gillard (1983) identified the characteristic overlap dip in the $Q_3$ branch of this band. The absence of the overlap contribution to the intensity of the first overtone band of $H_2$ is puzzling and has not been fully understood.

### 3.2. Profile Analysis

#### (a) Lineshape Functions

Following Mactaggart and Welsh (1973) and Reddy *et al.* (1977); who have analyzed the induced fundamental band of $H_2$ in the $H_2$ – inert gas mixtures and in the pure $H_2$ gas, respectively, the absorption coefficient $\bar{\alpha}_{qm}(\nu)$ $(=\alpha_{qm}(\nu)/\nu)$ at a given wavenumber $\nu$ of a specific molecular transition m arising from the quadrupolar induction mechanism can

conveniently be represented by

$$\tilde{\alpha}_{qm}(\nu) = A_q \int \tilde{\alpha}_{qm}(\nu)\, d\nu \; \frac{1}{1+(\Delta\nu/\delta_q)^2} \; \frac{1}{1+\exp(-hc\Delta\nu/kT)} \quad , \qquad (3.1)$$

where $\int \tilde{\alpha}_{qm}(\nu)\, d\nu$ is the integrated binary absorption coefficient of the mth transition and can be calculated theoretically, $\Delta\nu = \nu - \nu_m$, $\nu_m$ being the molecular wavenumber. h, c , and k are the fundamental constants and T is the absolute temperature. $A_q$ is a normalization factor for the lineshape used and is in fact the reciprocal of the area of the lineshape with height 0.5 at $\nu_m$.

$$\frac{1}{A_q} = \int \frac{1}{1+(\Delta\nu/\delta_q)^2} \; \frac{1}{1+\exp(-hc\Delta\nu/kT)} d\nu$$

$1/[1+(\Delta\nu/\delta_q)^2]$ is the dispersion type function which is symmetric about $\nu_m$, $\delta_q$ is the halfwidth at half height of the symmetrized line and the factor $1/[1+\exp(-hc\Delta\nu/kT)]$ is expected to convert the symmetrized lineform into the observed asymmetric lineshape. However, the absorption coefficient represented by Eq. (3.1) is not entirely satisfactory in the high wavenumber tail of the fundamental band ( see for example Reddy *et al.*, 1977, Reddy and Prasad, 1977 and Penney *et al.*, 1982). Reddy *et al.* 1980 included a $(\Delta\nu/\delta_{q4})^4$ term in the denominator of the dispersion-type function to account satisfactorily for the contribution of the quadrupolar wing in the region of the hexadecapolar U transitions in the fundamental band of $H_2$. To improve the fit between the observed and synthetic profiles we now propose the following lineshape function for the individual quadrupolar components (Lewis, 1983)

$$\tilde{\alpha}_{qm}(\nu) = A_q \int \tilde{\alpha}_{qm}(\nu)\, d\nu \times \frac{1}{1+(\Delta\nu/\delta_{q2})^2+(\Delta\nu/\delta_{q4})^4} \times \frac{1}{1+\exp(-hc\,\Delta\nu/kT)} \qquad (3.2)$$

where $\delta_{q2}$ is approximately the halfwidth at half height of the symmetrized line and is constant over the density range in which no diffusional narrowing sets in and $\delta_{q4}$ is a halfwidth parameter which mainly effects the high and low wavenumber tails of the line and is a function of the density of the gas. For clarification, the lineshapes described by Eqs. (3.1) and (3.2) are plotted in Fig. 9 with assumed parameters $\delta_{q2}=110\ cm^{-1}$ and $\delta_{q4}=230\ cm^{-1}$ for the $H_2$ gas at 295 K. The lineshape given by Eq. (3.1) is the solid curve and the one given by Eq. (3.2) is the dot-dash curve. It is clear that by using the $(\Delta\nu/\delta_{q4})^4$ term, the intensity of the line is reduced at the high and low wavenumbers with practically no change in the central section of the line.

The justification for the use of the $(\Delta\nu / \delta_{q4})^4$ term in Eq. 3.2 can be summarized as follows: An arbitrary lineshape can be expanded as a rational function. Also, the Lorentzian lineshape has been used in the past to produce an adequate fit of the experimental lineshape, over a small density range. It is therefore reasonable to seek a simple rational functional expression similar to the Lorentzian function. Lewis and Tjon (1978) have shown that the $(\Delta\nu / \delta_{q4})^4$ term will be the dominant asymptotic term for a hard repulsive force. While the lineshape with the $(\Delta\nu / \delta_{q4})^4$ term included in Eq. 3.2 is not exact, it should be a good approximation for the lines arising from the quadrupole-induced dipole moment, where the characteristic length scale for the induced dipole moment is greater than the length scale in which the radial motion of the colliding molecules

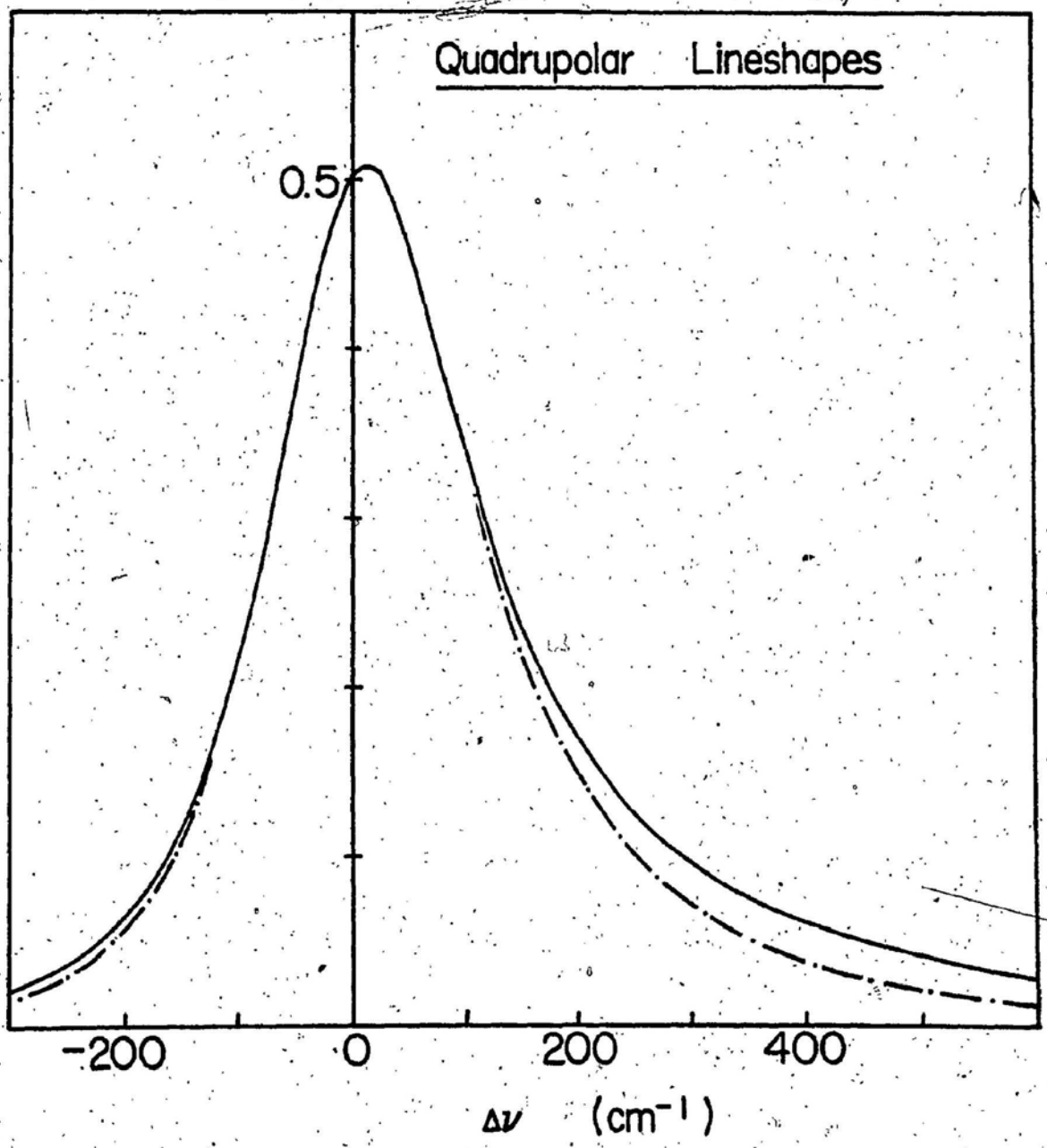


Fig. 9. A comparison of the collision-induced quadrupolar transition lineshapes. The solid line represents the observed lineshape given by Eq. (3.1) with $\delta_q$=110 $cm^{-1}$ and the dash-dot line represents the observed lineshape given by Eq. (3.2) with $\delta_{q2}$=110 $cm^{-1}$ and $\delta_{q4}$=230 $cm^{-1}$ at 295 K. The co-ordinate axis is in units of $A_q \int \tilde{\alpha}_{qm}(\nu) d\nu$.

reverses. Hence it is expected that the inclusion of the $(\Delta\nu / \delta_{q4})^4$ term should produce a reasonably good lineshape.

**(b) Intensities of Individual Lines**

The integrated absorption coefficient (in units of $cm^{-1}$ $amagat^{-2}$) for a given band due to quadrupolar induction and arising from binary collisions is expressed (Poll, 1971 and McKellar and Welsh, 1971) as

$$(1/\rho^2)\int\frac{\alpha(\nu)}{\nu}d\nu = \sum_m \int \bar{\alpha}_{qm}(\nu)\,d\nu \qquad (3.3)$$

$$= \frac{8\pi^3 e^2}{3hc} n_0^2 a_0^5 \left[\frac{a_0}{\sigma}\right]^5 J$$

$$\times \sum_{J_1=0}^{n}\sum_{J_2=0}^{n}\sum_{\frac{\Delta J_1}{2}=-1}^{1}\sum_{\frac{\Delta J_2}{2}=-1}^{1}\sum_{v'_1=0}^{N} X \,, \quad v'_2 = N - v'_1 \,; \qquad (3.4)$$

In this expression $\rho$ is the density of the gas in amagat units, e is the electron charge, $n_0$ is Loschmidt's number, $a_0$ is the first Bohr radius and the temperature-dependent dimensionless integral $J(T^*)$, where $T^* = kT/\epsilon$, represents the average dependence of the square of the induced dipole moment on the intermolecular separation R and is given (Van Kranendonk, 1958) by

$$J = 12\pi\int_0^\infty x^{-8} g(x) x^2 dx \,. \qquad (3.5)$$

Here $x = R/\sigma$ with $\sigma$ defined as the intermolecular separation when the intermolecular potential $V(\sigma) = 0$, and the pair correlation function of the gas at the low density limit, $g_0(x)$ is classically given by $\exp[-V^*(x)/T^*]$

with $V^*(x) = V(x)/\epsilon$, where $V(x)$ is assumed to be the Lennard-Jones intermolecular potential $V(x) = 4\epsilon(x^{-12} - x^{-6})$. Values of J and the appropriate quantum corrections to be applied to them have been recently reevaluated by Gibbs *et al.* (1977). The quantity X, representing a given transition is given by

$$X = P_{J_1} P_{J_2} [C(J_1\, 2J'_1; 00)^2 C(J_2\, 0J'_2; 00)^2$$

$$\times \langle 0J_1 | Q_1 | v'_1 J'_1 \rangle^2 \langle 0J_2 | \alpha_2 | v'_2 J'_2 \rangle^2 + Y/2\,] \qquad (3.6)$$

where $P_J$'s are the normalized Boltzmann factors (i.e., $\Sigma P_J = 1$) for the rotational level J and is given by

$$P_J = \frac{g_T(2J+1)\exp(-E_J/kT)}{\sum_J g_T(2J+1)\exp(-E_J/kT)} \qquad (3.7)$$

Here, the nuclear statistical weight factor $g_T$ is 1 and 3 for the even and odd J rotational states, respectively for $H_2$ and $E_J$ is the energy of the J th rotational level. For normal $H_2$ the conversion of ortho to para or vice versa is forbidden and the relation

$$\sum_{even J} P_J \Big/ \sum_{odd J} P_J = 1/3 \qquad (3.8)$$

is satisfied. In Eq. (3.6) subscripts 1 and 2 refer to the collision pair of molecules 1 and 2, respectively, the quantities $C(J\lambda J'; 00)$ with $\lambda = 0$ and 2 are the Clebsch-Gordan coefficients, and $\langle vJ|Q|v'J'\rangle$ and $\langle vJ|\alpha|v'J'\rangle$ with $v = 0$ in the present case are matrix elements of the quadrupole moment and the polarizability, respectively, of $H_2$ ( usually expressed in units of $ea_0^2$ and $a_0^3$, respectively).

The Y term in Eq. (3.6) accounts for the contribution of the anisotropy of the polarizability to the collision-induced absorption and is given by

$$Y = C(J_1 2J'_1;00)^2 C(J_2 2J'_2;00)^2 \left[\frac{2}{9}\left(\langle 0J_1|Q_1|v'_1J'_1\rangle^2 \langle 0J_2|\gamma_2|v'_2J'_2\rangle^2 + \langle 0J_2|Q_2|v'_2J'_2\rangle^2 \langle 0J_1|\gamma_1|v'_1J'_1\rangle^2\right) - \frac{4}{15}\langle 0J_1|Q_1|v'_1J'_1\rangle \times \langle 0J_2|\gamma_2|v'_2J'_2\rangle \langle 0J_2|Q_2|v'_2J'_2\rangle \langle 0J_1|\gamma_1|v'_1J'_1\rangle\right] , \quad (3.9)$$

where the $\langle 0J|\gamma|v'J'\rangle$ are matrix elements of the anisotropy of the polarizability. This term is small compared to X and contributes to purely anisotropic transitions in which both molecules of the collision pair change their rotational states; it also contributes a small amount to the transitions which mainly arise from the isotropic polarizability. In Eq. (3.4) the upper limit n of the first two summations is the maximum rotational state with any significant population of the molecules; the next two summations govern the selection rules for the quadrupolar induction mechanism (i.e., $\Delta J = -2(O)$, $0(Q)$ and $+2(S)$); and the final summation over $v'_1$ is taken up to a maximum value N with $v'_2$ having the constraint, $v'_2 = N - v'_1$. It is to be noted that N takes the values 0, 1, 2, ... etc. for the pure rotational, fundamental, first overtone bands, ... etc., respectively. A program written in HPL for a Hewlett-Packard model 9825A calculator uses Eq. (3.4) to calculate the integrated binary absorption coefficients $\int \tilde{\alpha}_{qm}(\nu)\,d\nu$, for all the individual quadrupolar transitions and is listed in Appendix A. Table 3-4 presents the transition intensities of $H_2$ in the first overtone region at 77, 201 and 295 K calculated with this program using the numerically calculated matrix elements of the quadrupole moment (Poll and Wolniewicz, 1978: Note that one-half of the numerical values were

TABLE 3-4 Transition Intensities of $H_2$ in the first overtone region

| Transition | Wavenumber ($cm^{-1}$) | Absolute Intensity ($cm^{-1}$ amagat$^{-2}$) | Relative Intensity | Relative Intensity (with 0.68 factor) |
|---|---|---|---|---|
| | | 77 K | | |
| $Q_2(1)$ | 8075.3 | .8678e-09 | .7416 | .7836 |
| $Q_2(0)+Q_0(0)$ | 8087.0 | .5537e-10 | .0473 | .0881 |
| $Q_1(1)+Q_1(1)$ | 8310.5 | .6073e-09 | .5190 | .9663 |
| $Q_1(1)+Q_1(0)$ | 8316.4 | .1958e-09 | .1673 | .3115 |
| $S_2(0)$ | 8406.4 | .6247e-09 | .5338 | .4616 |
| $Q_2(1)+S_0(0)$ | 8429.7 | .1468e-09 | .1255 | .2282 |
| $Q_2(0)+S_0(0)$ | 8441.4 | .4586e-10 | .0392 | .0730 |
| $S_2(1)$ | 8604.2 | .1170e-08 | 1.0000 | .8660 |
| $Q_1(1)+S_1(0)$ | 8653.1 | .4091e-09 | .3496 | .6509 |
| $Q_1(0)+S_1(0)$ | 8659.0 | .1285e-09 | .1098 | .2045 |
| $Q_2(1)+S_0(1)$ | 8662.3 | .2684e-09 | .2294 | .4171 |
| $Q_2(0)+S_0(1)$ | 8674.0 | .8382e-10 | .0716 | .1334 |
| $Q_1(1)+S_1(1)$ | 8868.2 | .6285e-09 | .5371 | 1.0000 |
| $Q_1(0)+S_1(1)$ | 8874.1 | .1970e-09 | .1683 | .3135 |
| $S_1(1)+S_0(0)$ | 8958.6 | .1718e-10 | .0147 | .0168 |
| $S_2(0)+S_0(1)$ | 8993.4 | .1493e-10 | .0128 | .0139 |
| $S_2(0)+S_1(0)$ | 8995.7 | .6813e-11 | .0058 | .0108 |
| $S_2(1)+S_1(1)$ | 9191.2 | .3152e-10 | .0269 | .0308 |
| $S_2(1)+S_0(0)$ | 9210.7 | .2177e-10 | .0186 | .0346 |
| $S_1(1)+S_1(1)$ | 9425.8 | .1733e-10 | .0148 | .0276 |

TABLE 3-4 Transition Intensities of $H_2$ in the first overtone region (cont'd)

| Transition | Wavenumber ($cm^{-1}$) | Absolute Intensity ($cm^{-1}$ amagat$^{-2}$) | Relative Intensity | Relative Intensity (with 0.68 factor) |
|---|---|---|---|---|
| | | 201 K | | |
| $O_2(3)$ | 7488.3 | .1304e-10 | .0108 | .0096 |
| $O_0^2(2)+Q_2(1)$ | 7720.9 | .8659e-11 | .0071 | .0135 |
| $Q_1(1)+O_1^2(3)$ | 7723.5 | .1984e-10 | .0163 | .0316 |
| $O_2^2(2)$ | 7732.6 | .3132e-10 | .0258 | .0231 |
| $Q_1^2(1)+O_1(2)$ | 7962.1 | .3787e-10 | .0312 | .0603 |
| $Q_1(0)+O_1^2(2)$ | 7968.0 | .8788e-11 | .0072 | .0140 |
| $Q_2(3)$ | 8017.2 | .2405e-10 | .0198 | .0234 |
| $Q_2^2(2)$ | 8052.0 | .6942e-10 | .0572 | .0667 |
| $Q_2^2(1)$ | 8075.3 | .9092e-09 | .7492 | .8275 |
| $Q_2^2(0)+Q_0(0)$ | 8087.0 | .4510e-10 | .0372 | .0718 |
| $Q_1(3)+Q_1^2(1)$ | 8281.1 | .3557e-10 | .0293 | .0566 |
| $Q_1(2)+Q_1^2(1)$ | 8298.7 | .1017e-09 | .0838 | .1619 |
| $Q_1(2)+Q_1^2(0)$ | 8304.6 | .1021e-10 | .0084 | .0162 |
| $Q_1(1)+Q_1^2(1)$ | 8310.5 | .6073e-09 | .5004 | .9663 |
| $Q_1(1)+Q_1^2(0)$ | 8316.4 | .1459e-09 | .1202 | .2322 |
| $Q_2(2)+S_0(0)$ | 8406.4 | .1067e-10 | .0088 | .0167 |
| $S_2^2(0)$ | 8406.4 | .4828e-09 | .3978 | .3568 |
| $Q_2^2(1)+S_0(0)$ | 8429.7 | .1094e-09 | .0902 | .1701 |
| $Q_2(0)+S_0^2(0)$ | 8441.4 | .2547e-10 | .0210 | .0405 |
| $S_2^2(1)$ | 8604.2 | .1214e-08 | 1.0000 | .8984 |
| $Q_2^2(3)+S_0(1)$ | 8604.2 | .9507e-11 | .0078 | .0149 |
| $Q_1^2(3)+S_1(1)$ | 8623.7 | .1062e-10 | .0088 | .0169 |
| $Q_2(2)+S_0^2(1)$ | 8639.0 | .2616e-10 | .0216 | .0409 |
| $Q_1^2(2)+S_1^2(0)$ | 8641.3 | .2952e-10 | .0243 | .0470 |
| $Q_1(1)+S_1^2(0)$ | 8653.1 | .3049e-09 | .2512 | .4852 |
| $Q_1(0)+S_1^2(0)$ | 8659.0 | .7140e-10 | .0588 | .1136 |
| $Q_2^2(1)+S_0(1)$ | 8662.8 | .2684e-09 | .2212 | .4171 |
| $Q_2^2(0)+S_0^2(1)$ | 8674.0 | .6247e-10 | .0515 | .0994 |
| $S_2^2(2)$ | 8785.5 | .1034e-09 | .0852 | .0767 |
| $Q_1^2(3)+S_1(1)$ | 8838.8 | .2187e-10 | .0180 | .0348 |
| $Q_1^2(2)+S_1^2(1)$ | 8856.4 | .6081e-10 | .0501 | .0968 |
| $Q_1(1)+S_1^2(1)$ | 8868.2 | .6284e-09 | .5178 | 1.0000 |
| $Q_1(0)+S_1^2(1)$ | 8874.1 | .1468e-09 | .1210 | .2336 |
| $Q_2(1)+S_0(2)$ | 8889.7 | .2277e-10 | .0188 | .0354 |

TABLE 3-4 Transition Intensities of $H_2$ in the first overtone region (cont'd)

| Transition | Wavenumber ($cm^{-1}$) | Absolute intensity ($cm^{-1}$ amagat$^{-2}$) | Relative intensity | Relative intensity (with 0.68 factor) |
|---|---|---|---|---|
| $S_2(3)$ | 8948.6 | .3435e-10 | .0283 | .0255 |
| $S_2(1) + S_0(0)$ | 8958.6 | .1280e-10 | .0105 | .0125 |
| $S_2(0) + S_0(1)$ | 8993.4 | .1113e-10 | .0092 | .0104 |
| $Q_1(1) + S_1(2)$ | 9072.3 | .4408e-10 | .0363 | .0701 |
| $Q_1(0) + S_1(2)$ | 9078.2 | .1027e-10 | .0085 | .0163 |
| $Q_2(1) + S_0(3)$ | 9109.9 | .7672e-11 | .0063 | .0119 |
| $S_2(1) + S_0(1)$ | 9191.2 | .3152e-10 | .0260 | .0308 |
| $S_1(1) + S_1(0)$ | 9210.7 | .1623e-10 | .0134 | .0258 |
| $Q_1(1) + S_1(3)$ | 9263.7 | .1206e-10 | .0099 | .0192 |
| $S_1(1) + S_1(1)$ | 9425.8 | .1733e-10 | .0143 | .0276 |

TABLE 3-4 Transition Intensities of $H_2$ in the first overtone region (cont'd)

| Transition | Wavenumber | Absolute Intensity | Relative Intensity | Relative Intensity (with 0.68 factor) |
|---|---|---|---|---|
| | ($cm^{-1}$) | ($cm^{-1}$ amagat$^{-2}$) | | |
| | | 295 K | | |
| $Q_2(1)+O_0(3)$ | 7488.3 | .1375e-10 | .0115 | .0238 |
| $O_2(3)$ | 7488.3 | .4899e-10 | .0410 | .0402 |
| $Q_1(3)+O_1(3)$ | 7694.1 | .9003e-11 | .0075 | .0160 |
| $Q_1(2)+O_1(3)$ | 7711.7 | .1176e-10 | .0098 | .0209 |
| $Q_2(1)+O_0(2)$ | 7720.9 | .1392e-10 | .0116 | .0241 |
| $Q_1(1)+O_1(3)$ | 7723.5 | .6791e-10 | .0568 | .1205 |
| $Q_1(0)+O_1(3)$ | 7729.4 | .1259e-10 | .0105 | .0223 |
| $O_2(2)$ | 7732.6 | .5528e-10 | .0463 | .0453 |
| $Q_1(3)+O_1(2)$ | 7932.7 | .8074e-11 | .0068 | .0143 |
| $Q_1(2)+O_1(2)$ | 7950.3 | .1055e-10 | .0088 | .0187 |
| $Q_1(1)+O_1(2)$ | 7962.1 | .6091e-10 | .0510 | .1080 |
| $Q_1(0)+O_1(2)$ | 7968.0 | .1129e-10 | .0094 | .0200 |
| $Q_2(3)$ | 8017.2 | .9073e-10 | .0759 | .0987 |
| $Q_2(2)$ | 8052.0 | .1230e-09 | .1030 | .1322 |
| $Q_2(1)$ | 8075.3 | .8980e-09 | .7516 | .9135 |
| $Q_2(0)+Q_0(J)$ | 8087.0 | .3606e-10 | .0302 | .0640 |
| $Q_1(3)+Q_1(3)$ | 8251.8 | .6529e-11 | .0055 | .0116 |
| $Q_1(3)+Q_1(2)$ | 8269.3 | .1768e-10 | .0148 | .0314 |
| $Q_1(3)+Q_1(1)$ | 8281.1 | .1217e-09 | .1019 | .2159 |
| $Q_1(2)+Q_1(2)$ | 8286.9 | .1195e-10 | .0100 | .0212 |
| $Q_1(3)+Q_1(1)$ | 8287.1 | .9352e-11 | .0078 | .0166 |
| $Q_1(2)+Q_1(1)$ | 8298.7 | .1636e-09 | .1369 | .2902 |
| $Q_1(2)+Q_1(0)$ | 8304.6 | .1312e-10 | .0110 | .0233 |
| $Q_1(1)+Q_1(1)$ | 8310.5 | .5447e-09 | .4559 | .9663 |
| $Q_1(1)+Q_1(0)$ | 8316.4 | .1046e-09 | .0875 | .1855 |
| $Q_2(3)+S_0(0)$ | 8371.6 | .1060e-10 | .0089 | .0185 |
| $Q_2(2)+S_0(0)$ | 8406.4 | .1371e-10 | .0115 | .0239 |
| $S_2(0)$ | 8406.4 | .3797e-09 | .3178 | .3129 |
| $Q_2(1)+S_0(0)$ | 8429.7 | .7842e-10 | .0656 | .1359 |
| $Q_2(0)+S_0(0)$ | 8441.4 | .1458e-10 | .0122 | .0259 |
| $S_2(1)$ | 8604.2 | .1195e-08 | 1.0000 | .9861 |
| $Q_2(3)+S_0(1)$ | 8604.2 | .3254e-10 | .0272 | .0568 |
| $Q_1(3)+S_1(0)$ | 8623.7 | .2904e-10 | .0243 | .0515 |
| $Q_2(2)+S_0(1)$ | 8639.0 | .4208e-10 | .0352 | .0734 |
| $Q_1(2)+S_1(0)$ | 8641.3 | .3793e-10 | .0318 | .0673 |

TABLE 3-4 Transition Intensities of $H_2$ in the first overtone region (cont'd)

| Transition | Wavenumber ($cm^{-1}$) | Absolute Intensity ($cm^{-1}$ amagat$^{-2}$) | Relative Intensity | Relative Intensity (with 0.68 factor) |
|---|---|---|---|---|
| $Q_1(1)+S_1(0)$ | 8653.1 | .2185e-09 | .1829 | .3876 |
| $Q_1(0)+S_1(0)$ | 8659.0 | .4088e-10 | .0342 | .0725 |
| $Q_2(1)+S_0(1)$ | 8662.3 | .2408e-09 | .2015 | .4171 |
| $Q_2(0)+S_0(1)$ | 8674.0 | .4477e-10 | .0375 | .0794 |
| $S_2(2)$ | 8785.5 | .1825e-09 | .1528 | .1509 |
| $Q_1(3)+S_1(1)$ | 8838.8 | .7486e-10 | .0627 | .1328 |
| $Q_1(2)+S_1(1)$ | 8856.4 | .9780e-10 | .0819 | .1735 |
| $Q_2(2)+S_0(2)$ | 8866.4 | .6398e-11 | .0054 | .0111 |
| $Q_1(1)+S_1(1)$ | 8868.2 | .5637e-09 | .4718 | 1.0000 |
| $Q_1(0)+S_1(1)$ | 8874.1 | .1052e-09 | .0881 | .1867 |
| $Q_2(1)+S_0(2)$ | 8889.7 | .3662e-10 | .0306 | .0634 |
| $Q_2(0)+S_0(2)$ | 8901.4 | .6806e-11 | .0057 | .0121 |
| $S_2(3)$ | 8948.6 | .1290e-09 | .1080 | .1069 |
| $Q_1(3)+S_1(2)$ | 9042.9 | .9403e-11 | .0079 | .0167 |
| $Q_1(2)+S_1(2)$ | 9060.5 | .1229e-10 | .0103 | .0218 |
| $Q_1(1)+S_1(2)$ | 9072.3 | .7089e-10 | .0593 | .1257 |
| $Q_1(0)+S_1(2)$ | 9078.2 | .1319e-10 | .0110 | .0234 |
| $Q_2(1)+S_0(3)$ | 9109.9 | .2626e-10 | .0220 | .0455 |
| $S_2(1)+S_0(1)$ | 9191.2 | .2828e-10 | .0237 | .0308 |
| $S_1(1)+S_1(0)$ | 9210.7 | .1163e-10 | .0097 | .0206 |
| $Q_1(2)+S_1(3)$ | 9251.9 | .7148e-11 | .0060 | .0127 |
| $Q_1(1)+S_1(3)$ | 9263.7 | .4129e-10 | .0346 | .0732 |
| $Q_1(0)+S_1(3)$ | 9269.6 | .7650e-11 | .0064 | .0136 |
| $S_1(1)+S_1(1)$ | 9425.8 | .1554e-10 | .0130 | .0276 |

used because of the definition adopted by these authors), and of the polarizability and the anisotropy of the polarizability (Kolos and Wolniewicz, 1967 and Poll, 1983). The values calculated numerically by Poll and Wolniewicz for the $H_2$ matrix elements are claimed to be accurate to 0.1%, 0.2% and 0.3% for the 0-1, 0-2 and 0-3 transitions respectively. The other matrix elements are expected to have similar errors. The matrix elements of the polarizability and the anisotropy of the polarizability are listed in Appendix C.

**(c) Method of Profile Analysis and Results**

The aim of the profile analysis is to obtain the best possible agreement between the experimental absorption profiles and the parameterized synthetic profile computed from the superposition of the individual absorption coefficients, $\sum_m \bar{\alpha}_{qm}(\nu)$ [$= (2.303/l\nu) \log_{10}(I_0(\nu)/I(\nu))$] which are given by Eq. (3.2). The two halfwidth parameters, $\delta_{q2}$ and $\delta_{q4}$, and the normalization factor $A_q$ were adjustable parameters in a non-linear least-squares fitting program written for the Hewlett-Packard model 9825A calculator and listed in Appendix B. Adjustment of the factor $A_q$ allowed a degree of freedom for the heights of the transition intensities. However, for Eq. (3.2) to have correct absolute intensity $A_q$ should be the reciprocal of the area of the lineshape with height 0.5 at $\nu_m$. The synthetic profile was fitted to the experimental absorption profile using these three parameters with the criterion that the sum of the squares of the residuals of $\log_{10}[I_0(\nu)/I(\nu)]$ be a minimum.

A representative fit for $H_2$ in the first overtone region at 77 K is shown in Fig. 10. As is evident there are large discrepancies between

the intensities of the peaks of the observed and calculated profiles. For clarification, the same experimental absorption profile is compared with an absolute synthetic profile and both are shown in Fig. 11. The calculated profile is the solid curve and uses the same fitted halfwidth parameters obtained from the fit shown in Fig. 10, however $A_q$ now takes its actual normalization value so that the intensities are in fact absolute. An examination of Fig. 11 reveals a trend between transitions of the pure overtone ($\Delta v = 2$) and those in which both molecules of the colliding pair undergo a fundamental ($\Delta v = 1$) transition. Specifically, the calculated intensities for transitions such as $Q_2(1)$, $S_2(0)$, $S_2(1)$, $Q_2(0)+S_0(0)$, $Q_2(1)+S_0(1)$ and $S_2(1)+S_0(1)$ are all too strong. A similar trend can be seen in the comparison between the experimental absorption profiles and the fitted synthetic profiles of $H_2$ at 201 and 295 K in Figs. 12 and 13, respectively; the calculated intensities of the transitions involving $\Delta v = 2$ transitions are also too high relative to the transitions involving $\Delta v = 1$. This trend was evident in all of the observed spectra. Similar observations have been made in the collision-induced absorption profiles of deuterium in the first overtone region (Gillard, 1983) under experimental conditions which are similar to those in the present work. This type of discrepancy is not evident in the collision induced fundamental bands of $H_2$ or $D_2$ because in these cases all transitions involve $\Delta v = 0$ and 1.

In order to improve the fit between the experimental and the synthetic profiles of $H_2$ in the first overtone region, the intensities of the $\Delta v = 2$ transitions must be reduced. Watanabe (1971) has suggested that these discrepancies can be explained in terms of a different density dependence for single and double transitions. This suggestion however seems to be

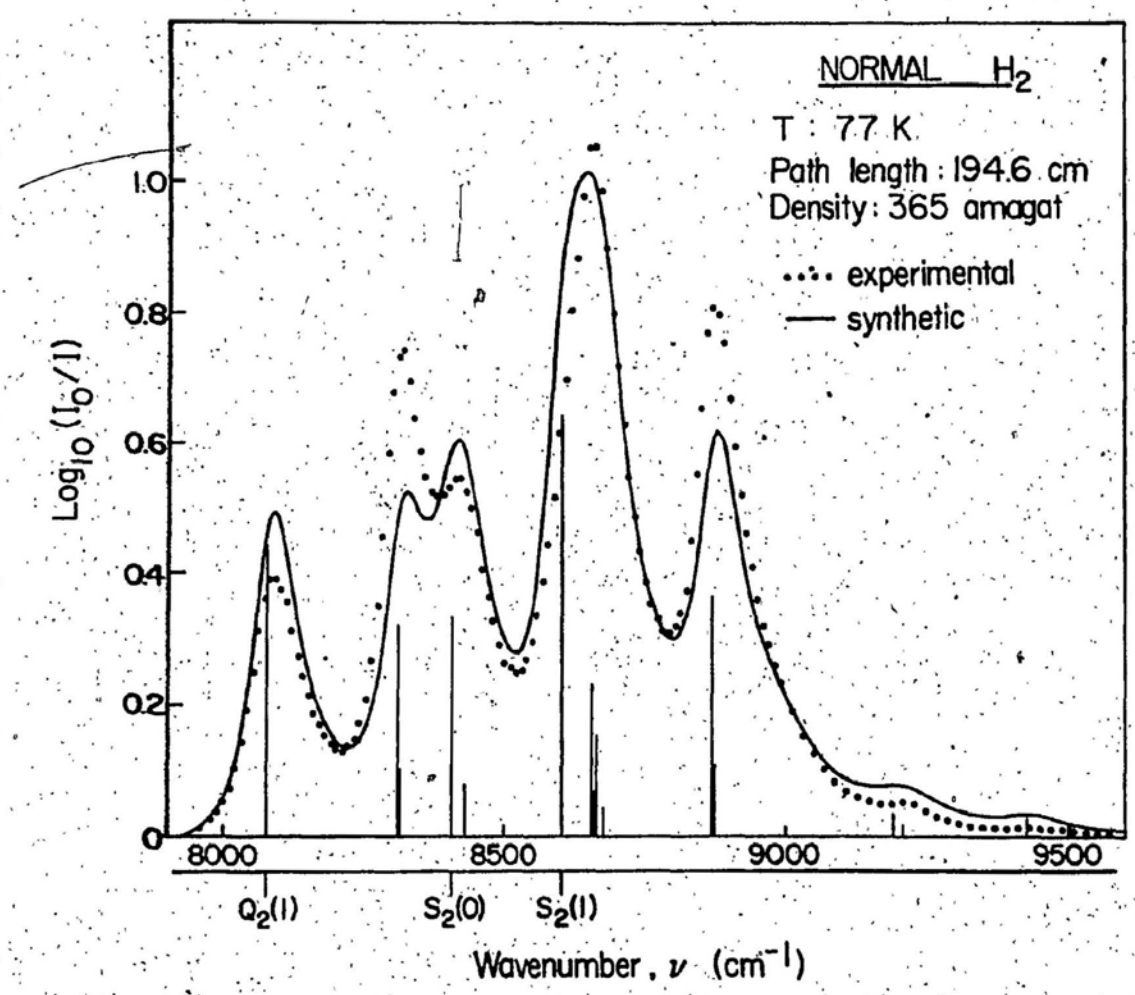


Fig. 10. Analysis of an absorption profile of normal $H_2$ in the pure gas at 77 K and 365 amagat in the first overtone region. The dotted curve is experimental; the solid curve, which is the sum of all the individual quadrupolar components, is a fitted theoretical profile obtained by using the relative intensities calculated with the available matrix elements $\langle|Q|\rangle$, $\langle|\alpha|\rangle$ and $\langle|\gamma|\rangle$ and the halfwidth parameters $\delta_{q2}=51.9\ cm^{-1}$ and $\delta_{q4}=226\ cm^{-1}$.

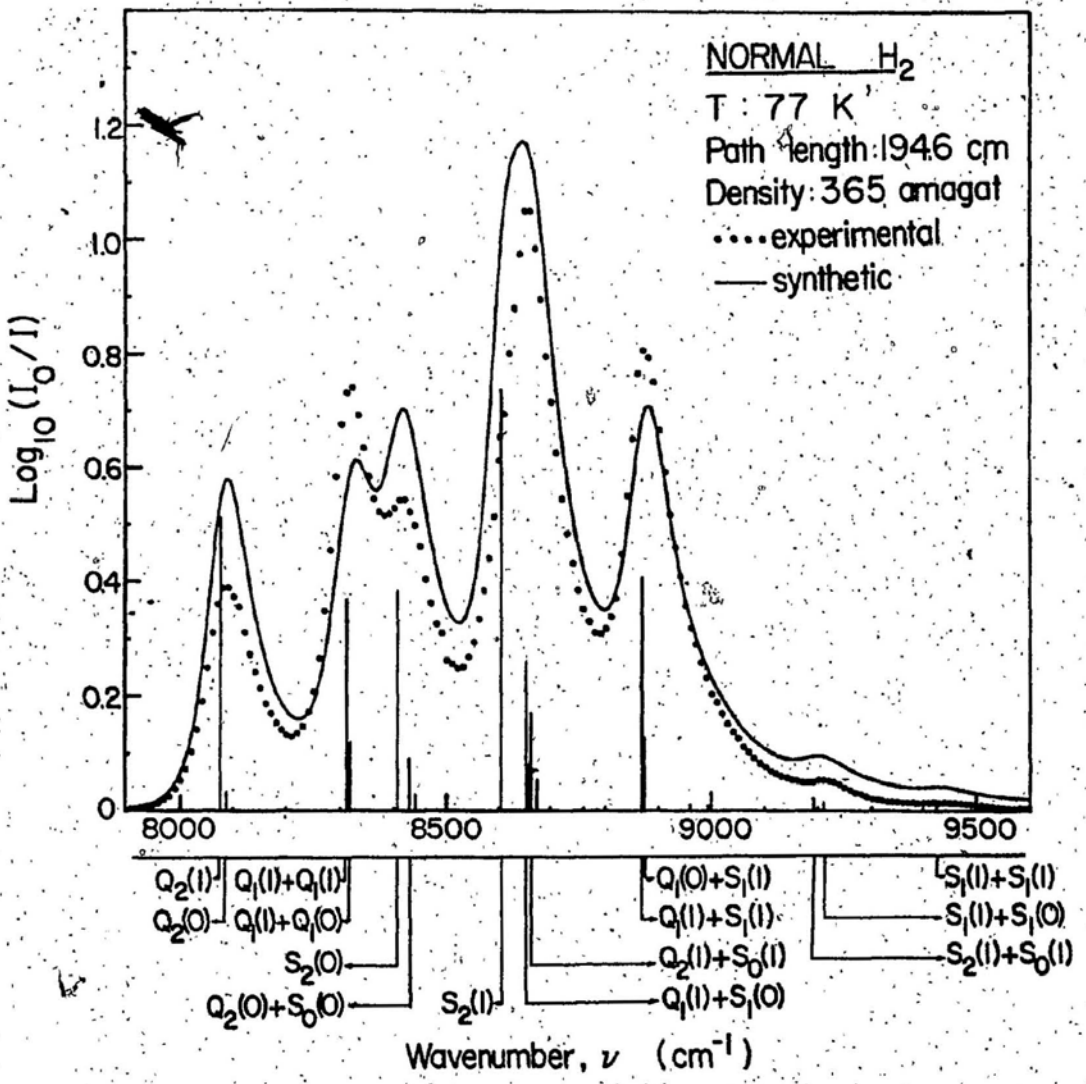


Fig. 11. Analysis of an absorption profile of normal $H_2$ in the pure gas at 77 K and 365 amagat in the first overtone region. The dotted curve, which is the same as the one shown in Fig. 10, is experimental; the solid curve, which is the sum of all the individual quadrupolar components, is a theoretical profile obtained by using the absolute intensities calculated with the available matrix elements and the halfwidths obtained from the fit shown in Fig. 10.

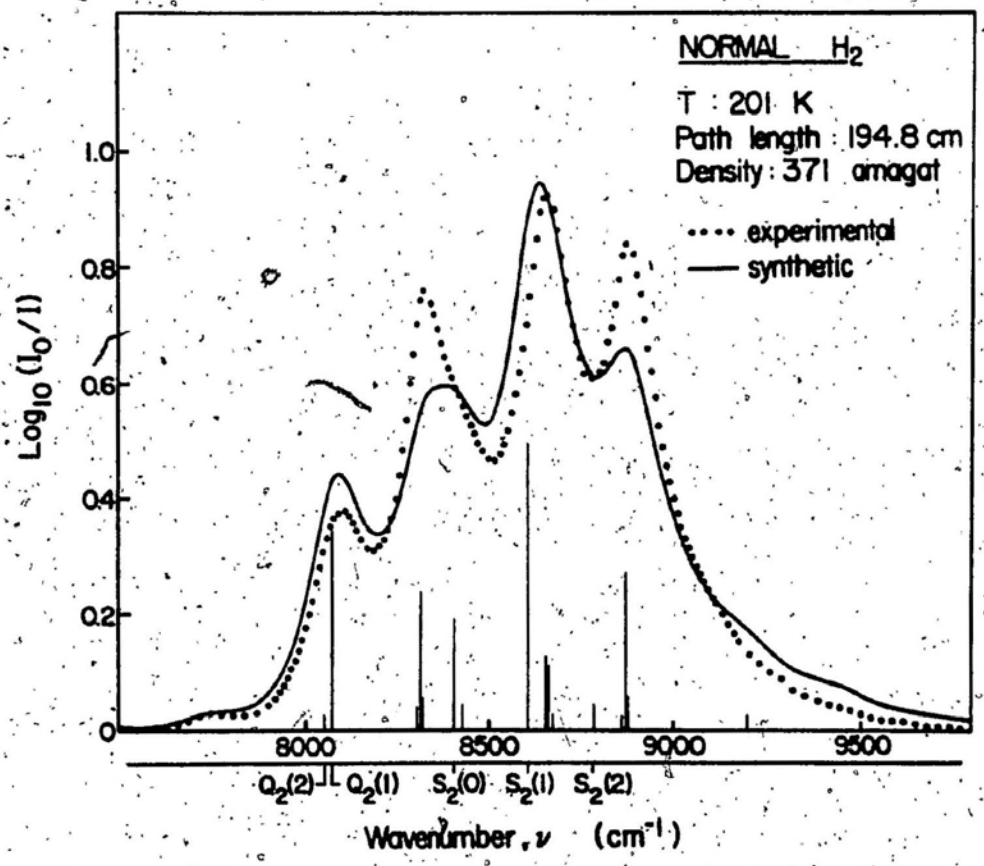


Fig. 12. Analysis of an absorption profile of normal $H_2$ in the pure gas at 201 K and 371 amagat in the first overtone region. The dotted curve is experimental; the solid curve is a fitted theoretical profile obtained by using the relative intensities calculated with the available matrix elements and the halfwidth parameters $\delta_{q2}$=97.8 $cm^{-1}$ and $\delta_{q4}$=281 $cm^{-1}$.

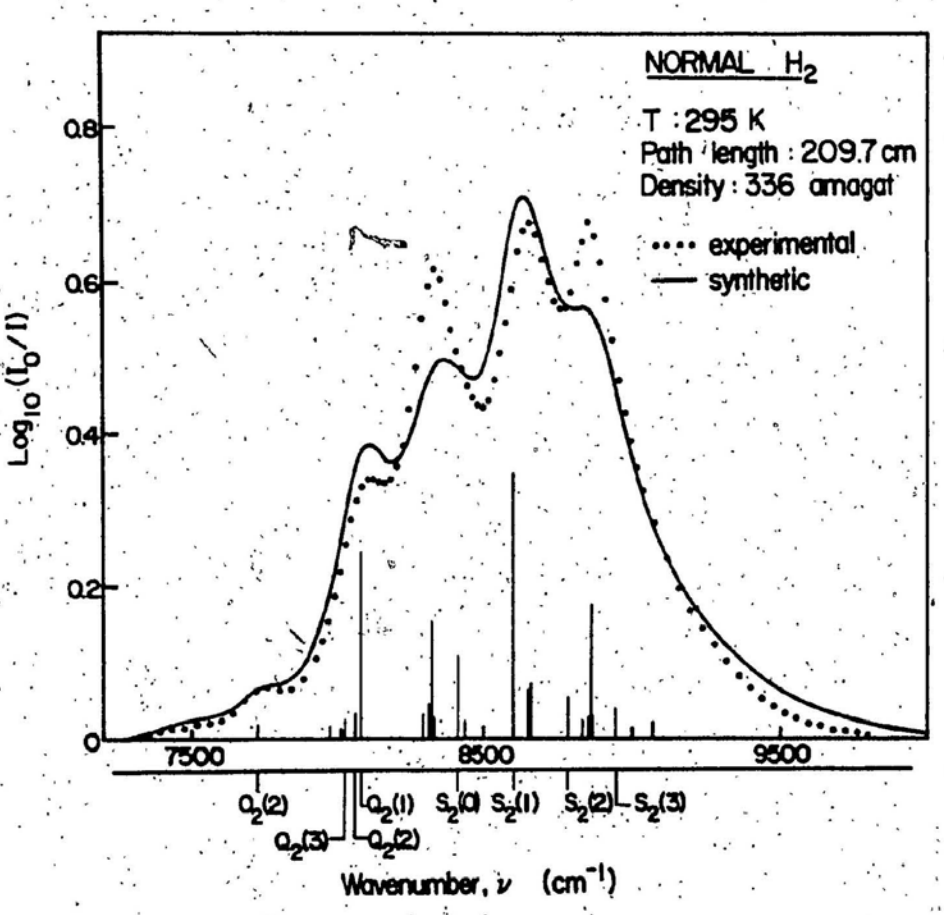


Fig. 13. Analysis of an absorption profile of normal $H_2$ in the pure gas at 295 K and 336 amagat in the first overtone region. The dotted curve is experimental; the solid curve is a fitted theoretical profile obtained by using the relative intensities calculated with the available matrix elements and the halfwidth parameters $\delta_{q2}$=127 $cm^{-1}$ and $\delta_{q4}$=278 $cm^{-1}$.

inadequate to explain the transitions such as $Q_2(J)+S_0(J)$ which are also too intense (see Fig. 11). As seen in chapter 4 the calculated intensity of the $S_2(J)+S_0(J)$ transition is also too intense relative to the corresponding experimental intensity, as compared to the case of $S_1(J)+S_1(J)$. Thus it appears that the calculated intensities of the $\Delta v=2$ transitions, no matter whether they are single or double, are too high compared to the corresponding experimental intensities. Consideration of Eq. (3.6) indicates that the best way to affect all $\Delta v=2$ transitions in a similar manner is through the quadrupole matrix elements since they occur in both isotropic and anisotropic contributions. Also, adjustment of the isotropic polarizability matrix elements is ruled out because of the restriction of the Clebsch-Gordan coefficient $C(J0J';00)$ governing these matrix elements. Any adjustment would not affect transitions in which there is a change in the rotational state of the molecule associated with the polarizability matrix elements since the Clebsch-Gordan coefficient is zero. Therefore different $\Delta v=2$ transitions would respond differently depending on the change in rotational states. It was therefore decided to reduce the values of the quadrupole moment matrix elements for the $\Delta v=2$ transitions systematically until a better agreement was obtained between the experimental profiles and the fitted theoretical profiles. Transitions involving $\Delta v=2$ are also accompanied by a $\Delta v=0$ change in the collision partner. Therefore the overall transition intensity can be reduced by changing either the $\Delta v=2$ or the $\Delta v=0$ quadrupole matrix elements. However, in the analysis of the collision-induced pure rotational ($\Delta v=0$) spectra of hydrogen, Brachet *et al.* (1983) have shown that the calculated absorption agrees satisfactorily with the experimental absorption. Therefore

in the present work the intensities of the lines involving $\Delta v = 2$ were adjusted by reducing the values of the $\Delta v = 2$ quadrupole moment matrix elements. The values of these matrix elements were reduced systematically in steps and each set was used to calculate new synthetic profiles for the collision-induced first overtone region. These were least squares fitted to the experimental spectra obtained at all the three temperatures and the best adjustment factor for the matrix elements was determined from the fits using the least squares criterion for the differences. Finally, a reduction of the $\Delta v = 2$ quadrupole matrix elements by a factor 0.68 gave very good agreement between the experimental profiles and the fitted synthetic profiles thus obtained. Results of the new analysis for the three profiles shown earlier in Figs. 10, 12 and 13, with the adjustment factor for the $\Delta v = 2$ quadrupole moment matrix elements are shown in Figs. 14, 15 and 16. The agreement between the synthetic and experimental spectra is very much improved in all the cases. A low density (161 amagat) experimental profile at 77 K was fitted to a synthetic profile using the 0.68 adjustment factor for the $\Delta v = 2$ quadrupole matrix elements and is shown in Fig. 17. The agreement between the observed and synthetic profiles is again very good. Therefore, a variation in density has very little effect on the observed discrepancy of the $\Delta v = 2$ transitions. The results of the new analysis of the experimental absorption profiles at all recorded gas densities using the adjusted quadrupole matrix elements are presented in Table 3-5. The values of $\delta_{q2}$ agree favorably with the values 53, 86 and 107 $cm^{-1}$ for the quadrupolar halfwidth parameter obtained in the analysis of the collision-induced fundamental band of $H_2$ at 77, 196 and 298 K, respectively (Reddy *et al.*, 1977). The halfwidths $\delta_{q2}$ have been plotted

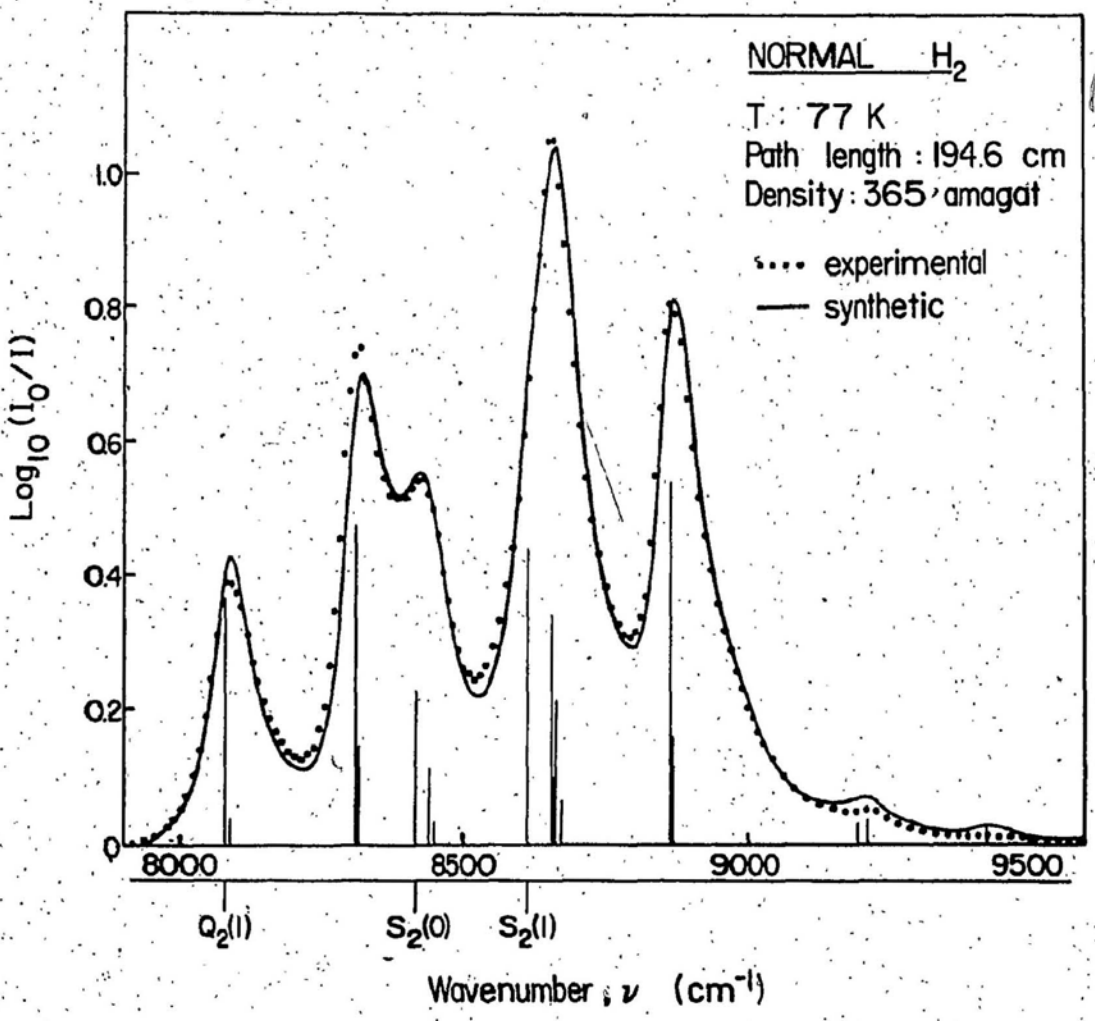


Fig. 14. Analysis of an absorption profile of normal $H_2$ in the pure gas at 77 K and 365 amagat in the first overtone region. The dotted curve, which is the same as the one shown in Fig. 10, is experimental. The solid curve is a fitted theoretical profile obtained by using the relative intensities calculated with the $\Delta v=2$ quadrupole moment matrix elements multiplied by the adjustment factor of 0.68 and the values of $\langle|\alpha|\rangle$ and $\langle|\gamma|\rangle$ and the halfwidth parameters $\delta_{q2}=48.2\ cm^{-1}$ and $\delta_{q4}=167\ cm^{-1}$.

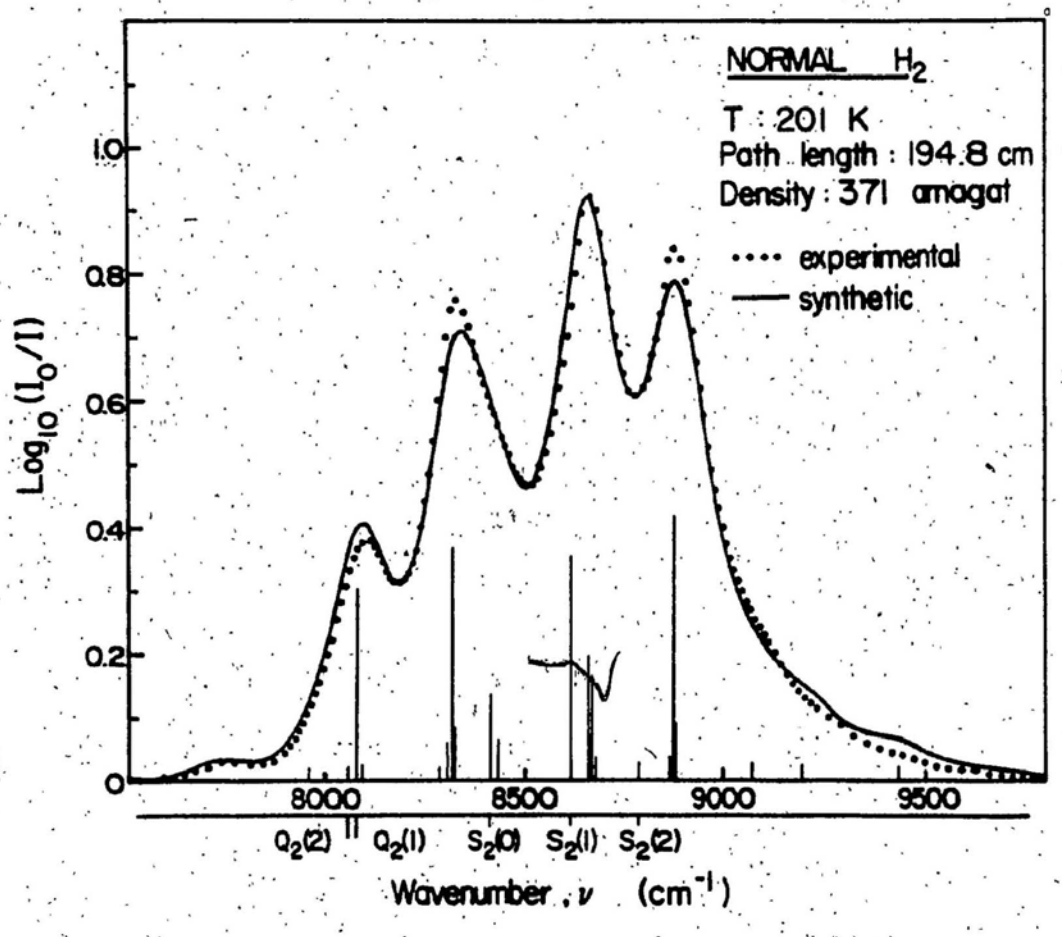


Fig. 15. Analysis of an absorption profile of normal $H_2$ in the pure gas at 201 K and 371 amagat in the first overtone region. The dotted curve, which is the same as the one shown in Fig. 12, is experimental. The solid curve is a fitted theoretical profile obtained by using the relative intensities calculated with the $\Delta v=2$ quadrupole moment matrix elements multiplied by the adjustment factor of 0.68 and the values of $<|\alpha|>$ and $<|\gamma|>$ and the halfwidth parameters $\delta_{q2}=87.4\ cm^{-1}$ and $\delta_{q4}=229\ cm^{-1}$.

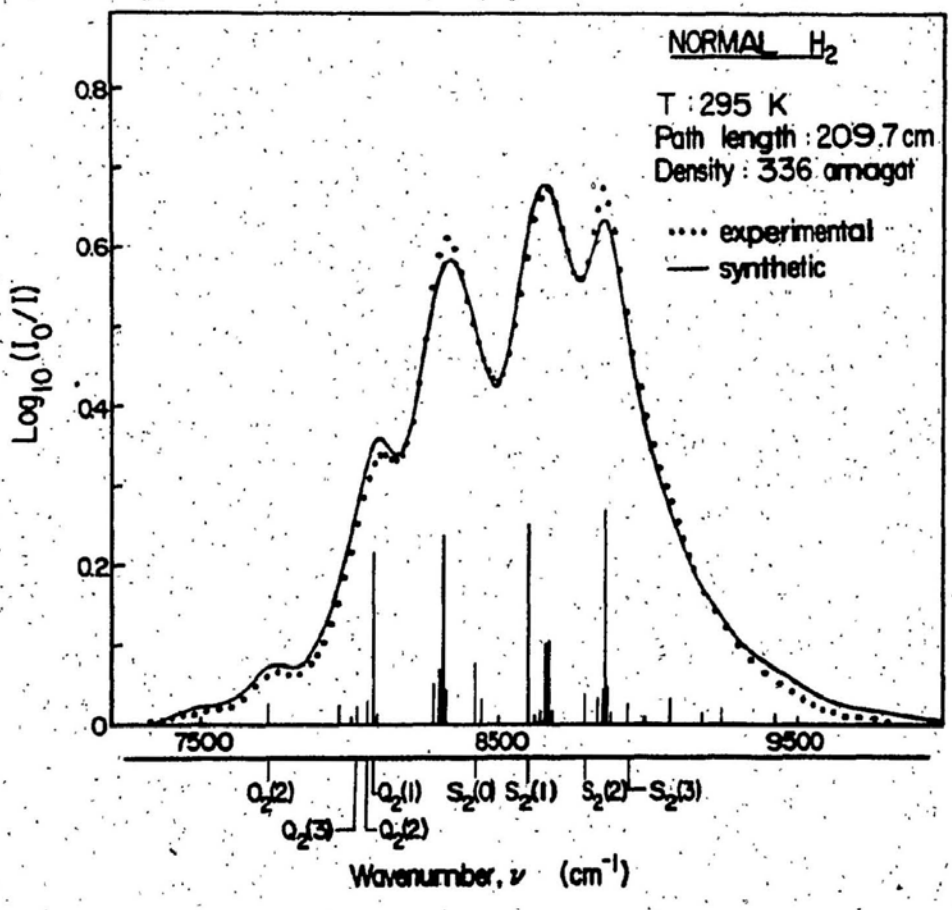


Fig. 16. Analysis of an absorption profile of normal $H_2$ in the pure gas at 295 K and 336 amagat in the first overtone region. The dotted curve, which is the same as the one shown in Fig. 13, is experimental. The solid curve is the fitted theoretical profile obtained by using the relative intensities calculated with the $\Delta v=2$ quadrupole moment matrix elements multiplied by the adjustment factor of 0.68 and the values of $\langle|\alpha|\rangle$ and $\langle|\gamma|\rangle$ and the halfwidth parameters $\delta_{q2}=110\ cm^{-1}$ and $\delta_{q4}=245\ cm^{-1}$.

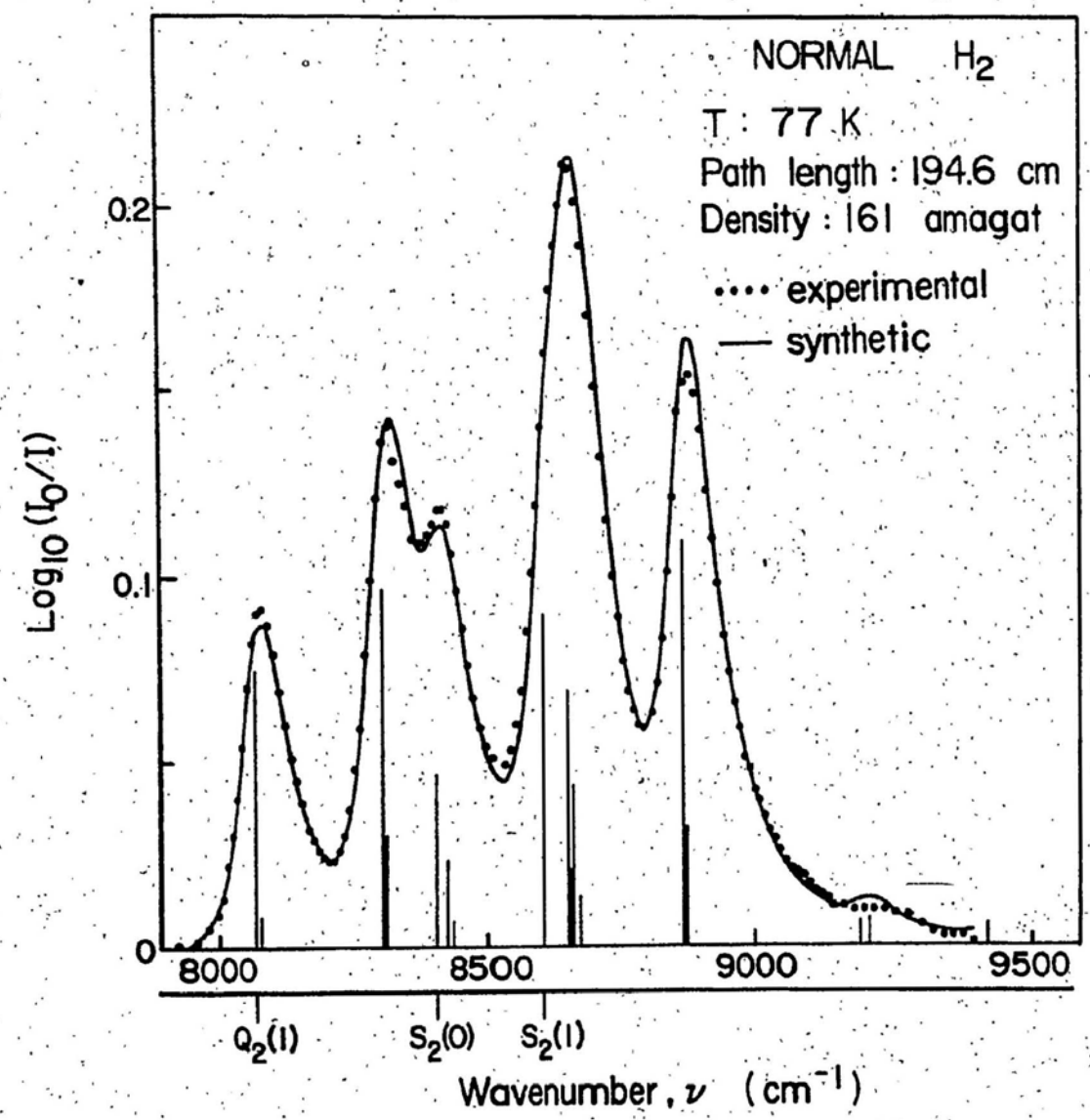


Fig. 17. Analysis of a lower density absorption profile of normal $H_2$ in the pure gas at 77 K and 161 amagat in the first overtone region. The dotted curve is experimental. The solid curve is the fitted theoretical profile obtained by using the relative intensities calculated with the $\Delta v=2$ quadrupole moment matrix elements multiplied by the adjustment factor of 0.68 and the values of $\langle|\alpha|\rangle$ and $\langle|\gamma|\rangle$ and the halfwidth parameters $\delta_{q2}=49.3\ cm^{-1}$ and $\delta_{q4}=148\ cm^{-1}$.

against the square root of the temperature in Fig. 18 which shows the straight line agreement required by the kinetic nature of the linewidths. A linear fit to the points gives the relation $\delta_{q2}=6.4T^{1/2}$. The corresponding relation for the fundamental band of $H_2$ (Reddy *et al.*, 1977) is $\delta_{q2}=6.16T^{1/2}$ where the difference in the constant coefficients results from the introduction of the term $(\Delta\nu/\delta_{q4})^4$ in the denominator of the dispersion lineshape in the present study. Over the range of the gas densities studied, the parameter $\delta_{q2}$ remains constant, however the parameter $\delta_{q4}$ shows a definite increase with the density as shown in Fig. 19. Thus the central portion of the lineshape remains the same while the tail ends of the lineshape become broader with density. This increase in the width of the base of the lineshape is in general agreement with the prediction of Lewis and Tjon (1978) who studied computer-simulated collision-induced absorption in a two-dimensional Lorentz gas. They argue that the lineshape consists of two components, a narrow Lorentzian component and a broad component. In the notation used in this thesis, $\delta_{q2}$ is the characteristic halfwidth parameter representing the narrow Lorentzian component and $\delta_{q4}$ characterizes the broad component.

It is also interesting to note that the 0.68 adjustment factor for the $\Delta v=2$ quadrupole moment matrix elements is also the same for the collision-induced absorption profiles of deuterium in the first overtone region (Gillard, 1983). Figure 20 illustrates the good agreement between the experimental profile of $D_2$ at 77 K in the first overtone region and the synthetic profile using the adjustment factor of 0.68 for the $\Delta v=2$ quadrupole moment matrix elements. It should be noted that although the relative intensities of the transitions have been improved, there is still a

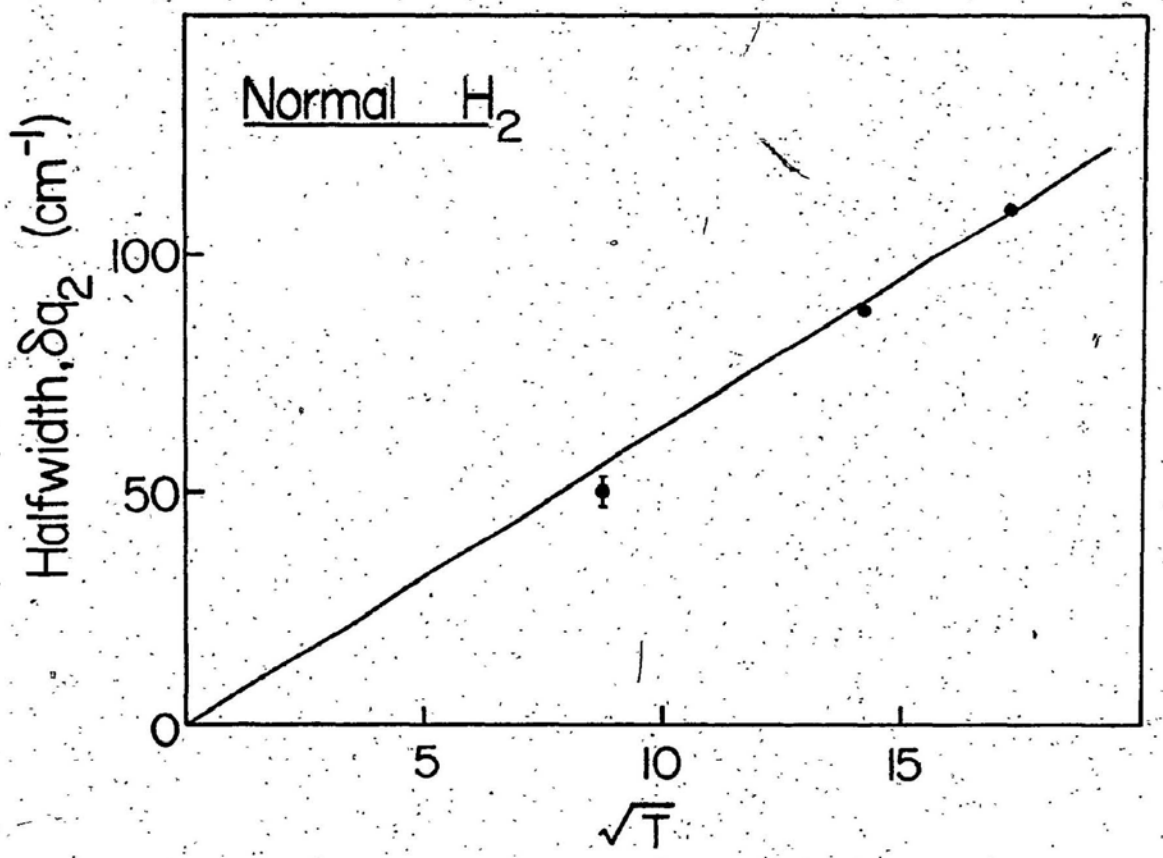


Fig. 18. The quadrupolar halfwidth $\delta_{q2}$ versus the square root of the absolute temperature.

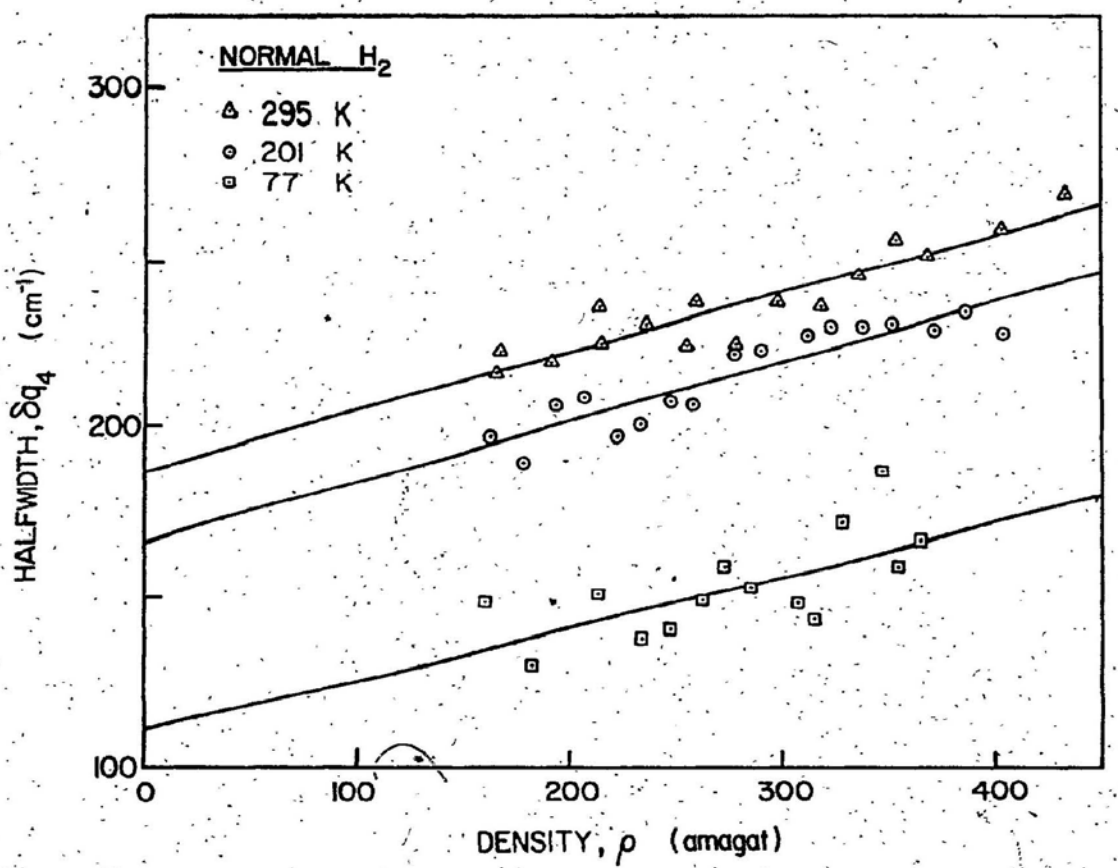


Fig. 19. Variation of the quadrupolar halfwidth $\delta_{q4}$ as a function of the gas density. The straight lines represent a linear least squares fit through the points at each temperature.

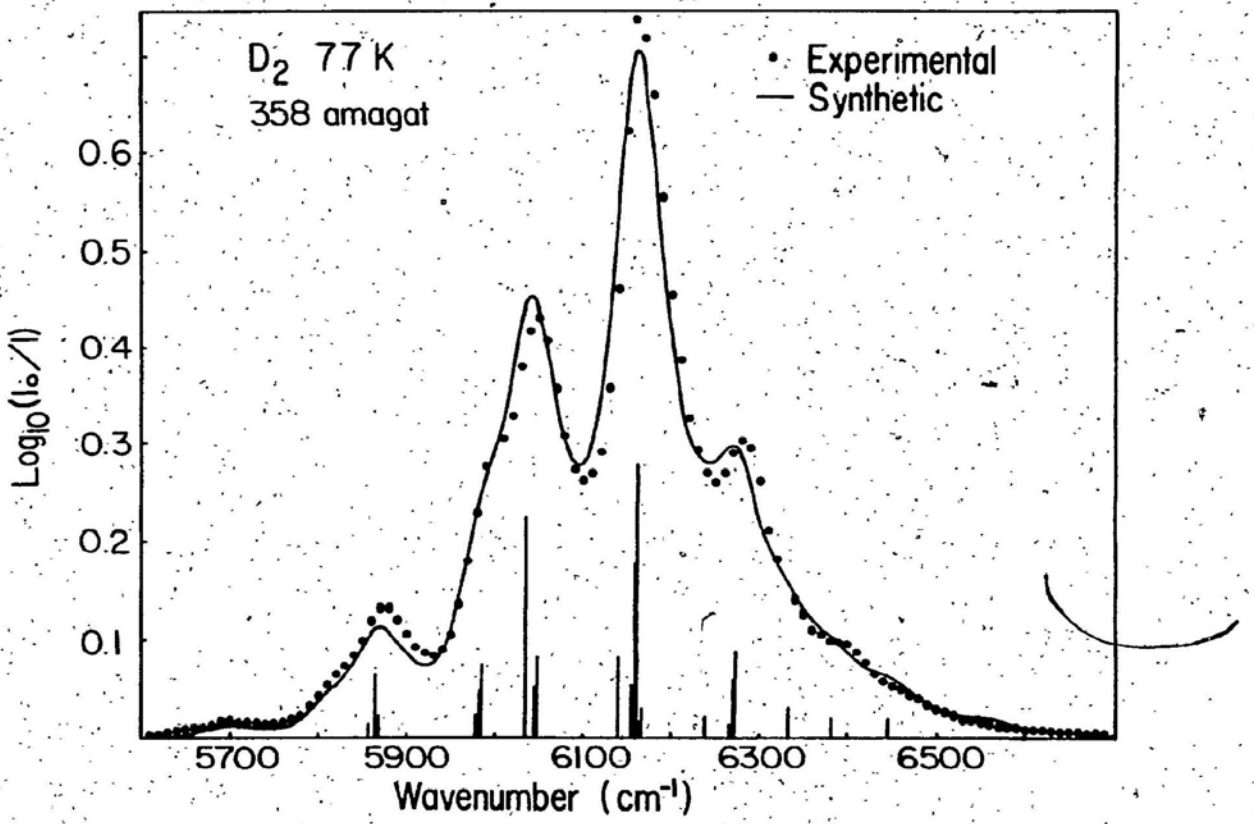


Fig. 20. Analysis of an absorption profile of normal $D_2$ in the pure gas at 77 K and 358 amagat in the first overtone region. The dotted curve is experimental. The solid curve is a fitted theoretical profile obtained by using the relative intensities calculated with the $\Delta v=2$ quadrupole moment matrix elements multiplied by the adjustment factor of 0.68 and the values $<|\alpha|>$ and $<|\gamma|>$ and the halfwidth parameters $\delta_{q2}=37.2\ cm^{-1}$ and $\delta_{q4}=88.0\ cm^{-1}$. (Gillard, 1983)

TABLE 3-5. Results of profile analysis [a]

| Temperature | Halfwidth parameter [b] | |
|---|---|---|
| (K) | $\delta_{q2}$ ($cm^{-1}$) | $\delta_{q4}$ ($cm^{-1}$) |
| 77 | 49 ± 2 | 135 - 185 |
| 201 | 88 ± 1 | 190 - 230 |
| 295 | 110 ± 1 | 220 - 270 |

[a] The errors quoted are standard deviations.
[b] The values quoted for $\delta_{q4}$ represent the range over which the halfwidth varies from low to high density.

discrepancy between the observed spectra and the profile synthesized using the calculated absolute intensities as shown in Fig. 21, namely the calculated absorption is less than the experimental absorption.

### 3.3. The Absorption Coefficients

The analysis of the absorption profiles reported in Sec. 3.2 is based on the assumption that the total contribution to the intensity of the band comes from binary collisions only. However, ternary collisions also contribute a small amount to the total intensity. The integrated absorption coefficient, $\int \alpha(\nu)\, d\nu$ can generally be expanded in a power series of the gas density $\rho_{H_2}$ $(=\rho_a)$ in the form

$$\int \alpha(\nu)\ d\nu = \alpha_{1a}\rho_a^2 + \alpha_{2a}\rho_a^3 + \cdots \qquad (3.10)$$

or

$$(1/\rho_a^2) \int \alpha(\nu)\ d\nu = \alpha_{1a} + \alpha_{2a}\rho_a + \cdots \ . \qquad (3.11)$$

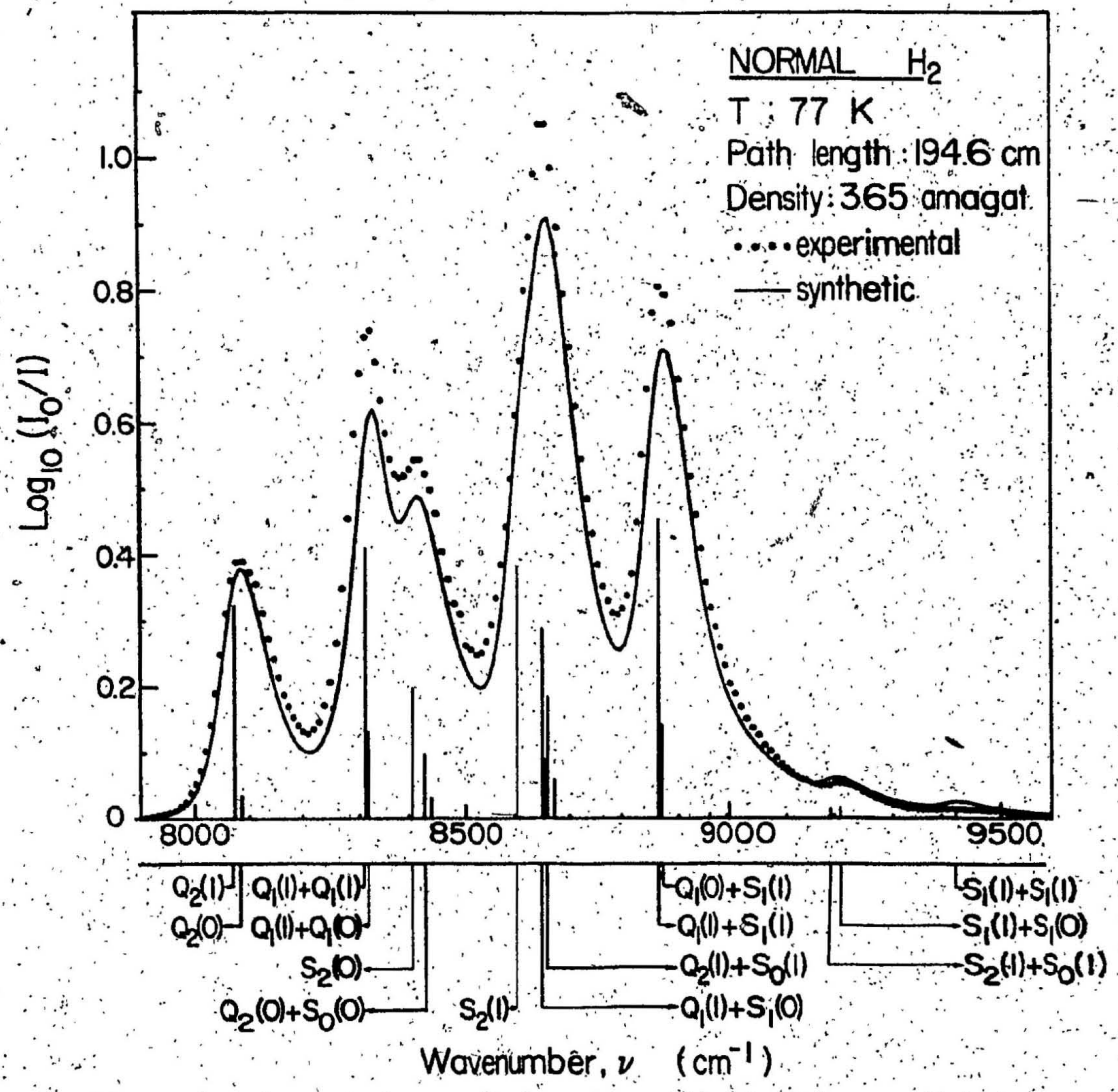


Fig. 21. Analysis of an absorption profile of normal $H_2$ in the pure gas at 77 K and 365 amagat in the first overtone region. The dotted curve, which is the same as the one shown in Fig. 10, is experimental. The solid curve is a theoretical profile obtained by using the absolute intensities calculated with the $\Delta v=2$ quadrupole moment matrix elements multiplied by the adjustment factor of 0.68 and the values of $\langle|\alpha|\rangle$ and $\langle|\gamma|\rangle$ and the halfwidth parameters obtained from the fit shown in Fig. 14.

where $\alpha_{1a}$ and $\alpha_{2a}$ are the binary and ternary absorption coefficients, respectively. The experimental values of the integrated absorption coefficient are determined from the areas under the experimental profiles. Figure 22 shows plots of $(1/\rho_a^2)\int \alpha(\nu)\, d\nu$ against $\rho_a$, where the intercept and slope (i.e., $\alpha_{1a}$ and $\alpha_{2a}$, respectively) were obtained from a linear least squares fit of the data.

An alternate form of the integrated absorption coefficient, $\int \tilde{\alpha}(\nu)\, d\nu$ $(= \int \alpha(\nu)/\nu \; d\nu)$ can be expressed as

$$c \int \tilde{\alpha}(\nu)\; d\nu = \tilde{\alpha}_{1a}\rho_a^2 n_0^2 + \tilde{\alpha}_{2a}\rho_a^3 n_0^3 + \cdots , \tag{3.12}$$

where c is the speed of light and $n_0$ is Loschmidt's number. The new binary and ternary absorption coefficients ($\tilde{\alpha}_{1a}$ and $\tilde{\alpha}_{2a}$, respectively) are related to $\alpha_{1a}$ and $\alpha_{2a}$ by the expressions

$$\tilde{\alpha}_{1a} = \frac{c}{n_0^2 \overline{\nu}}\, \alpha_{1a} \tag{3.13}$$

and

$$\tilde{\alpha}_{2a} = \frac{c}{n_0^3 \overline{\nu}}\, \alpha_{2a} , \tag{3.14}$$

where $\overline{\nu}$ is the band center given by

$$\overline{\nu} = \int \alpha(\nu)\, d\nu \Big/ \int \alpha(\nu)/\nu \; d\nu . \tag{3.15}$$

The binary and ternary absorption coefficients for the first overtone region of hydrogen are presented in Table 3-6.

The experimental binary absorption coefficient for the first overtone region can be compared with the calculated binary absorption by dividing $\alpha_{1a}$ by the band center $\overline{\nu}$.

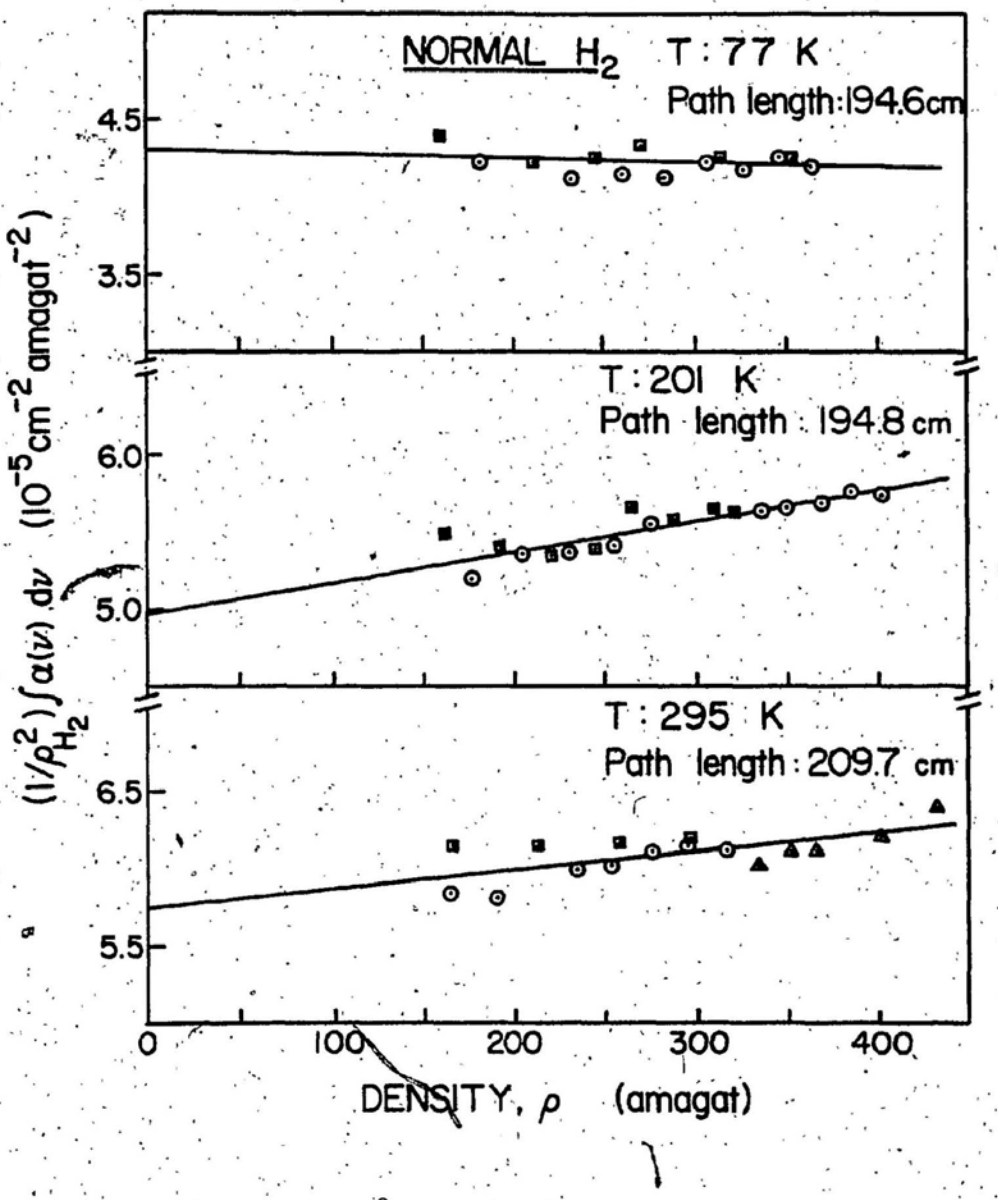


Fig. 22. Plots of $(1/\rho^2)\int\alpha(\nu)d\nu$ versus $\rho$ for normal $H_2$ in the pure gas at 77, 201 and 295 K in the collision-induced first overtone region. The different symbols refer to different experimental trials.

TABLE 3-6. Absorption coefficients* of $H_2$ in its first overtone region

| T (K) | Binary absorption coefficient $\alpha_{1a}$ ($10^{-5}$ $cm^{-2}$ $amagat^{-2}$) | $\tilde{\alpha}_{1a}$ ($10^{-37}$ $cm^6$ $s^{-1}$) | Ternary absorption coefficient $\alpha_{2a}$ ($10^{-9}$ $cm^{-2}$ $amagat^{-3}$) | Ref. |
|---|---|---|---|---|
| 77 | 4.31±0.09 | 2.86 | −0.3±0.3 | (a) |
| 80 | 3.5 | | | (b) |
| 85 | 4.16 | | | (c) |
| 201 | 4.99±0.08 | 2.44 | 1.9±0.3 | (a) |
| 295 | 5.8±0.1 | 2.1 | 1.2±0.3 | (a) |
| 300 | 6.2 | | | (b) |

* The errors quoted are standard deviations.
(a) Present work
(b) Welsh *et al.* (1951)
(c) McKellar and Welsh (1971)

$$\sum_m \int \tilde{\alpha}_{qm}(\nu)\,d\nu = \alpha_{1a}/\bar{\nu}$$

The experimental and calculated values of the absorption coefficient are compared in Table 3-7 for the temperatures 77, 201 and 295 K. The first calculated column is the sum of the integrated binary absorption $\int \tilde{\alpha}_{qm}(\nu)\,d\nu$ over all significant transitions using the unadjusted matrix elements. The last column represents the integrated binary absorption calculated with the 0.68 adjustment factor for the $\Delta v=2$ quadrupole moment matrix elements.

TABLE 3-7: Comparison of experimental and calculated binary absorption coefficients ( in units of $10^{-9}$ $cm^{-1}$ $amagat^{-2}$)

| T (K) | Experimental * | Calculated (unadjusted) | Calculated (with 0.68 adjustment factor) |
|---|---|---|---|
| 77 | 5.1±0.1 | 5.80 | 4.37 |
| 201 | 5.88±0.09 | 6.21 | 4.70 |
| 295 | 6.9±0.1 | 6.71 | 5.08 |

* The errors quoted are standard deviations.

### 3.4. Conclusions

In this chapter we have presented the results of a comprehensive study of the collision-induced absorption of $H_2$ in the first overtone region in the pure gas at 77, 201 and 295 K for densities up to 430 amagat. In all cases, the absence of a dip in the Q branch and the fact that the detailed profile analysis, carried out assuming only the quadrupolar absorption, accounted for the absorption in the Q branch indicates that there is no direct contribution from the overlap induction mechanism to the absorption in the first overtone region; this conclusion is in agreement with the earlier observations. The analysis of the experimental profiles has shown that there are discrepancies between the observed and calculated absorption profiles. It is found that by reducing the $\Delta v = 2$ quadrupole moment matrix elements by a factor of 0.68 a satisfactory agreement could be obtained between the experimental absorption profiles and the fitted synthetic profiles for all the recorded spectra. Bragg *et al.* (1982), in

their study of the allowed quadrupole transitions in the 1-0 through 4-0 bands of $H_2$ arising from free molecules, have found that the measured quadrupole line strengths agree within 10 % with the corresponding theoretical line strengths based on the same quadrupole moment matrix elements, as are used in the present work. The exact reasons for the large discrepancy between the observed collision-induced spectra of $H_2$ in the first overtone region and the corresponding computed spectra without the adjustment factor for the quadrupole moment matrix elements are not immediately clear. However one must realize that the quadrupole moment matrix elements used in the present profile analysis have been numerically evaluated for the free molecules only. One possible reason for the discrepancy between the experimental and calculated profiles (without the adjustment factor) could be the occurence of negative interference between the quadrupole-induced dipole and the anisotropic overlap-induced dipoles in the collision process (see for example Poll *et al.*, 1975, 1981 and Bachet *et al.*, 1983 ). A theoretical investigation to account for the results obtained in the present analysis of the first overtone band of $H_2$ is highly desireable.

## CHAPTER 4

## DOUBLE TRANSITIONS $S_2(J)+S_0(J)$ AND $S_1(J)+S_1(J)$ OF $H_2$ IN THE FIRST OVERTONE REGION AT 77 K

### 4.1. Introduction

As discussed earlier in Chapters 1 and 3, in the quadrupolar induction mechanism pertaining to the collision-induced absorption in the first overtone region, the isotropic part of the polarizability of the colliding pair of molecules contributes to the intensity of the following transitions: pure overtone transitions $O_2(J)$, $Q_2(J)$, $S_2(J)$, $Q_2(J)+O_0(J)$ and $Q_2(J)+S_0(J)$ and double fundamental transitions $Q_1(J)+O_1(J)$, $Q_1(J)+Q_1(J)$ and $Q_1(J)+S_1(J)$; however, the anisotropic component of the polarizability contributes to the intensity of the pure overtone double S transitions $S_2(J)+S_0(J)$ and the double fundamental S transitions $S_1(J)+S_1(J)$, (which do not have any contribution from the isotropic polarizability), and approximately 5 % to the intensities of the main transitions. Pure rotational double transitions $S_0(J)+S_0(J)$ of $H_2$ were observed experimentally by Kiss and Welsh (1959) and later studied by Bachet *et al.* (1983). Recently in our laboratory, double transitions $S_1(J)+S_0(J)$ of $H_2$ at 77 K were observed and analyzed by Sen *et al.* (1980). A reanalysis of the experimental absorption profiles of the $S_1(J)+S_0(J)$ region will be presented in Chapter 5.

The investigation to be described in the present chapter was undertaken to observe the collision-induced spectra of the double transitions $S_2(J)+S_0(J)$ and $S_1(J)+S_1(J)$ of normal $H_2$ at 77 K with significant intensity and to analyze the observed spectra. These spectra were obtained when the experiment was performed with a 2 m absorption cell for $H_2$ gas densities in the range 640 – 940 amagat at 77 K. At this

temperature only seven double S transitions (four of which are of pure overtone type and the remaining three are of double fundamental type) arising from J = 0 and 1 states are important. The contribution of the individual transitions of this group to the intensity of the observed spectra was separated by the method of profile analysis. The adjustment factor of 0.68 used for the $\Delta v = 2$ quadrupole moment matrix elements of $H_2$ in Chapter 3 was also found necessary to calculate the intensities of the $S_2(J) + S_0(J)$ components in order to obtain satisfactory fits of the theoretical synthetic profiles to the experimental profiles.

It should be pointed out that transitions of the type $O_2(J) + S_0(J)$, $O_1(J) + O_1(J)$ and $O_1(J) + S_1(J)$ are expected to contribute to the intensity of the first overtone region because of the Y term in Eqs. (3.6) and (3.9). However, for the $H_2$ spectra at 77 K, these transitions are too weak and can be neglected.

Experimental details for the study of the double S transitions of $H_2$ in the first overtone region are described in Chapter 2.

## 4.2. Absorption Profiles

Three representative collision-induced absorption profiles of $H_2$ in the first overtone region at 77 K in the spectral region 8900 - 10200 $cm^{-1}$ for the gas densities 644, 794 and 914 amagat are shown in Fig. 23. The distinct peaks superimposed on the high wavenumber tail of the main band can be attributed to the $S_{\Delta v}(J) + S_{\Delta v}(J)$ transitions. The positions of these transitions are calculated from the free molecular constants and are marked along the wavenumber axis. The lower density absorption profiles of $H_2$ in the first overtone region at 77 K shown in Chapter 3, indicate

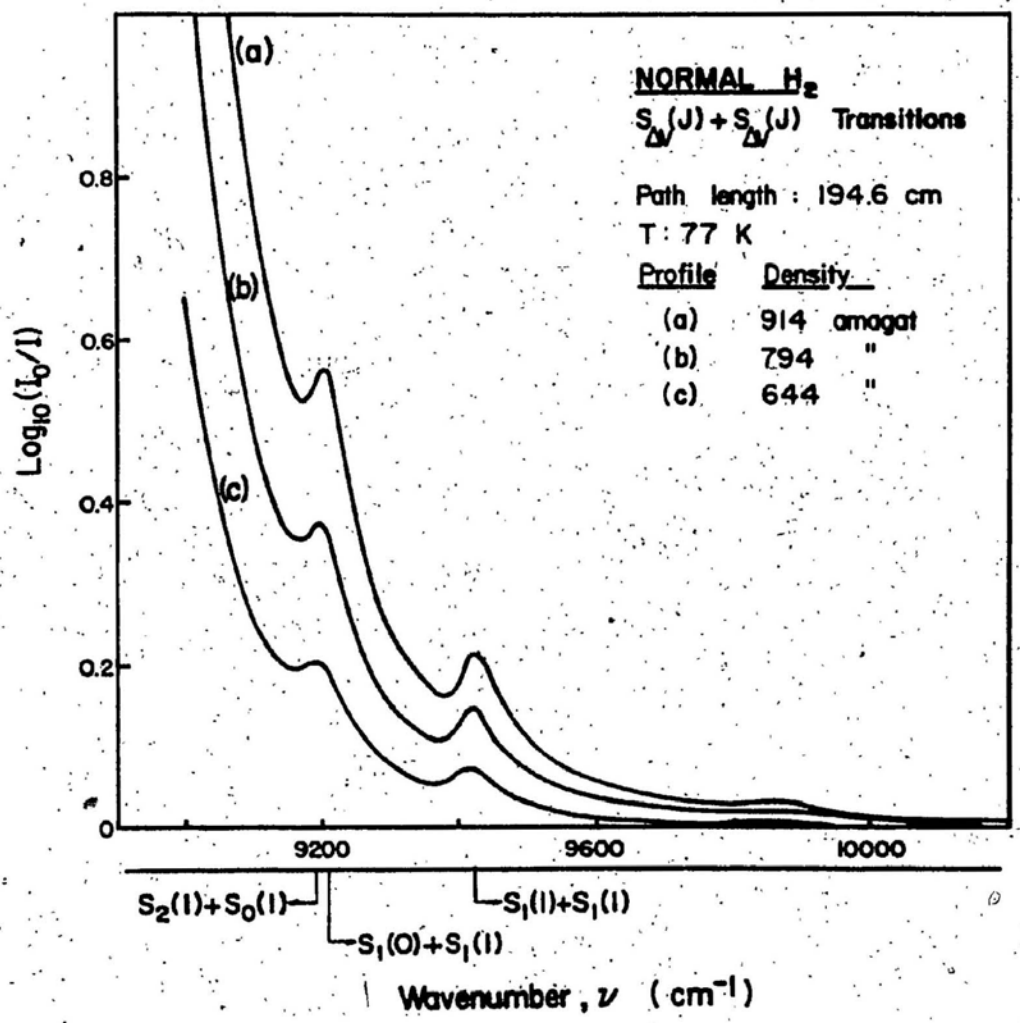


Fig. 23. Collision-induced absorption profiles of $H_2$ at three different densities of the gas at 77 K in the spectral region 8900 - 12000 $cm^{-1}$ where the double transitions $S_2(1) + S_0(1)$, $S_1(0) + S_1(1)$ and $S_1(1) + S_1(1)$ appear prominently.

the presence of these transitions, however their intensities are too weak for a proper analysis. Gas densities above 600 amagat cause the absorption of the main band in the spectral region below 8900 $cm^{-1}$ to exceed the limit of detection of the recording system but give a significant amount of absorption in the spectral region of the $S_{\Delta v}(J)+S_{\Delta v}(J)$ transitions so that a meaningful analysis of the profiles can be performed in this region.

The absorption peak at ~ 9195 $cm^{-1}$ corresponds to the sum of the two components $S_2(1)+S_0(1)$ (9191.2 $cm^{-1}$) and $S_1(1)+S_1(0)$ (9210.7 $cm^{-1}$). The second distinct peak at ~9425 $cm^{-1}$ corresponds to the $S_1(1)+S_1(1)$ (9425.8 $cm^{-1}$) transition. The three transitions $S_2(1)+S_0(0)$, $S_2(0)+S_0(1)$ and $S_1(0)+S_1(0)$ (8958.6, 8993.4 and 8995.7 $cm^{-1}$ respectively) which are hidden under the wing of the main band transitions were also included in the analysis. A small absorption feature observed at ~9860 $cm^{-1}$ in the profile at 914 amagat corresponds to the $Q_1(1)+U_1(1)$ (9850.7 $cm^{-1}$) and $Q_1(0)+U_1(1)$ (9856.6 $cm^{-1}$) transitions arising from the hexadecapolar induction mechanism.

### 4.3. Profile Analysis

From the analysis of the lower density absorption profiles of $H_2$ in the first overtone region at 77 K shown in Fig. 14 (Chapter 3), it is evident that the high wavenumber wing can very well be represented by assuming that its contribution to the absorption arises from a single component at the position of the $Q_1(1)+S_1(1)$ transition (8868.2 $cm^{-1}$). Following Reddy *et al.* (1980), who analyzed the U transitions in the fundamental band of $H_2$, we propose to represent the wing with a modified dispersion lineshape of a single line. The absorption coefficient of the main band

wing $\bar{\alpha}_w(\nu)$, is therefore represented by

$$\bar{\alpha}_w(\nu) = \frac{a_1}{1 + (\Delta\nu/a_2)^2 + (\Delta\nu/a_3)^4} \quad (4.1)$$

where $a_1$, $a_2$ and $a_3$ are independent adjustable parameters, $\Delta\nu = \nu - \nu_m$ and $\nu_m$ is the molecular wavenumber of the $Q_1(1) + S_{1(1)}$ transition.

The absorption coefficient $\bar{\alpha}_{qm}(\nu)$ for each of the double S transitions used in the profile analysis is represented by

$$\bar{\alpha}_{qm}(\nu) = A_q \int \bar{\alpha}_{qm}(\nu)\, d\nu \; x \; \frac{1}{(1 + (\Delta\nu/\delta_q)^2)} \; x \; \frac{1}{1 + \exp(-hc\Delta\nu/kT)} \quad (4.2)$$

where $\int \bar{\alpha}_{qm}(\nu)\, d\nu$ is the integrated binary absorption coefficient of the mth transition, $A_q$ is a normalization factor equal to the reciprocal of the area of the lineshape with height 0.5 at $\nu_m$ as defined in Chapter 3 and $\delta_q$ is the halfwidth at half height of the symmetric dispersion type function. The factor $1/[1 + \exp(-hc\Delta\nu/kT)]$ converts the symmetrized form into the observed asymmetric lineshape. The halfwidth parameter $\delta_{q4}$ which was used in the analysis of the main band presented in Chapter 3 was removed from the present analysis to reduce the number of parameters in the least squares fitting. It was believed that an additional parameter would allow too much freedom when considered with the three adjustable parameters of the wing contribution.

The values of $\int \bar{\alpha}_{qm}(\nu)\, d\nu$ for the double S transitions of $H_2$ in the first overtone region were calculated with Eqs. (3.4) and (3.6) using the Y term defined by Eq. (3.9) which accounts for the contribution of the anisotropy of the polarizability to the induced absorption. These intensities were calculated using the available matrix elements of the quadrupole

moment, polarizability and anisotropy of the polarizability as cited in Chapter 3. Table 4-1 lists the theoretical intensities calculated both with the unadjusted matrix elements and with the $\Delta v = 2$ quadrupole moment matrix elements multiplied by the adjustment factor of 0.68, as used in the analysis of the main band.

A synthetic profile of the collision-induced absorption of $H_2$ in the first overtone region above 8900 $cm^{-1}$ was computed from the superposition of the absorption coefficient $\tilde{\alpha}_w(\nu)$ of the main band wing given by Eq. (4.1) and the sum of the individual absorption coefficients $\sum_m \tilde{\alpha}_{qm}(\nu)$ of the double S transitions which are given by Eq. (4.2). The three parameters $a_1$, $a_2$, and $a_3$ in the lineshape of the main band wing, the quadrupolar halfwidth $\delta_q$ and the factor $A_q$ were used as adjustable parameters for a non-linear least squares fit to the experimental absorption profile. A wavenumber shift was introduced as an additional adjustable parameter. This accounted for any shift from the transition wavenumbers calculated from the constants of the free $H_2$ molecule which may arise from perturbations of the vibrational levels. The factor $A_q$ allows a degree of freedom for the height of the transition intensities in the fitting, but when absolute intensity calculations are made $A_q$ is the normalization of the lineshape.

Following the results of Chapter 3, the synthetic profiles were fitted to the experimental absorption profiles using the relative intensities calculated with the $\Delta v = 2$ quadrupole moment matrix elements multiplied by the adjustment factor of 0.68. The synthetic and experimental profiles for an intermediate gas density are compared in Fig. 24. The agreement

TABLE 4-1 Intensities of the first overtone S+S transitions at 77 K

| Transition | Wavenumber ($cm^{-1}$) | Absolute intensity $\int \tilde{\alpha}_{qm}(\nu) d\nu$ ($cm^{-1}$ $amagat^{-2}$) | Relative intensity | Relative intensity (with 0.68 factor) |
|---|---|---|---|---|
| $S_2(0)+S_0(0)$ | 8760.7 | .8135e-11 | .0137 | .0145 |
| $S_2(1)+S_0(0)$ | 8958.6 | .1718e-10 | .0289 | .0319 |
| $S_2(0)+S_0(1)$ | 8993.4 | .1493e-10 | .0251 | .0265 |
| $S_1(0)+S_1(0)$ | 8995.7 | .6815e-11 | .0114 | .0206 |
| $S_2(1)+S_0(1)$ | 9191.2 | .3153e-10 | .0529 | .0586 |
| $S_1(1)+S_1(0)$ | 9210.7 | .2178e-10 | .0366 | .0659 |
| $S_1(1)+S_1(1)$ | 9425.8 | .1733e-10 | .0291 | .0525 |

between the two is good and indicates that the relative intensities of the transitions is satisfactory when the adjusted quadrupolar matrix elements are used. If an adjustment factor were not used for the $\Delta v = 2$ matrix elements the $S_2(1)+S_0(1)$ transition intensity would have been too high.

For the range of gas densities used in the present work, there is a noticeable narrowing of the S+S quadrupolar lines. This is the first indication of diffusional pressure narrowing for quadrupolar lines of $H_2$ in the first overtone region. Recently Gillard (1983) has also observed the same effect in the collision-induced 2-0 band of deuterium. De Remigis *et al.* (1971) first observed pressure narrowing in $H_2$-Ar gas mixtures at 152 K for Ar densities in the range 300 to 833 amagat. Their study focused on

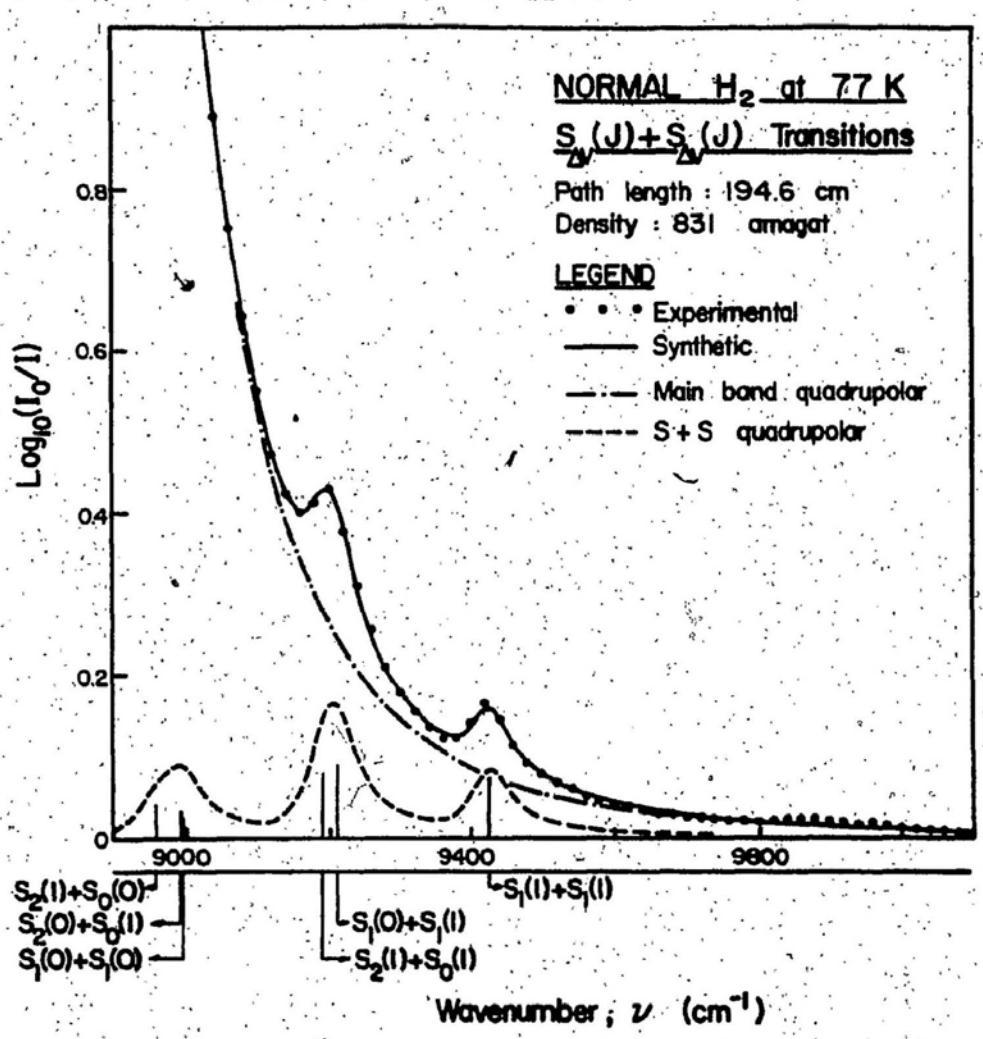


Fig. 24. Analysis of a collision-induced absorption profile of normal $H_2$ at 77 K in the spectral region 8900 - 11000 $cm^{-1}$. The dots represent the experimental data. The solid curve is the total synthetic profile which is the sum of the dash-dot curve representing the wing of the main quadrupolar-induced transitions and the dashed curve representing the sum of the individual transitions $S_2(J) + S_0(J)$ and $S_1(J) + S_1(J)$.

the $S_1(1)$ quadrupolar line of the fundamental band. For argon gas densities up to 300 amagat the halfwidth remained constant at 55 $cm^{-1}$ but decreased to 25 $cm^{-1}$ at the highest gas density. Van Kranendonk (1978) interpreted this narrowing in terms of a diffusion effect in which the line width is proportional to the diffusion coefficient for the gas at high densities. At high argon densities the $H_2$ molecule undergoes collisions not only with one argon atom but also with other argon atoms and the motion of the $H_2$ molecule becomes characteristic of diffusion. The argon atoms therefore act as a cage around the $H_2$ molecule and the effective collision duration is increased, resulting in reduced halfwidths for the quadrupolar lines. Pressure narrowing in $H_2$-foreign gas mixtures was further investigated by Mactaggart *et al.* (1973) in both the gas and liquid phases. For each gas mixture they showed that the quadrupolar halfwidth remained constant up to a certain density and then decreased linearly. The initial flat plateau defines the region in which the absorption arises primarily from isolated binary collisions. They have also pointed out that the pressure narrowing in the liquid phase is very similar to that for the corresponding dense binary gas mixture.

In the present work, the $S_{\Delta v}(J) + S_{\Delta v}(J)$ collision-induced transitions of $H_2$ in the pure gas at 77 K in the first overtone region have been studied in the density range 640 to 940 amagat. Within this density range the halfwidth of the lines is found to decrease from 40 to 30 $cm^{-1}$. The points are shown in Fig. 25 and are compared with the halfwidths of the quadrupolar lines of the fundamental band (Reddy *et al.*, 1977) and the first overtone main band. In both the fundamental and first overtone regions there is no indication of a decreasing halfwidth at the densities

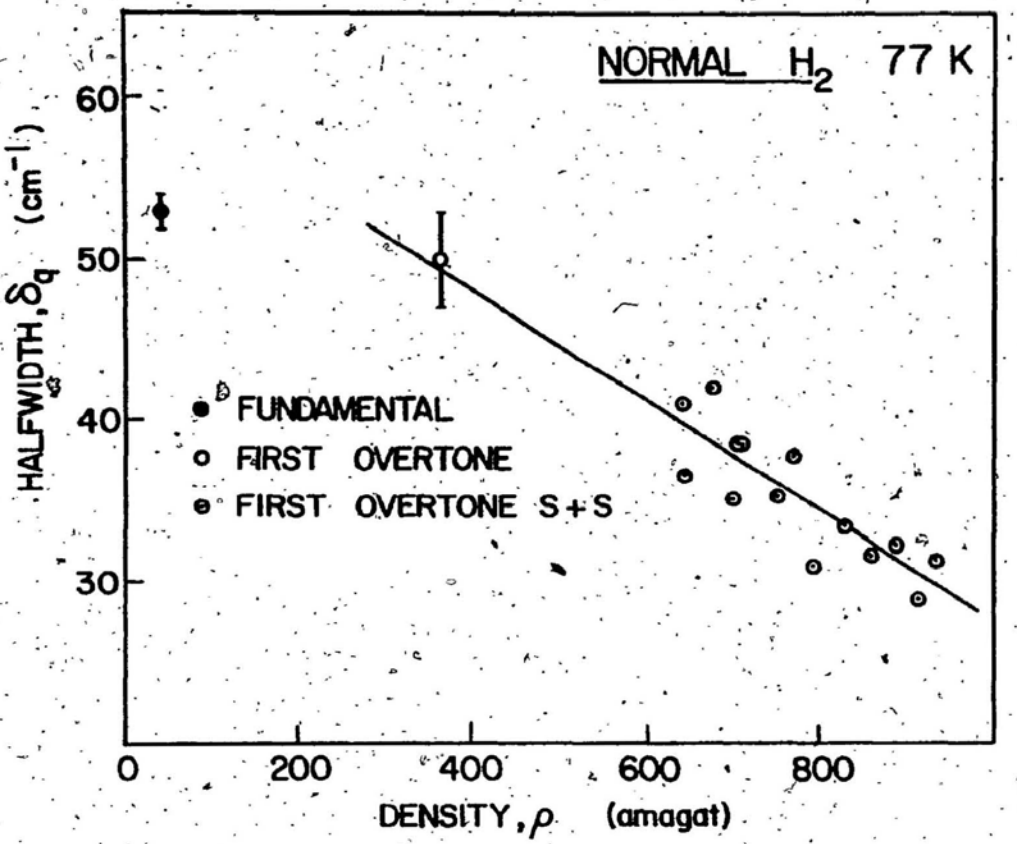


Fig. 25. Variation of the quadrupolar halfwidth $\delta_q$ as a function of the gas density $\rho$. The line is a least squares fit through the data points of the double S transitions of $H_2$ in the first overtone region. Data points for the main quadrupolar transitions of the fundamental and first overtone regions are also shown.

studied and the points plotted indicate the maximum density and the average halfwidth. In comparison with the earlier studies of the pressure narrowing, it would seem that these two points are representative of a constant halfwidth plateau at 52 $cm^{-1}$. The line shown is a linear least squares fit of the halfwidths of S+S transitions only and indicates that the pressure narrowing of hydrogen in the pure gas starts at approximately 350 amagat at 77 K. An attempt to determine the self diffusion coefficient for hydrogen is not feasible because the model discussed by Zaidi and Van Kranendonk(1971) has considered only mixtures of hydrogen with heavier inert gases and is too simple for the pure gas.

### 4.4. Absorption Coefficients of the $S_1(1)+S_1(1)$ Transition

The areas under the computed profiles for the $S_1(1)+S_1(1)$ component shown in Fig. 24 have been determined from a numerical integration of Eq. 4.2 using the least squares fitted values of the adjustable parameters $A_q$ and $\delta_q$ for each gas density. The integrated absorption coefficient $\int \alpha(\nu)\, d\nu$ can be expanded ( Eq. 3.10 and 3.12 ) in powers of the gas density to define the binary ($\alpha_{1a}$ and $\tilde{\alpha}_{1a}$) and ternary ($\alpha_{2a}$ and $\tilde{\alpha}_{2a}$) absorption coefficients. The values $(1/\rho_a^2)\int \alpha(\nu)\, d\nu$ are plotted against gas density $\rho_a$ in Fig. 26 and a linear least squares fit is obtained. The binary and ternary absorption coefficients given by the intercept and slope, respectively, are presented in Table 4-2. The statistical errors in the absorption coefficients could be reduced by extending the range of the gas densities towards lower densities. To obtain significant absorption at lower densities a longer path length would be required.

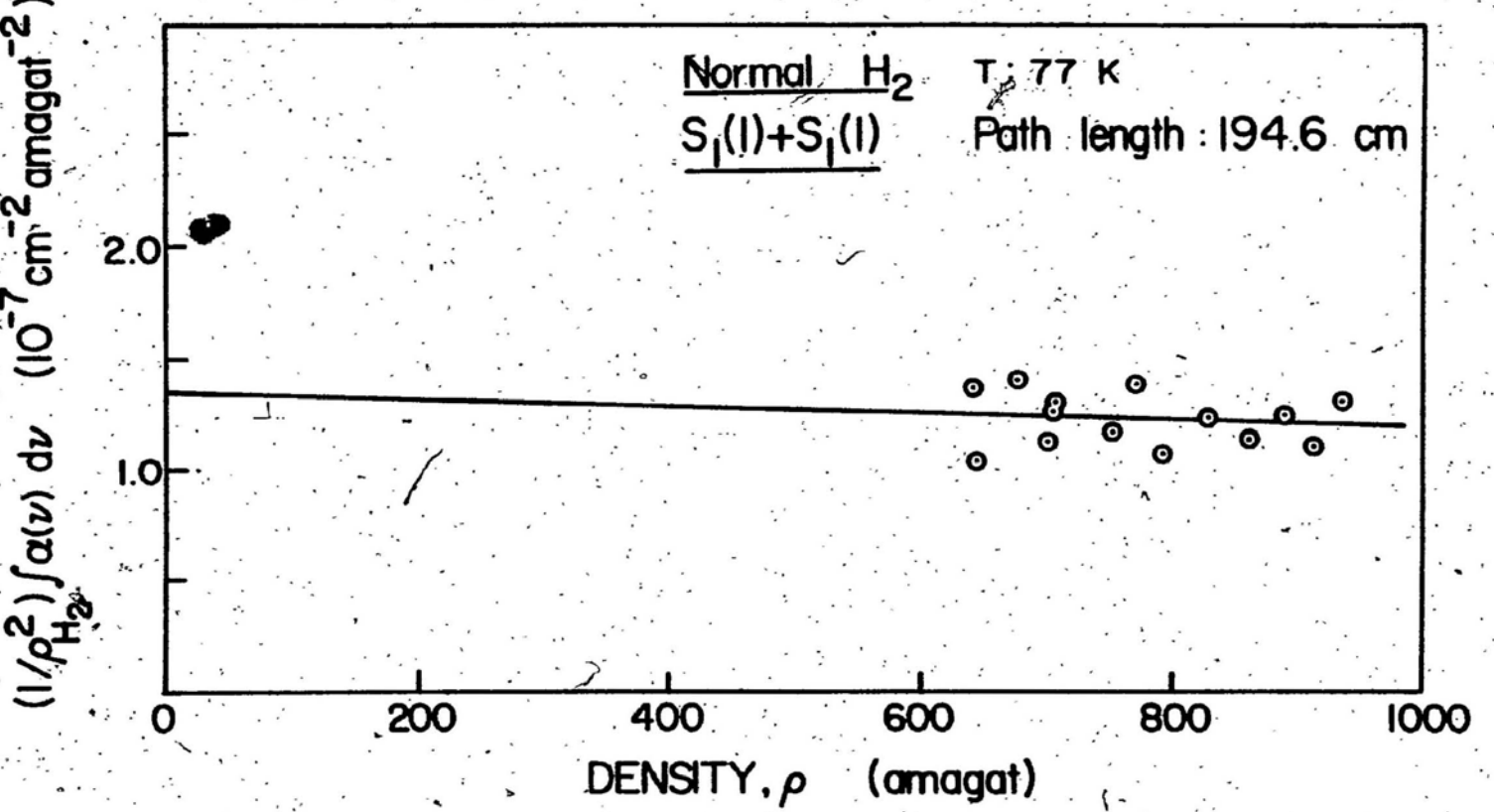


Fig. 26. Plots of $(1/\rho^2)\int\alpha(\nu)d\nu$ versus $\rho$ for the $S_1(1) + S_1(1)$ quadrupolar transition of $H_2$.

TABLE 4-2. Absorption Coefficients of the $S_1(1)+S_1(1)$ Transition of $H_2$ at 77 K

| Binary Absorption Coefficient | | Ternary Absorption Coefficient |
|---|---|---|
| $\alpha_{1a}$ ($10^{-7}$ $cm^{-2}$ $amagat^{-2}$) | $\tilde{\alpha}_{1a}$ ($10^{-40}$ $cm^6$ $s^{-1}$) | $\alpha_{2a}$ ($10^{-11}$ $cm^{-2}$ $amagat^{-3}$) |
| 1.4 ± 0.3 | 6.2 | -2 ± 3 |

## 4.5. Conclusions

The profile analysis presented in Fig. 24 definitely shows that the discrepancies occurring in the relative intensities of the first overtone region lies in the difference between the pure overtone and the double fundamental transitions rather than between the single and double transitions. The adjustment factor of 0.68 for the $\Delta v=2$ quadrupole moment matrix elements provides relative intensities for the $S_{\Delta v}(J)+S_{\Delta v}(J)$ transitions which give satisfactory fits to the experimental profiles. As shown in Table 4-1 the calculated binary absorption for the $S_1(1)+S_1(1)$ transition is $1.73 \times 10^{-11}$ $cm^{-1}amagat^{-2}$ with the 0.68 adjustment factor. This can be compared with the experimental absorption by dividing the binary absorption coefficient $\alpha_{1a}$ given in Table 4-2 by $\bar{\nu}$ (9426 $cm^{-1}$). This gives the result $1.5 \pm 0.3 \times 10^{-11}$ $cm^{-1}amagat^{-2}$ which agrees with the calculated result within the bounds of the stated error.

## CHAPTER 5

## A RE-ANALYSIS OF THE $S_1(J)+S_0(J)$ TRANSITIONS IN THE COLLISION-INDUCED FUNDAMENTAL BAND OF HYDROGEN

The $S_1(J)+S_0(J)$ transitions of the fundamental band arise solely because of the anisotropy of the polarizability. These transitions occur on the high wavenumber wing of the overlap and main quadrupolar transitions of the $H_2$ fundamental band and are somewhat similar to the S + S transitions in the first overtone region. In this chapter a re-analysis of the absorption profiles of $H_2$ at 77 K obtained earlier in this laboratory by Sen *et al.* (1980) will be presented.

### 5.1. Absorption Profiles

The absorption profiles considered in the following analysis were obtained earlier by Reddy and his co-workers (see for example Sen et al., 1980). The absorption spectra were recorded at 77 K in the pure gas for densities in the range 150 to 350 amagat. Some typical profiles are shown in Fig. 27. As a result of the high densities the stronger transitions of the main band have saturated the sensitivity of the recording system below 4800 $cm^{-1}$. Also the weaker $S_1(J)+S_0(J)$ transitions appear as two individual peaks at 5075 $cm^{-1}$ and 5300 $cm^{-1}$. As indicated along the base of the Fig. 27, the peak at 5075 $cm^{-1}$ corresponds to the two transitions $S_1(1)+S_0(0)$ (5067.3 $cm^{-1}$) and $S_1(0)+S_0(1)$ (5084.8 $cm^{-1}$), while the distinct peak at 5300 $cm^{-1}$ corresponds to the $S_1(1)+S_0(1)$ (5299.9 $cm^{-1}$) transition. The $S_1(0)+S_0(0)$ (4852.2 $cm^{-1}$) transition, which was also used in the analysis, is masked by the stronger main band transitions.

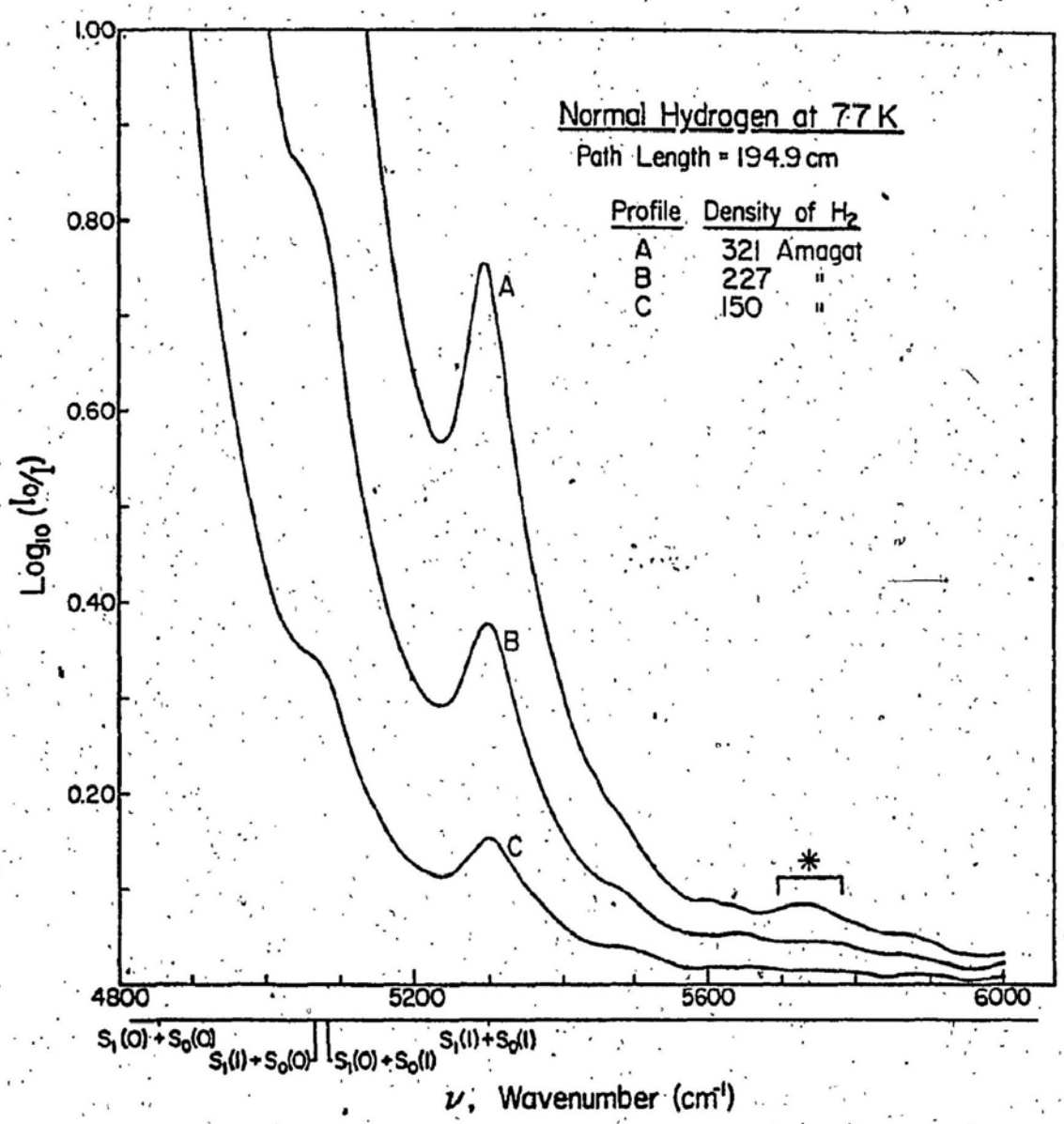


Fig. 27. Collision-induced absorption profiles of $H_2$ in the fundamental band at three different densities of the gas at 77 K in the spectral region 4800 - 6000 $cm^{-1}$. The positions of the $S_1(J) + S_0(J)$ transitions are marked along the base of the figure. (Sen et al., 1980)

## 5.2. Profile Analysis

At 77 K the halfwidths of the stronger components of the main fundamental band are still broad enough so that their high wavenumber wings contribute significantly in the region of the weaker $S_1(J)+S_0(J)$ transitions. In order to obtain useful information about the weaker transitions it is necessary to separate them from the absorption of the main band.

The present work considers the study of the $H_2$ fundamental band at low densities by Reddy et al. (1977) as a starting point. The analyzed absorption profile shown in Fig. 28 is reproduced from their paper. This profile was analyzed by assuming a Levine-Birnbaum lineshape (Levine and Birnbaum, 1967) and Van Kranendonk's dispersion type lineshape (Van Kranendonk, 1968) for the intracollisional and intercollisional components, respectively, of the overlap induction and a Boltzmann modified dispersion lineshape was used for the quadrupolar transitions. It is clear from Fig. 28 that in the region of the $S_1(J)+S_0(J)$ transitions (i.e., above 4800 $cm^{-1}$) the only significant contribution from the main band is due to the quadrupolar transitions. The contribution of the overlap absorption, centered about the $Q_1(J)$ position, is negligible in the region above 4800 $cm^{-1}$. However, the earlier work of Sen *et al.* assumed that there was a significant contribution from the overlap absorption. In the present analysis the overlap contribution in the fundamental S + S region was assumed to be zero.

The high wavenumber wing of the main band consists of the superposition of the tail ends of a number of strong quadrupolar lines. As proposed for the analysis of the S + S transitions of $H_2$ in the first overtone region (Chapter 4), the high wavenumber wing is represented by a

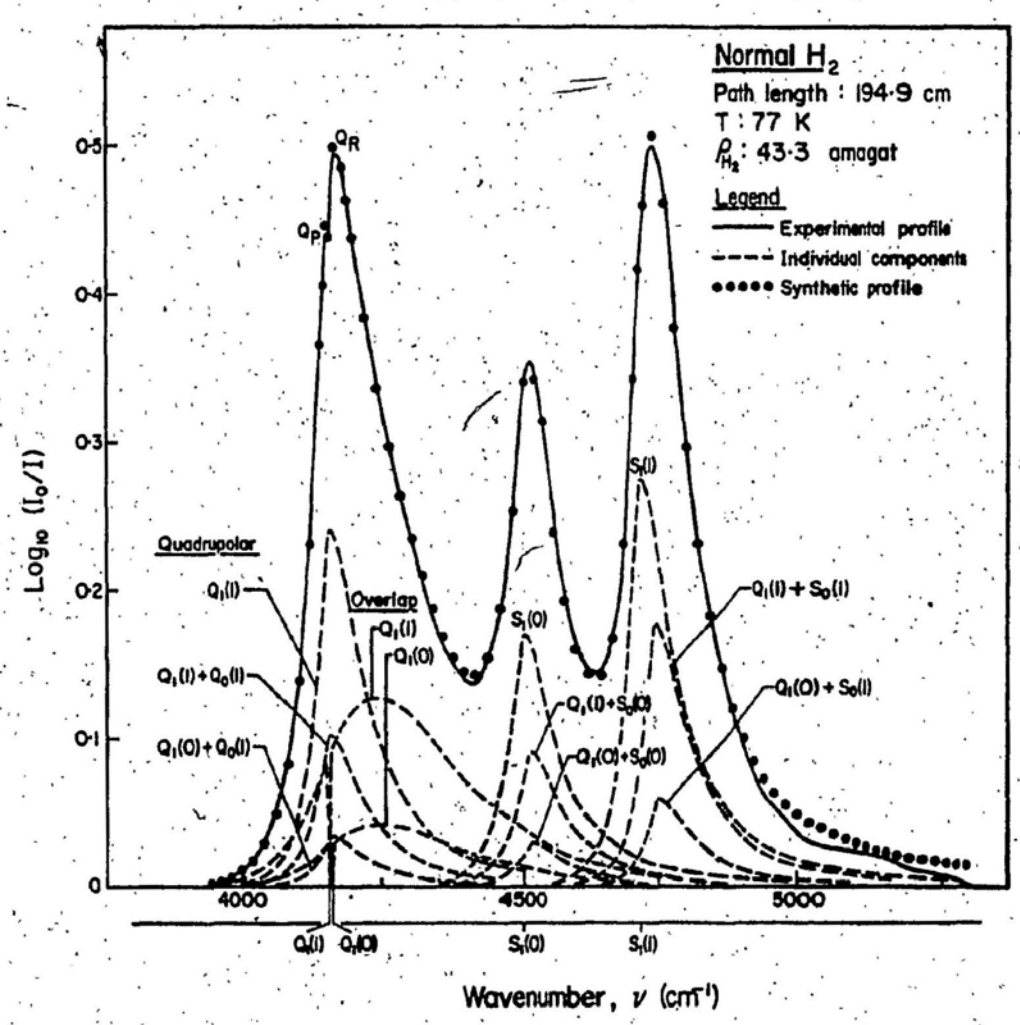


Fig. 28. Analysis of an absorption profile of normal $H_2$ in the pure gas at 77 K and 43.3 amagat in the fundamental band. The solid curve is the experimental profile. The dashed curves represent two overlap-induced and nine quadrupole-induced computed components and the dots represent the summation of these. (Reddy et al., 1977)

modified dispersion lineshape of a single line. The absorption coefficient for the wing of the main band, $\tilde{\alpha}_w(\nu)$ is therefore given by

$$\tilde{\alpha}'_w(\nu) = \frac{a_1}{1 + (\Delta\nu/a_2)^2 + (\Delta\nu/a_3)^4} , \qquad (5.1)$$

where $a_1$, $a_2$ and $a_3$ are adjustable parameters and $\Delta\nu = \nu - \nu_m$. The origin of the lineshape, $\nu_m$ was assumed to be at the position of the nearest strong quadrupolar transition, namely $S_1(1)$ at 4712.9 $cm^{-1}$.

The absorption coefficient, $\tilde{\alpha}_{qm}(\nu)$ for the $S_1(J)+S_0(J)$ transitions is represented by the symmetrized dispersion lineshape (see Mactaggart and Welsh (1973) and Reddy *et al.* (1977)). As described by Eq. (3.1) it is written as

$$\tilde{\alpha}_{qm}(\nu) = A_q \int \tilde{\alpha}_{qm}(\nu)\, d\nu \times \frac{1}{1+(\Delta\nu/\delta_q)^2} \times \frac{1}{1+\exp(-hc\,\Delta\nu/kT)} \qquad (5.2)$$

The calculated intensities $\int \tilde{\alpha}_{qm}(\nu)\, d\nu$, for the S + S transitions of the fundamental band are presented in Table 5-1.

In the fitting procedure both $a_2$ in Eq. (5.1) and $\delta_q$ in Eq. (5.2) were considered to be the same adjustable parameter under the assumption that the main quadrupolar lines and the $S_1(J)+S_0(J)$ lines have the same halfwidth. $A_q$ is also an adjustable parameter to allow a degree of freedom for the height of the transitions. However, in order for Eq. 5.2 to represent the theoretical absorption coefficient, $A_q$ must be the reciprocal of the area of the lineshape with height 0.5 at $\nu_m$. An adjustable shift parameter for the molecular wavenumber $\nu_m$ is used to account for any possible perturbation of the vibrational levels calculated from constants of the free $H_2$ molecule. In the analysis, the five parameters are

TABLE 5-1 Calculated intensities of the fundamental S+S transitions in normal $H_2$ at 77 K

| Transition | Wavenumber ($cm^{-1}$) | Absolute intensity $\int \tilde{\alpha}_{qm}(\nu) d\nu$ ($cm^{-1}$ amagat$^{-2}$) | Relative intensity |
|---|---|---|---|
| $S_1(0)+S_0(0)$ | 4852.2 | .4186e-09 | 0.3288 |
| $S_1(1)+S_0(0)$ | 5067.3 | .6965e-09 | 0.5471 |
| $S_1(0)+S_0(1)$ | 5084.9 | .7650e-09 | 0.6009 |
| $S_1(1)+S_0(1)$ | 5299.9 | .1273e-08 | 1.0000 |

assumed to be the same for all the four $S_1(J)+S_0(J)$ transitions and are allowed to vary with density in order to obtain the best least squares fit between the calculated and experimental profiles.

A comparison between a typical experimental profile and the corresponding least squares fitted synthetic profile is shown in Fig. 29. The agreement between them is very good. The contribution of the wing of the main band and the quadrupolar transitions arising from the anisotropy of the polarizability are shown separately in this figure. The sticks represent the positions and heights of the individual $S_1(J)+S_0(J)$ transitions. Eleven profiles obtained by Sen *et al.* (1980) have been reanalyzed and the results are given in Table 5-2.

### 5.3. Absorption Coefficients of $S_1(1)+S_0(1)$

As discussed earlier in Sec. 3.3, the integrated absorption coefficient

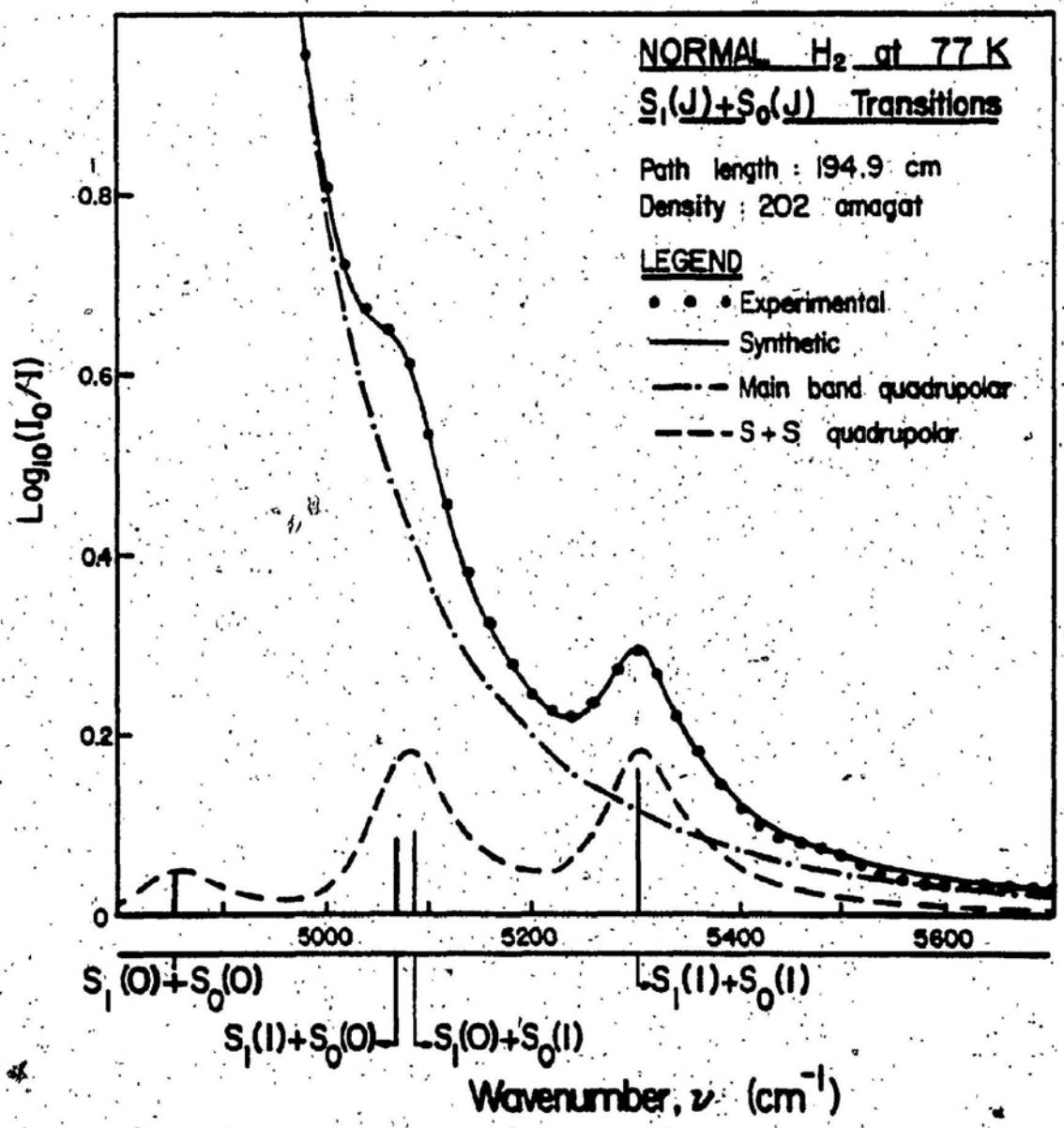


Fig. 29. Analysis of a collision-induced absorption profile of normal $H_2$ in the fundamental band at 77 K in the spectral region 4800 - 5700 $cm^{-1}$. The dots represent the experimental data. The solid curve is the total synthetic profile which is the sum of the dash-dot curve representing the wing of the main quadrupolar-induced transitions and the dashed curve representing the sum of the individual $S_1(J) + S_0(J)$ transitions.

TABLE 5-2. Results of profile analysis of the fundamental S + S transitions of $H_2$ at 77 K

| Quadrupolar half-width $\delta_q$ ($cm^{-1}$) | Collision duration* $\tau_q$ ($10^{-14}$ s) | Molecular shift of quadrupolar components ($cm^{-1}$) | Reference |
|---|---|---|---|
| 45 ± 3 | 11.8 | −7 ± 2 | Present work |
| 54 ± 2 | 9.83 | −9 ± 2 | Sen et al. (1980) |

* $\tau_q = \frac{1}{2\pi c \delta_q}$

$\int \alpha(\nu)\, d\nu$ can be expanded in a power series of the gas density $\rho_a$ with the expansion coefficients representing the binary and ternary absorption coefficients ($\alpha_{1a}$ and $\alpha_{2a}$ or $\tilde{\alpha}_{1a}$ and $\tilde{\alpha}_{2a}$ respectively). The observed value of the integrated absorption coefficient for the $S_1(1)+S_0(1)$ transition is determined by numerically integrating Eq. 5.2 over the wavenumber range, using the fitted values for the parameters $A_q$ and $\delta_q$ at each density. Figure 30 shows a plot of $(1/\rho_a^2) \int \alpha(\nu)\, d\nu$ versus $\rho_a$ and a linear least squares fit to the experimental points. The values of the binary and ternary coefficients for the $S_1(1)+S_0(1)$ transition are presented in Table 5-3 and are compared with the earlier work of Sen *et al.* (1980).

## 5.4. Conclusions

We have shown in the present chapter that the calculated relative intensities of the S + S transitions of the fundamental band give satisfactory fits of the synthetic profiles to the experimental profiles. However,

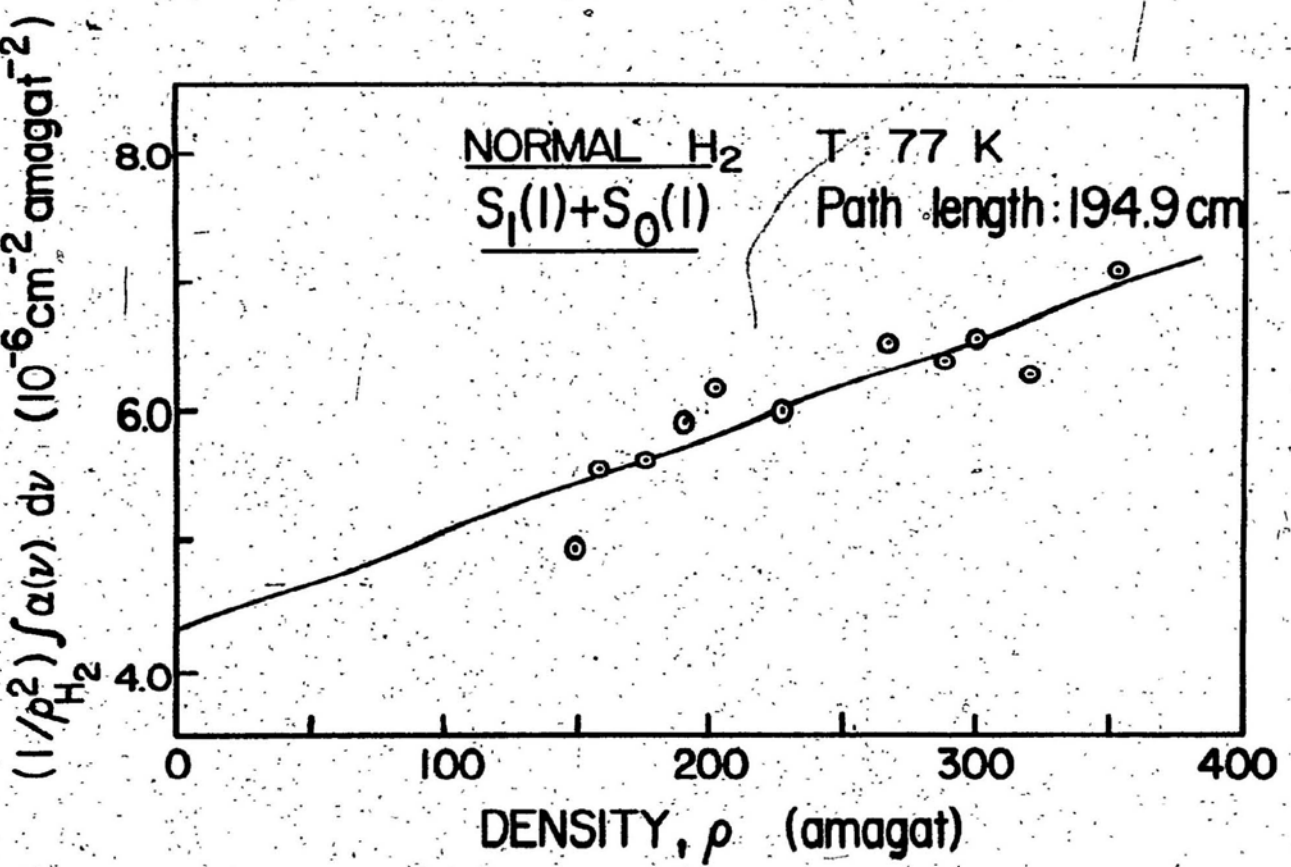


Fig. 30. Plots of $(1/\rho^2)\int\alpha(\nu)d\nu$ versus $\rho$ for the $S_1(1) + S_0(1)$ quadrupolar transition of $H_2$.

TABLE 5-3. Absorption Coefficients of the $S_1(1)+S_0(1)$ Transition of $H_2$ at 77 K

| Binary absorption coefficient | | Ternary absorption coefficient | Ref. |
|---|---|---|---|
| $\alpha_{1a}$ ($10^{-6}$ $cm^{-2}$ $amagat^{-2}$) | $\bar{\alpha}_{1a}$ ($10^{-38}$ $cm^6$ $s^{-1}$) | $\alpha_{2a}$ ($10^{-9}$ $cm^{-2}$ $amagat^{-3}$) | |
| 4.3 ± .3 | 3.3 | 7 ± 1 | (a) |
| 6.84 ± .21 | 5.26 | 7.08 ± 0.98 | (b) |

(a) Present work
(b) Sen *et al.* (1980)

there is considerable discrepancy between the calculated absolute values and the experimental values of the binary absorption coefficient. Actually, the calculated binary absorption for the $S_1(1)+S_0(1)$ is $1.27\times10^{-9}$ $cm^{-1}$ $amagat^{-2}$ (Table 5-1) and the corresponding experimental value is $8.0\pm0.6\times10^{-10}$ $cm^{-1}$ $amagat^{-2}$ (which is obtained by dividing the binary absorption coefficient $\alpha_{1a}$ by $\bar{\nu}$ (5358 $cm^{-1}$)). The calculated and experimental results differ by approximately 40 %. The differences between the values of the transition halfwidth and the absorption coefficients obtained by Sen *et al.* (1980) and by the present analysis can be attributed to the differences in the method of analysis. In their analysis Sen *et al.* considered all of the transitions of the fundamental band individually in the fitting of the synthetic profiles to the absorption profiles in S + S region above 4800 $cm^{-1}$. Because of the freedom of the parameters the overlap contribution in this region was found by them to be greater than that of the main band quadrupolar transitions. However, in the present analysis

we have represented the high wavenumber wing of the main band transitions by a single line and assumed that the overlap contribution to the S + S region is zero.

# APPENDIX A

## PROGRAM TO CALCULATE THE INTENSITIES OF THE QUADRUPOLE-INDUCED TRANSITIONS

Program to calculate the integrated binary absorption coefficient $\int \alpha_{qm}(\nu) d\nu$, for all of the individual quadrupolar transitions of a given band. (Written in HPL for the Hewlett-Packard model 9825A calculator.)

```
0: dsp "calculate quadrupolar intensities";stp
1: "the output will be the integrated binary ":
2: "absorption coefficient as defined by Poll 1970":
3: ent "no. of vibrational states",N
4: dim R,O,Q,U,O[2,10],I[3,150],U[2,10],E[2],P[2]
5: dim Q[-1:1,0:N,0:4],A[0:N,0:4],G[-1:1,0:N,0:4],B[0:N]
6: dim D[0:N],H[0:N],W[0:N],X[-1:1,0:N,0:4,-1:1,0:4]
7: ent "temperature",R;1.438832042/R→T;fxd 5
8: wrt 6,"temperature",R;wrt 6
9: ent "output file no. (track 0)",S
10: "ent 'relative intensity cutoff',C":0→C
11: wrt 6,"relative intensity cutoff ",C;fxd 0
12: dsp "if no file is to be created,";wait 1000
13: ent "press continue,else press 1",Z
14: if flg13;gto "load"
15: dsp "enter spectroscopic constants";stp
16: for I=0 to N
17: dsp "B(",I,")";ent "",B[I]
18: dsp "D(",I,")";ent "",D[I]
19: dsp "H(",I,")";ent "",H[I]
20: dsp "v(",I,")";ent "",W[I]
21: next I
22: dsp "enter polarizability matrix";stp
23: for V=0 to N
24: for J=0 to 4
25: dsp "a(v=",V,",J=",J,")";ent "",A[V,J]
26: next J
27: next V
28: dsp "enter quadrupole matrix elements";stp
29: for K=-2 to 2 by 2
30: for V=0 to N
31: for J=max(0,-K) to 4
32: dsp "Q(dJ=",K,",v'=",V,",J=",J,")";ent "",Q;Q→Q[K/2,V,J]
33: next J
34: next V
35: next K
36: dsp "enter anisotropic matrix elements";stp
37: for K=-2 to 2 by 2
38: for V=0 to N
39: for J=max(0,-K) to 4
40: dsp "G(dJ=",K,",v'=",V,",J=",J,")";ent "",G;G→G[K/2,V,J]
41: next J
```

```
42: next V
43: next K
44: rcf F,Q[*],A[*],G[*],B[*],D[*],H[*],W[*]
45: gto "run"
46: "load":ldf 27,Q[*],A[*],G[*],B[*],D[*],H[*],W[*]
47: fxd 3;ent "fudge factor for V=2 A matrix",r0
48: if flg13;gto "fA"
49: wrt 6,"polarizability adjustment factor", r0
50: for J=0 to 4
51: A[2,J]*r0→A[2,J]
52: next J
53: "fA":ent "anisotropic adjustment factor", r0
54: if flg13;gto "fQ"
55: wrt 6,"anisotropic polarizability fudge factor",r0
56: for K=-2 to 2 by 2
57: for J=max(0,-K) to 4
58: for V=0 to N
59: G[K/2,V,J]*r0→G[K/2,V,J]
60: next V
61: next J
62: next K
63: "fQ":ent "adjustment factor for V=2 Q matrix", r0
64: if flg13;gto "run"
65: wrt 6,"quadrupole adjustment factor", r0
66: for K=-2 to 2 by 2
67: for J=max(0,-K) to 4
68: Q[K/2,2,J]*r0→Q[K/2,2,J]
69: next J
70: next K
71: "run":dsp "to print matrix elements ,";wait 1000
72: dsp "press 1 , else press continue";ent "",Z
73: if flg13;gto "overlay"
74: wrt 6,"    SPECTROSCOPIC CONSTANTS";wrt 6;wrt 6
75: fmt 3,8x,"B",14x,"D",14x,"H",13x,"v"
76: wrt 6.3
77: fmt 4,4e15.6
78: for V=0 to N
79: wrt 6.4,B[V],D[V],H[V],W[V]
80: next V
81: wrt 6;wrt 6
82: wrt 6,"    polarizability matrix elements";wrt 6
83: fmt 5,f15.7,z
84: for V=0 to N
85: for J=0 to 4
86: wrt 6.5,A[V,J]
87: next J
88: wrt 6
89: next V
90: wrt 6;wrt 6;wrt 6
91: wrt 6,"    quadrupole matrix elements";wrt 6
92: for K=-2 to 2 by 2
93: for V=0 to N
```

```
94: for J=0 to 4
95: wrt 6.5,Q[K/2,V,J]
96: next J
97: wrt 6
98: next V
99: wrt 6
100: next K
101: wrt 6;wrt 6;wrt 6
102: wrt 6,"     anisotropic matrix elements";wrt 6
103: for K=-2 to 2 by 2
104: for V=0 to N
105: for J=0 to 4
106: wrt 6.5,G[K/2,V,J]
107: next J
108: wrt 6
109: next V
110: wrt 6
111: next K
112: fmt 1,4f5.0,f15.3,2x,e15.6,2x,4f15.5
113: "overlay":
114: for K=-2 to 2
115: for V=0 to N
116: for J=0 to 4
117: for L=-2 to 2
118: for I=0 to 4
119: 0→X[K/2,V,J,L/2,I]
120: next I
121: next L
122: next J
123: next V
124: next K
125: wrt 6;wrt 6;wrt 6;wrt 6,"output file #",S
126: fxd 0;wrt 6;wrt 6;wrt 6;wrt 6,"output file #",S
127: 0→Y;0→W
128: for J=1 to 5 by 2
129: (2*J+1)*exp(-F(J,0)*T)+W→W
130: (2*J-1)*exp(-F(J-1,0)*T)+Y→Y
131: next J
132: (4*Y)^2→H;3*Y/W→W;0→Y
133: fxd 3;wrt 6,"statistical weights for normal H2",1,W
134: wrt 6;wrt 6
135: "LOAD SECOND PART OF PROGRAM":
136: trk 1;ldf 26,5
137: stp
138: "F":p1*(p1+1)→p3
139: B[p2]*p3-D[p2]*p3^2+H[p2]*p3^3+W[p2]→p3;ret p3
140: end
```

Second part of program to calculate the integrated binary absorption coefficient for the quadrupolar transitions.

```
0: dsp "CALCULATION 23/12/82";trk 0
1: wrt 6,"normal hydrogen"
2: for K=-2 to 2 by 2
3: for V=0 to N
4: for J=max(-K,0) to 4
5: 'F'(J,0)→E[1]
6: 1→G;if int(J/2)<J/2;W→G
7: G*(2*J+1)*exp(-E[1]*T)/H→P[1]
8: for L=-2 to 2 by 2
9: for I=max(-L,0) to 4
10: 'F'(I,0)→E[2]
11: 1→G;if int(I/2)<I/2;W→G
12: G*(2*I+1)*exp(-E[2]*T)→P[2]
13: P[1]*P[2]→P;0→Z
14: if L≠0;Z+'C'(J,K)*(Q[K/2,V,J]*A[N-V,I])^2→Z
15: 0→A
16: (Q[K/2,V,J]*G[L/2,N-V,I])^2+(Q[L/2,N-V,I]*G[K/2,V,J])^2→A
17: 2/9*A→A
18: A-4/15*Q[K/2,V,J]*G[L/2,N-V,I]*Q[L/2,N-V,I]*G[K/2,V,J]→A
19: "the factor 1/2 arises from van K and Kiss 1959 eq.19":
20: 'C'(J,K)*'C'(I,L)*A/2→A
21: Z+A→Z
22: Z*P→X
23: if V<=N-V;V→B;K/2→F;J→M;L/2→Q;I→Y;gto "cont"
24: N-V→B;L/2→F;I→M;K/2→Q;J→Y
25: "cont":0→Z
26: X[F,B,M,Q,Y]→Z
27: Z+X→X[F,B,M,Q,Y]
28: next I;next L;next J;next V;next K
29: "sum all V = N transitions with K , i.e. dJ(1) = 0":
30: for L=-2 to 2 by 2
31: for I=0 to 4
32: for J=1 to 4
33: X[0,0,0,L/2,I]+X[0,0,J,L/2,I]→X[0,0,0,L/2,I]
34: 0→X[0,0,J,L/2,I]
35: next J
36: next I
37: next L
38: "collect identical terms when v = N/2":
39: int(N/2)→B
40: if B*2#N;gto "norm"
41: for K=-2 to 2 by 2
42: for J=max(-K,0) to 4
43: for L=-2 to 2 by 2
44: J→F
45: if K=L;J+1→F
46: for I=F to 4
47: X[K/2,B,J,L/2,I]→Y
48: Y+X[L/2,B,I,K/2,J]→X[K/2,B,J,L/2,I]
```

```
49: 0→X[L/2,B,I,K/2,J]
50: next I
51: next L
52: next J
53: next K
54: "norm":
55: "find maximum intensity":
56: fmt 9,e10.4
57: 0→Y
58: for K=-2 to 2 by 2
59: for V=0 to N
60: for J=max(-K,0) to 4
61: for L=-2 to 2 by 2
62: for I=max(-L,0) to 4
63: if X[K/2,V,J,L/2,I]>Y;X[K/2,V,J,L/2,I]→Y
64: next I
65: next L
66: next J
67: next V
68: next K
69: wrt 6.9,"maximum value of X is ",Y
70: "the value of F is the constant coefficient ":
71: "of X as defined by McKellar and Welsh 1971":
72: if R=77;6.215199e-7→F
73: if R=201;6.656299e-7→F
74: if R=295;7.175405e-7→F
75: wrt 6;wrt 6;wrt 6;0→Q
76: wrt 6,"   molecule 1      molecule 2";wrt 6
77: wrt 6," dJ1  dV1   J1   dJ2  dV2   J2";wrt 6
78: fmt 2,6f5.0,f15.3,e15.8,e15.8
79: for K=-2 to 2 by 2
80: for V=0 to N
81: for J=max(0,-K) to 4
82: 'F'(J,0)→E[1];'F'(J+K,V)-E[1]→D
83: for L=-2 to 2 by 2
84: for I=max(-L,0) to 4
85: X[K/2,V,J,L/2,I]→X
86: 'F'(I,0)→E[2];'F'(I+L,N-V)-E[2]+D→E
87: .001→C
88: if X/Y>C;Q+1→Q;E→I[1,Q];X*F→I[2,Q];X/Y→I[3,Q]
89: if X/Y>C;wrt 6.2,K,V,J,L,N-V,I,E,X*F,X/Y
90: next I
91: next L
92: next J
93: next V
94: wrt 6
95: next K
96: prt Q,"quadrupole lines"
97: trk 0;rcf S,R,O,Q,U,O[*],I[*],U[*]
98: stp
99: "Clebsch-Gordan coefficients":
100: "C":if p2=-2;3*p1*(p1-1)/(2*(2*p1-1)*(2*p1+1))→p3;ret p3
```

```
101: if p2=0;p1*(p1+1)/((2*p1-1)*(2*p1+3))→p3;ret p3
102: if p2=2;3*(p1+1)*(p1+2)/(2*(2*p1+1)*(2*p1+3))→p3;ret p3
103: dsp "error";beep;stp
104: "energy of the vib-rotational levels":
105: "F":p1*(p1+1)→p3
106: B[p2]*p3-D[p2]*p3^2+H[p2]*p3^3+W[p2]→p3;ret p3
107: end
```

# APPENDIX B

PROGRAM TO FIT THE SYNTHETIC PROFILE TO THE EXPERIMENTAL PROFILE

Non-linear least squares program to fit the synthetic profile to the experimental profile. (Written for the Hewlett-Packard model 9825A calculator.)

```
0: trk 0;dsp "LINESHAPE PROGRAM 10-10-81";stp
1: 240→C;dim R,O,Q,U,O[2,10],Q[3,150],U[2,10],N,T[2],X[C]
2: dim Y[C],C[3],A[2,5],D[10],S[10,11],G[4],V[2],B[2]
3: ent "graph y-max for log10",G[4];if flg13;gto "start"
4: ent "starting frequency",G[1],"end frequency",G[2];0→G[3]
5: scl G[1],G[2],G[3],G[4]
6: "start":ent "calculated data file #",F;1→V
7: ldf F,R,O,Q,U,O[*],Q[*],U[*];if O=0;4→V;0→r1;1→r2;1→r3
8: fmt 4,f5.0,f10.3,2el4.7
9: 0→A
10: for J=1 to Q
11: Q[2,J]+A→A
12: next J
13: fmt 1,"sum of calculated transition intensities",el4.5
14: fmt 5," temperature = ",f6.1,/,/
15: wrt 6.5,R;1.438832042/R→R;0→T[2]
16: ent "to cancel printing, enter 1",r0;if r0=1;gto "in"
17: if O=0;gto "q"
18: fmt 6,15x,"overlap",/,8x,"waveno.",5x,"intensity",/
19: wrt 6.6
20: for I=1 to O;wrt 6.4,I,U[1,I],O[2,I];next I
21: "q":if Q=0;gto "u"
22: fmt 7,/,12x,"quadrupolar",/,8x,"waveno.",5x,"intensity",/
23: wrt 6.7
24: for I=1 to Q;wrt 6.4,I,Q[1,I],Q[2,I],Q[3,I];next I
25: "u":if U=0;gto "in"
26: fmt 8,/,12x,"anisotropic",/,8x,"waveno.",5x,"intensity",/
27: wrt 6.8
28: for I=1 to U;wrt 6.4,I,U[1,I],U[2,I];next I
29: "in":ent "track # for experimental data",Z;trk Z
30: ent "experimental data file #",F;F→G
31: ent "# of parameters",P,"increment",H,"fract. error",E
32: P+V-1→P
33: P+1→K;rdm D[P],S[P,K]
34: for I=V to P;ent rI;next I
35: "nextfil":fmt 9,/,/,"track ",f2.0,3x,"file ",f3.0
36: fmt 8,"delta ",f9.6,4x," error ",f9.6
37: wrt 6.9,Z,F;wrt 6.8,H,E;T[2]→V[2]
38: wrt 6;wrt 6.1,A
39: fmt 1,6el5.7
40: F→G;ldf G,N,T[*],X[*],Y[*]
41: 0→A;0→B;X[3]-X[2]→T
```

```
42: for J=1 to N
43: Y[J]/1000→Y[J];Y[J]+A→A;Y[J]*X[J]+B→B
44: next J
45: fmt 1,"area under profile log10 Io/I",e14.5
46: wrt 6;wrt 6.1,B*T;wrt 6
47: fmt 2,"area under profile (1/waveno.)log10 Io/I",e14.5
48: wrt 6.2,A*T
49: wrt 6;fmt 3,"area under profile ln Io/I",e14.5
50: wrt 6.3,2.303*B*T;wrt 6
51: fmt 4,"area under profile(1/waveno.)*ln Io/I",e14.5
52: wrt 6.4,2.303*A*T
53: fmt 4,f3.0,2x,f12.2,6f12.6
54: fmt 5,3x,"temperature",2x,f6.1,4x,"pressure",2x,f7.1,/
55: wrt 6;wrt 6.5,T[1],T[2]
56: if abs(T[1]-1.438832042/R)>.01;dsp "bad temperature";stp
57: if V[2]#0;r4*(T[2]/V[2])^2→r4
58: fmt 1,9e15.7
59: wrt 6.1,r1,r2,r3,r4,r5,r6,r7
60: "fit":for I=1 to P
61: for J=1 to P+1
62: 0→S[I,J];next J
63: next I
64: 0→I;fxd 0;if F=G;gto "31"
65: F→G
66: "30":ldf G,N,T[*],X[*],Y[*]
67: "31":for L=1 to C
68: I+1→I;dsp I,N;X[L]→X;gsb "cal"
69: Y→D
70: for J=V to P
71: rJ*H→K;rJ+K→rJ;gsb "cal"
72: rJ-K→rJ;(Y-D)/K→D[J];next J
73: for J=V to P
74: for K=V to P;S[J,K]+D[J]*D[K]→S[J,K];next K
75: S[J,P+1]+(Y[L]-D)*D[J]→S[J,P+1];next J
76: if I>=N;fxd 5;gto "solve"
77: next L
78: G+1→G;gto "30"
79: "solve":for K=V to P
80: if S[K,K]=0;prt "matrix is singular";gto "start"
81: for J=K+1 to P+1;S[K,J]/S[K,K]→S[K,J]
82: for I=V to P;if K#I;S[I,J]-S[I,K]*S[K,J]→S[I,J]
83: next I
84: next J
85: next K
86: for I=V to P;rI+S[I,P+1]→rI;next I
87: wrt 6.1,r1,r2,r3,r4,r5,r6
88: for I=V to P
89: if abs(S[I,P+1]/rI)>E;gto "fit"
90: next I
91: if r0=1;gto "plot"
92: wtb 6,10,10,10
93: fmt 3,21x,"OBS",8x,"CALC",7x,"DIFF",11x,"OVERLAP QUAD"
```

```
94: wrt 6,3;for I=1 to 5;0→A[1,I];0→A[2,I];next I
95: 0→I;0→D;if G=F;gto "47"
96: F→G
97: "46":ldf G,N,T[*],X[*],Y[*]
98: "47":2*X[1]-X[2]→L
99: fmt 4,f3.0,2x,7f12.4
100: for J=1 to C
101: I+1→I;X[J]→X;X*(X-L)/2→V[1];X→L;gsb "cal"
102: for K=3 to 5
103: (A[1,K]+C[K-2])*V[1]+A[2,K]→A[2,K];C[K-2]→A[1,K]
104: next K
105: (A[1,1]+Y[J])*V[1]+A[2,1]→A[2,1]
106: (A[1,2]+Y)*V[1]+A[2,2]→A[2,2]
107: Y[J]→A[1,1];Y→A[1,2];(Y[J]-Y)*X→K;D+K*K→D
108: wrt 6.4,I,X,Y[J]*X,Y*X,K
109: if I>=N;gto "area"
110: next J
111: G+1→G;gto "46"
112: "area":fmt 9,/,8x,"area",5x,f12.4
113: wrt 6.9,A[2,1],A[2,2],A[2,1]-A[2,2],A[2,3],A[2,4],A[2,5]
114: fmt 2,/,"standard error =",e12.4;wrt 6.2,√D/(N-P)
115: "plot":if G[4]=0;G+1→F;gto "nextfil"
116: if V[2]#0;gto "skp"
117: axe G[1],0,100,.1;csiz 1.2
118: plt G[1],G[4],1;cplt 2,-2;lbl "+ OBSERVED"
119: plt G[1],G[4],1;cplt 2,-5;lbl "- CALCULATED";csiz .6
120: "skp":0→I;if G=F;gto "57"
121: F→G
122: "56":ldf G,N,T[*],X[*],Y[*]
123: "57":for J=1 to C
124: 1+I→I;plt X[J],Y[J]*X[J],1;cplt -.3,-.3;lbl "+"
125: if I>=N;iplt 0,0,1;gto "65"
126: next J
127: G+1→G;gto "56"
128: "65":csiz .6;0→I;if G=F;gto "67"
129: F→G
130: "66":ldf G,N,T[*],X[*],Y[*]
131: "67":for J=1 to 200
132: G[1]+(G[2]-G[1])/200*J→X;gsb "cal"
133: plt X,Y*X,-2
134: next J
135: "pltline":if V[2]#0;gto "back"
136: for I=1 to O
137: plt O[1,I],0,1;plt O[1,I],O[2,I]*O[1,I]*r1/2,2
138: cplt -.3,-.3;lbl "-"
139: next I
140: for I=1 to Q
141: if Q[3,I]<.05;gto 144
142: plt Q[1,I],0,1;plt Q[1,I],Q[3,I]*Q[1,I]*r4/2,2
143: cplt -.3,-.3;lbl "-"
144: next I
145: "back":plt 0,0,1;G+1→F;wtb 6,13,10,10,10,10,10
```

```
146: gto "nextfil"
147: "cal is a subrutine containing the ":
148: "lineshape functions":
149: "cal":0→C[1];if O=0;gto "Q"
150: for M=1 to O
151: X-O[1,M]→T
152: r1*O[2,M]*(1-1/(1+(T/r2)^2))/(1+exp(-R*T))→Y
153: abs(2*T/r3)→W;gsb "mbess"
154: C[1]+Y*S→C[1];next M
155: "Q":0→C[2];if Q=0;gto "U"
156: for M=1 to Q
157: X-Q[1,M]→T
158: Q[3,M]/((1+(T/r5)^2+(T/r6)^4)*(1+exp(-R*T)))+C[2]→C[2]
159: next M
160: r4*C[2]→C[2]
161: "U":0→C[3];if U=0;gto "add"
162: for M=7 to P;X-U[1,M-6]→T
163: rM*(1-1/(1+(T/r2)^2))/(1+exp(-R*T))→Y
164: abs(2*T/r3)→W;gsb "mbess"
165: C[3]+abs(Y*S)→C[3];next M
166: "add":C[1]+C[2]+C[3]→Y
167: ret
168: "modified Bessel function of the 2nd kind":
169: "mbess":if W>0;gto "1600"
170: 2→S;ret
171: "1600":if W>2;gto "1800"
172: (W/3.75)^2→T;.0360768+.0045813*T→Z
173: 3.0899424+T*(1.2067492+T*(.2659732+T*Z))→A
174: 1+T*(3.5156229+T*A)→A
175: .00301532+.00032411*T→Z
176: .51498869+T*(.15084934+T*(.02658733+T*Z))→B
177: .5+T*(.87890594+T*B)→B
178: (W/2)^2→T;-.00110404-.00004686*T→Z
179: -.67278579+T*(-.18156897+T*(-.01919402+T*Z))→Z
180: 1+T*(.15443144+T*Z)→Z
181: 2*Z+W*W*ln(T)*B→B
182: .0001075+.0000074*T→Z
183: .23069756+T(.0348859+T*(.00262698+T*Z))→Z
184: -.57721566+T*(.4227842+T*Z)→Z
185: -A*ln(T)/2+Z→A
186: A*W*W+B→S;ret
187: "1800":2/W→T;.00325614-.0006825*T→Z
188: -.0365562+T*(.01504268+T*(-.00780353+T*Z))→A
189: 1.25331414+T*(.23498619+T*A)→A
190: 2*A*exp(-W)*√W→A;.00587872+T*(-.00251154+T*.00053208)→Z
191: T*(-.07832358+T*(.02189568+T*(-.01062446+T*Z)))→B
192: 1.25331414+B→B
193: B*exp(-W)*W*√W→B;A+B→S;ret
194: end
```

# APPENDIX C

## POLARIZABILITY MATRIX ELEMENTS OF MOLECULAR HYDROGEN
## ( POLL, 1983 )

# APPENDIX C

## POLARIZABILITY MATRIX ELEMENTS OF MOLECULAR HYDROGEN

TABLE C-1 Matrix elements[a] of the isotropic, $\alpha$ and anisotropic, $\gamma$ polarizability of $H_2$ in $a_0^3$ units.

| | v | J | $\langle vJ \mid \alpha \mid v'J \rangle$ | $\langle vJ \mid \gamma \mid v'J \rangle$ | $\langle vJ \mid \gamma \mid v'J+2 \rangle$ |
|---|---|---|---|---|---|
| $\Delta v = 0$ | 0 | 0 | 5.41381 | 2.02377 | 2.03510 |
| | 0 | 1 | 5.42342 | 2.03159 | 2.05003 |
| | 0 | 2 | 5.44262 | 2.04724 | 2.07248 |
| | 0 | 3 | 5.47134 | 2.07074 | 2.10246 |
| | 0 | 4 | 5.50951* | 2.10211* | 2.13998* |
| $\Delta v = 1$ | 0 | 0 | −0.73922 | 0.61001 | 0.57084 |
| | 0 | 1 | −0.74026 | 0.61176 | 0.54630 |
| | 0 | 2 | −0.74233 | 0.61524 | 0.52323 |
| | 0 | 3 | −0.74542 | 0.62047 | 0.50152 |
| | 0 | 4 | −0.74880* | 0.62747* | 0.48106* |
| $\Delta v = 2$ | 0 | 0 | 0.07129 | 0.01224 | 0.02100 |
| | 0 | 1 | 0.07152 | 0.01246 | 0.02639 |
| | 0 | 2 | 0.07197 | 0.01288 | 0.03147 |
| | 0 | 3 | 0.07264* | 0.01305* | 0.03624* |
| | 0 | 4 | 0.07353* | 0.01432* | 0.04707* |

* extrapolated values.

[a] Poll (1983)

## REFERENCES

Bachet, G., Cohen, E.R., Dore, P. and Birnbaum, G. Can J. Phys. **61**, 591 (1983).

Birnbaum, G., and Cohen, E.R. Can. J. Phys. **54**, 593 (1976).

Birnbaum, G., Guilliot, B. and Bratos, S. Adv. Chem. Phys. **51**, 49 (1982).

Bragg, S.L., Brault, J.W. and Smith, W.H. Astrophys. J. **263**, 999 (1982).

Chang, K.S. Ph.D Thesis, Memorial University of Newfoundland, St. John's, Newfoundland (1974).

Chisholm, D.A., MacDonald, J.C.F., Crawford, M.F. and Welsh, H.L. Phys. Rev. **88**, 957 (1952).

Crawford, M.F., Welsh, H.L. and Locke, J.L. Phys. Rev. **75**, 1607 (1949).

Crawford, M.F., Welsh, H.L., MacDonald, J.C.F. and Locke, J.L. Phys. Rev. **80**, 469 (1950).

De Remigis, J., Mactaggart, J.W. and Welsh, H.L. Can. J. Phys. **49**, 381 (1971).

Downie, A.R., Magoon, M.C., Purcell, T. and Crawford, B. J. Opt. Soc. Amer. **43**, 941 (1953).

Fink, U., Wiggins T.A. and Rank D.A. J. Mol. Spect. **18**, 384 (1965).

Foltz, J.V., Rank, D.H. and Wiggins, T.A. J. Mol. Spect. **21**, 203 (1966).

Gibbs, P.W., Gray, C.G., Hunt, J.L., Reddy, S.P., Tipping, R.H. and Chang, K.S. Phys. Rev. Lett. **33**, 256 (1974).

Gillard, P. Ph.D Thesis, Memorial University of Newfoundland, St. John's, Newfoundland (1983; unpublished).

Goorvitch, D., Silvaggio, P.M., and Boese, R.W. J. Quant. Spectrosc. Radiat. Transfer **25**, 237 (1981).

Gray, C.G. J. Phys. B: Proc. Phys. Soc., London **4**, 1661 (1971).

Hare, W. F. J. and Welsh, H. L. Can. J. Phys. **36** , 88 (1958).

Karl, G. and Poll, J. D. J. Chem. Phys. **46** , 2944 (1967).

Kiss, Z. K. and Welsh, H. L. Can. J. Phys. **37** , 1249 (1959).

Levine, H. B. and Birnbaum, G. Phys. Rev. **154** , 172 (1967).

Lewis, J. C. Physica A **82** , 500 (1976) and references therein.

Lewis, J. C. Private communication (1983).

Lewis, J. C. and Van Kranendonk, J. Phys. Rev. Lett. **24** , 802 (1971).

Lewis, J. C. and Van Kranendonk, J. Can. J. Phys. **50** , 325 (1972a).

Lewis, J. C. Can. J. Phys. **50** , 2881 (1972b).

Lewis, J. C. and Van Kranendonk, J. Can. J. Phys. **50** , 2902 (1972c).

Lewis, J. C. and Tjon, J. A. Physica A **91** , 161 (1978).

Lewis, J. C. Can. J. Phys. **61** , 440 (1983).

Mactaggart, J. W. and Hunt, J. L. Can. J. Phys. **47** , 65 (1969).

Mactaggart, J. W., De Remegis, J. and Welsh, H. L. Can. J. Phys. **51** , 1971 (1973).

Mactaggart, J. W. and Welsh, H. L. Can. J. Phys. **51** , 158 (1973).

McCarty, R. D., Hord, J. and Roder, H. M. Natl. Bur. Standards Monograph **168** (1981).

McKellar, A. R. W. and Welsh, H. L. Proc. Roy. Soc. London **A322** , 421 (1971).

Michels, A., De Graaff, W., Wassennaar, T., Levelt, J. M. H., and Louwerse, P. Physica **25** , 25 (1959).

Penney, R. J., M. Sc. Thesis, Memorial University of Newfoundland, St. John's, Newfoundland (1980; unpublished).

Penney, R. J., Prasad, R. D. G. and Reddy, S. P. J. Chem. Phys. **77** , 131 (1982).

Plyler, E. K., Gallar, N. M. and Wiggins, T. A. J. Res. Natl. Bur. Standards, **48** , 221 (1952).

Poll, J.D. Private communications (1983).

Poll, J.D. **Proceedings I.A.U. Symposium 40 on Planetary Atmospheres** (Reidel, Dordrecht), 384 (1971).

Poll, J.D. Hunt, J.L. and Mactaggart, J.W. Can. J. Phys. **53**, 954 (1975).

Poll, J.D. and Wolniewicz, L. J. Chem. Phys. **68**, 3053 (1978).

Poll, J.D. and Hunt, J.L. Can. J. Phys. **59**, 1448 (1981).

Prasad, R.D.G., Ph.D. Thesis, Memorial University of Newfoundland, St. John's Newfoundland (1976; unpublished).

Reddy, S.P. and Kuo, C.Z. J. Mol. Spectrosc. **37**, 327 (1971).

Reddy, S.P., Varghese, G. and Prasad R.D.G. Phys. Rev. A **15**, 975 (1977).

Reddy, S.P. and Prasad, R.D.G. J. Chem. Phys. **66**, 5259 (1977).

Reddy, S.P., Sen, A. and Prasad, R.D.G. J. Chem. Phys. **72**, 6102 (1980).

Rich, N.H. and McKellar, A.R.W. Can. J. Phys. **54**, 486 (1976).

Sen, A., Prasad, R.D.G. and Reddy, S.P. J. Chem. Phys. **72**, 1716 (1980).

Silvaggio, P.M., Goorvitch, D. and Boese, R.W. J. Quant. Spectrosc. Radiat. Transfer **26**, 103 (1981).

Van Kranendonk, J. Physica **23**, 825 (1957).

Van Kranendonk, J. Physica **24**, 347 (1958).

Van Kranendonk, J. Can. J. Phys. **46**, 1173 (1968).

Van Kranendonk, J. Physica **73**, 156 (1974).

Van Kranendonk, J. and Bird, R.B. Physica **17**, 953 (1951a)

Van Kranendonk, J. and Bird, R.B. Physica **17**, 968 (1951a)

Van Kranendonk, J. **Intermolecular Spectroscopy and Dynamical Properties of Dense Systems**, edited by J. Van Kranendonk (North-Holland Publishing Company, Amsterdam), 77 (1980)

Watenabe, A. Can. J. Phys. **49**, 1320 (1971).

Watanabe, A. and Welsh, H.L. Can. J. Phys. **45**, 2859 (1967).

Watanabe, A., Hunt, J.L. and Welsh, H.L. Can. J. Phys. **49**, 860 (1971).

Welsh, H.L. **MTP International Review of Science, Physical Chemistry, Vol. 3, Spectroscopy**, edited by D.A. Ramsay (Butterworths, London) (1972) and references therein.

Welsh, H.L., Crawford, M.F. and Locke, J.L. Phys. Rev. **76**, 580 (1949).

Welsh, H.L., Crawford, M.F., MacDonald, J.C.F. and Chisholm, D.A. Phys. Rev. **83**, 1264 (1951).

Zaidel, A.N., Prokofer, V.K., Raisku, S.M., Slavnyi, V.A. and Shreider, E.Ya. **Tables of Spectral Lines** (IFI/Plenum, New York-London.) (1970).

Zaidi, H.R. and Van Kanendonk, J. Can. J. Phys. **49**, 385 (1971).